

General Disclaimer

One or more of the Following Statements may affect this Document

- This document has been reproduced from the best copy furnished by the organizational source. It is being released in the interest of making available as much information as possible.
- This document may contain data, which exceeds the sheet parameters. It was furnished in this condition by the organizational source and is the best copy available.
- This document may contain tone-on-tone or color graphs, charts and/or pictures, which have been reproduced in black and white.
- This document is paginated as submitted by the original source.
- Portions of this document are not fully legible due to the historical nature of some of the material. However, it is the best reproduction available from the original submission.

NASA CR-159424
PWA-5616

(NASA-CR-159424) COMPRESSOR SEAL RUB
ENERGETICS STUDY Final Report, 8 Apr. 1977
- 8 Apr. 1978 (Pratt and Whitney Aircraft
Group) 139 p HC A07/MF A01 CSCI 21E

N78-32096

G3/07 Unclass
31638



COMPRESSOR SEAL RUB ENERGETICS STUDY

FINAL REPORT

By W. F. Lavery

PRATT & WHITNEY AIRCRAFT GROUP
COMMERCIAL PRODUCTS DIVISION
UNITED TECHNOLOGIES CORPORATION

Prepared For

NATIONAL AERONAUTICS AND SPACE ADMINISTRATION

NASA Lewis Research Center
Contract NAS3-20613



FOREWORD

This report describes the work accomplished under contract NAS3-20613, Perform a Compressor Seal Rub Energetics Study, by Pratt & Whitney Aircraft (P&WA) Group, Commercial Products Division of United Technologies Corporation for the Lewis Research Center of the National Aeronautics and Space Administration. The technical effort was initiated 8 April 1977 and completed on 8 April 1978.

Mr. Lawrence Ludwig of the National Aeronautics and Space Administration (NASA) was the Project Manager and Mr. Leonard W. Schopen of the NASA Research Center was the Contracting Officer. Mr. Ludwig was replaced as Project Manager by Dr. Robert C. Bill, also of NASA, in April 1978.

Dr. William F. Lavery was the Program Manager for Pratt & Whitney Aircraft.

Appreciation is extended to the following P&WA personnel for their assistance: William F. Otfinoski, Assistant Project Engineer, for overall program assistance; Paul J. Dziorny, Analytical Engineer, for conducting the test program and completing the data reduction and analysis; Gary O'Dell, Engineering Technician, for conducting the tests and related setup and wear measurements; Frederick E. Dauser, Assistant Statistical Project Engineer, for statistically planning the test program and analyzing the data; Martin J. Reiner, Assistant Materials Project Engineer, and Arnold S. Grot and Robert J. Van Cleaf, Materials Engineers, for providing metallographic services and analyses.

PRECEDING PAGE BLANK NOT FILMED

TABLE OF CONTENTS

Section	Title	Page No.
1.0	SUMMARY AND CONCLUSIONS	1
	1.1 Summary of Results	1
	1.2 Conclusions	2
2.0	RECOMMENDATIONS	4
3.0	INTRODUCTION	5
	3.1 Background	5
	3.2 Program Overview	7
4.0	TECHNICAL PROGRAM	8
	4.1 Test Configuration	8
	4.2 Measurement of Rub Energy	9
	4.2.1 Total Rub Energy	9
	4.2.2 Blade Heating and Interface Temperature	11
	4.2.3 Heat to Abradable and Wear Debris	12
	4.2.4 Supplementary Instrumentation	12
	4.2.5 Convective "h" Determination	13
	4.3 Statistical Test Matrix	14
	4.4 Method of Test	14
	4.5 Fundamental Rub Interaction Tests	16
	4.5.1 Wear Analysis	18
	4.5.2 Metallographic Analysis	19
	4.6 Data Reduction and Analysis	21
	4.6.1 Total Rub Energy	21
	4.6.2 Rub Heat Into The Blade	22
	4.6.3 Rub Heat Into The Disk and Debris	25
	4.6.4 Statistical Analysis of The Data	27
	4.6.5 Summary of Task I Test Results	30
	4.7 Detailed Investigation of Significant Parameters	31
	4.7.1 Energy Measurements and Test Method	31
	4.7.2 Visual Test Results	32
	4.7.3 Wear Analysis	33
	4.7.4 Metallographic Analysis	34
	4.7.5 Data Reduction and Analysis	36
	4.7.6 Summary of Task III Test Results	36
	REFERENCES	39
	SYMBOLS	40

LIST OF TABLES

Table No.		Page No.
I	Statistical Test Matrix for Task I	42
II	Wear Measurements for the Task I Tests	43
III	Wear Results for the Task I Tests	44
IV	Task I Test Conditions, Wear and Data Analysis Results	45
V	Pyrometer Readings and Calculated Bulk Temperatures	47
VI	Basic Independent Parameters and Their Numerical and Coded Values	48
VII	Regression Equation Coefficients	49
VIII	Significance of Terms – % Variation Accounted for by Independent Variable	51
IX	Test Matrix for Tasks I and III	52
X	Task III Test Conditions and Wear Results	53
XI	Percent of Debris Particles Found Within a Given Size Range	54
XII	Task III Test Conditions, Wear and Data Analysis Results	55

LIST OF ILLUSTRATIONS

Figure No.	Title	Page No.
1	Test Rig Setup for Rub Energy Test	57
2	Schematic of Test Setup	57
3	Schematic of Rotor System	58
4	Instrumented Rub Test Blade	58
5	Specimen for Convective Heat Transfer Coefficient Evaluation Testing	59
6	Results of Convective Heat Transfer Coefficient Evaluation	60
7	Setup to Determine Multiple Blade Heat Transfer Coefficients	61
8	Results of Testing to Determine Frictional Resistance Torque	62
9	Post Test Cross-sections of Task I Test Seals	63
10	Post Test Cross-sections of Task I Test Seals	64
11	Post Test Cross-sections of Task I Test Seals	65
12	Post Test Cross-sections of Task I Test Seals	66
13	Photographs of Hastelloy X Fibermetal Abradable Seals from Test 9 and Test 10	67
14	Transverse Section Through Test Blade #11 Showing Transfer	68
15	Top View of Test Blade #1 Showing Transfer	69
16	Transverse Section Through Tip of 8-1-1 Titanium Blade From Test 9	70
17	Longitudinal Section Through Tip of 8-1-1 Titanium Blade From Test 12	71
18	Task I Test 1 Data Reduction Results	72

LIST OF ILLUSTRATIONS (continued)

Figure No.	Title	Page No.
19	Task I Test 3 Data Reduction Results	73
20	Task I Test 4 Data Reduction Results	74
21	Task I Test 5 Data Reduction Results	75
22	Task I Test 8 Data Reduction Results	76
23	Task I Test 9 Data Reduction Results	77
24	Task I Test 11 Data Reduction Results	78
25	Task I Test 12 Data Reduction Results	79
26	Model for Thermal Analysis of Blade	80
27	Test 7 – Thermocouple Trace During Test	81
28	Test 7 – Blade Heating Data Reduction	82
29	Task I Test 2 Data Reduction Results	83
30	Task I Test 7 Data Reduction Results	84
31	Task I Test 10 Data Reduction Results	85
32	Data Fit to Model Using Least Squares Criterion	86
33	Regression Analysis for Task I Average Total Energy	87
34	Regression Analysis for Task I Average Total Energy, Including Data from Expansion of 1.0 mm Tests	88
35	Regression Analysis for Task I Peak Total Energy	89
36	Regression Analysis for Task I Peak Total Energy, Including Data from Expansion of 1.0 mm Tests	90
37	Regression Analysis for Task I Average Heat to Blade	91
38	Regression Analysis for Task I Average Heat to Blade, Including Data from Expansion of 1.0 mm Tests	92
39	Regression Analysis for Task I Peak Heat to Blade	93

LIST OF ILLUSTRATIONS (continued)

Figure No.	Title	Page No.
40	Regression Analysis for Task I Peak Heat to Blade, Including Data from Expansion of 1.0 mm Tests	94
41	Regression Analysis for Task I Maximum Blade Temperature	95
42	Regression Analysis for Task I Maximum Blade Temperature, Including Data from Expansion of 1.0 mm Tests	96
43	Regression Analysis for Task I Adjusted Blade Wear and Transfer	97
44	Task III Blade Thermocouple Installation	98
45	Test Setup for Task III, Multi-bladed Test	99
46	Cross-sections of Seals from Task III Tests	100
47	Cross-sections of Seals from Task III Tests	101
48	Photograph Showing Absence of Smearing and Glazing on Seal Surface for Test 15	102
49	Photograph Showing Absence of Smearing and Glazing on Seal Surface for Test 13	103
50	Blade Rub Surface from Test 15	103
51	Sections of Recrystallization at the Blade Rub Interface for Test 13	104
52	Cross-section of Blade from Test 17 Showing Decomposition of the Grain Structure	104
53	Seal Surface from Test 17 Showing Heavy Surface Glazing	105
54	Cross-section Through Blade from Test 13 Showing Region of Maximum Transfer	105
55	Blade Tip #1 from Test 14	106
56	Blade Tip #2 from Test 14	107

LIST OF ILLUSTRATIONS (continued)

Figure No.	Title	Page No.
57	Blade Tip #3 from Test 14	108
58	Burrs at Leading and Trailing Edges of Blade Tip from Test 14	109
59	A Section of the Rub Surface where Mixing has Occurred	109
60	Photograph of Blade Tip Showing Surface Layer of Titanium with Traces of Hastelloy X for Test 14	110
61	Photomicrograph of the Rubstrip for Test 14 Showing Densification at the Rub Surface	110
62	Blade Tip #1 from Test 16	111
63	Blade Tip #2 from Test 16	112
64	Blade Tip #3 from Test 16	113
65	Cross-section of Blade from Test 16 Showing Burr at Leading Edge	114
66	Plan View of Rubstrip from Test 16 Showing Heavily Glazed Striations	115
67	Typical Particle of Rub Debris from Test 14	116
68	Hastelloy X Abradable Seal Fiber Dislodged During Rub	116
69	Task III Test 13 Data Reduction Results	117
70	Task III Test 14 Data Reduction Results	118
71	Task III Test 15 Data Reduction Results	119
72	Task III Test 16 Data Reduction Results	120
73	Task III Test 17 Data Reduction Results	121
74	Task III Test 14 Strain Gauge Results	122
75	Task III Test 16 Strain Gauge Results	123

LIST OF ILLUSTRATIONS (continued)

Figure No.	Title	Page No.
76	Comparison of Task III Data with Task I Model — Average Total Energy	124
77	Comparison of Task III Data with Task I Model — Peak Total Energy	125
78	Comparison of Task III Data with Task I Model — Average Heat to Blade	126
79	Comparison of Task III Data with Task I Model — Peak Heat to Blade	127
80	Comparison of Task III Data with Task I Model — Maximum Blade Temperature	128
81	Comparison of Task III Data with Task I Model — Adjusted Blade Wear and Transfer	129

1.0 SUMMARY AND CONCLUSIONS

1.1 SUMMARY OF RESULTS

Twelve fundamental rub interaction tests using compressor blade/shroud materials (titanium blades and Feltmetal[®] fibermetal rubstrips) were instrumented and run under simulated engine conditions. The first 10 tests were statistically planned. The eleventh was run as a repeat of test 6, a test in which the rub speed dropped to zero prior to completion of the test. Test 12 was chosen, using linear regression and correlation analysis, to provide additional test data in a region of high rub energy and severe wear.

The tests were conducted with single stationary blades rubbing against seal material bonded to rotating test disks. The instantaneous rub torque, speed, incursion rate and blade temperatures were continuously measured and recorded. Incursion rate, rub depth, abradable density, blade thickness and rub velocity were varied to simulate engine compressor rub conditions. Data was obtained to determine the effect these rub parameters have on rub energy and heat split between the blade, rubstrip and rub debris. A statistical linear regression analysis was used to determine the relationship of the rub parameters to such dependent variables as total rub energy, heat to the blade, interface temperature and blade wear/transfer. All correlations were determined to be significant with total rub energy being the most, blade heating in the middle and blade temperature and wear the least significant. Each independent variable was also ranked as to its significance. Incursion rate was determined to have the strongest influence on the rub phenomenon, followed by rub velocity and blade thickness which are substantially lower in influence but still show a significant effect. Incursion depth and abradable density were found to have minimal influence on rub energy and blade heating, temperature and wear.

Observations and measurements of the first twelve tests indicated the strong influence of incursion rate. The rub modes ranged from clean rubs with very low rub energy, relatively low blade tip temperatures and low blade wear for the 0.0025 mm per second incursion rate to high rub energy, extreme blade tip temperatures and high blade wear and/or seal material transfer for the 0.25 mm per second incursion rate. At the intermediate incursion rate (0.025 mm per second) blade wear was low but transfer occurred.

Rub velocity, a less significant variable, had its strongest effect on interface temperature which was noted to be 320°K higher by the regression analysis at the lower rub velocity. Blade wear and transfer also showed a corresponding increase as the rub velocity was decreased from 213 to 152 mps.

Blade thickness proved to be of the same order of importance as rub velocity, its strongest effect being on rub energy terms which increased with increased blade thickness.

Both incursion depth and abradable density produced no significant effects on rub energy or interface temperature but an apparent increase in blade wear plus transfer was observed for the higher density abradable.

A high degree of confidence in the data was realized from the statistical analysis of the first twelve tests. This left the final five programmed tests to extend the range of investigation to determine the effect of a change in blade material and the addition of blades for multiple blade testing.

Three nickel base alloy (Incoloy 901) blade tests were conducted. The major difference between the Incoloy 901 and titanium testing was the interface temperature which was considerably lower for the Incoloy 901. This is reasonable because the softening or reduced strength temperature for Incoloy 901 is much less than for titanium. This limited testing indicated that blade material does not have a significant effect on blade wear. The testing also indicated that blade material does not have an effect on the transfer phenomenon.

The tests with multiple blades did not reduce the work per blade and did increase the rub energy of the system. Both the thin and thick blades did not produce the blade wear reduction expected; the wear for each thicker blade, in fact, was three times that for the single blade in a comparative test. It was noted that the close blade spacing prevented abradable cooling between rubs resulting in continuous rubbing of all blades and intensification of the heating effects.

1.2 CONCLUSIONS

This program was designed to investigate the rub phenomenon associated with a compressor blade/seal system subjected to simulated engine conditions. The testing conducted provided the following conclusions:

- Statistical test planning and analysis of the data was very successful.
- All statistical correlations to determine the main linear effects were determined to be significant. The ranking of the importance of each individual independent variable is:
 - incursion rate — very important
 - rub velocity — moderate importance
 - blade thickness — moderate importance
 - incursion depth — low importance
 - abradable density — low importance
- Incursion rate, the most important variable, increased rub energy and blade wear with increasing values of incursion rate.
- Statistical analysis of the interactive effects of two combined variables did not reveal any significant relationships.

- Three distinct rub modes were identified.
 - A low energy, low blade wear mode which occurred at low incursion rates.
 - Transfer of seal material to the blade tips which occurred at moderate and high incursion rates.
 - A high rub energy, high wear rate rub mode which predominated under combined high incursion rate, low rub velocity and thick blades.
- Testing indicated that blade material does not have a significant effect on blade wear for the blade materials tested.
- Testing revealed no effect of blade material on the transfer phenomenon.
- Testing with multiple blades did not greatly reduce the work per blade and did increase the rub energy of the system. Close blade spacing was noted to prevent abradable cooling between rubs resulting in the abnormal event of all blades continuously rubbing and intensification of the heating effects.

2.0 RECOMMENDATIONS

The systematic testing completed in the present program has provided a sound foundation for additional testing to further investigate compressor seal rub phenomena. Several different rub modes have been identified including a low rub energy clean cutting mode, a high rub energy mode with transfer of abradable material to the blade and some seal surface densification and a high rub energy mode with high blade wear, high interface temperatures and substantial seal surface densification and glazing. Although rub conditions required to produce each of these rub modes were identified further work is required to determine how the various independent rub parameters influence the transition from one rub mode to another so that the causes of high energy rub phenomena can be understood and controlled.

Testing with multiple blades produced the unexpected result that high rub energy was not eliminated when more blades were provided to reduce the cutting effect required for each blade. While this result was attributed, in these tests, to close blade spacing which prevented cooldown of the seal surface between rubs, additional work is needed to determine the effect of blade spacing and multiple blade rubbing on the rub energetics.

In order to focus on the numerous geometric and rate related rub variables, the testing conducted in this program was limited to one compressor abradable material. Future work should extend the range of investigation to other abradables. Both advanced sprayed abradables and current competitive high pressure compressor abradables should be considered for such work.

Development of low rub energy abradable seal systems remains a key to achievement of improved compressor performance goals for future engines and a means of improving the initial performance and reducing its deterioration in current generation engines. The performance of high pressure ratio machines, which will be required to meet the nation's energy efficient engine objectives, will be even more sensitive to maintenance of tight compressor blade tip seal clearances than that of current generation engines. For this reason the disciplined approach to development of improved compressor blade tip sealing which has been initiated in this program must be continued to assure that superior abradable seal systems are available as they are needed.

3.0 INTRODUCTION

Gas path sealing is a critical factor in gas turbine engine performance and fuel consumption. As the engine cycle has moved toward higher compressor pressure ratios, blade tip clearance in the high pressure compressor has become an area of increasing concern (references 1 and 2). If the detrimental effects of tip leakage are to be minimized, engines must be able to operate with minimum tip clearance at all flight conditions while avoiding interference between blade tip and shroud through all engine transients. Additionally, the engine must be designed to successfully withstand blade tip/shroud rubs resulting from maneuver and surge deflections. Since the clearance increase produced by rubbing wear will be minimized if the wear occurs preferentially on the shroud with negligible wear on the blade tips, static shrouds in modern gas turbine engines incorporate surface layers of abradable materials.

Abradable materials which will yield minimum wear of blade tip and labyrinth seals have been the object of extensive and continuing effort at Pratt & Whitney Aircraft (references 3 and 4). Efforts to date have provided some answers for the overall rub mechanics question (references 5 and 6) but the formulation of a rub mechanics model for compressor blade tips against the various current and advanced compressor abradables has not been fully addressed. To establish such a model for use in setting abradability criteria and goals for advanced compressor abradables, rub energy and heat split data are required from controlled testing of the major variables. The program was designed to investigate the rub mechanics of compressor abradable blade tip seals for a range of rub conditions representative of actual flight engine service occurrences.

3.1 BACKGROUND

The purpose of compressor tip seals is to minimize the leakage air across the blade tips from the pressure to the suction side of the blades. Such leakage results in irrecoverable losses which translate into compressor efficiency loss. Since an aerodynamically smooth surface is needed for the compressor endwall, tip sealing is accomplished by maintaining a minimum clearance between the blade tip and the opposing shroud. Beyond the tolerance limitations inherent in various fabrication and assembly procedures there are a number of factors which lead to compressor tip clearance variations during engine operation. These are maneuver and landing g-loads, rotor and stator deflection during off-design engine operation (e.g. surge-induced deflection), thermal transient mismatch between rotating and static seal components, rotor whirl, engine case distortion due to engine mount loads and structural vibration and instability. For engines which are built with initially tight tip clearances these effects result in rubbing between the blade tips and shroud which produces wear of the blades or the shroud or both, with an attendant increase in tip clearance. Shrouds that are truly abradable result in localized shroud wear, rather than full circumferential blade wear, and thus result in a minimum increase in tip leakage due to rub interactions. The abradables used in current engines only partially meet this objective. The resulting blade wear has not only produced immediate losses in engine performance but has become a major cost factor in engine overhaul since worn blades must be replaced in order to restore a compressor to its original efficiency and flow capacity.

The primary objective for an abradable material is that it be readily removable by the rubbing action of the compressor blades. Since it is advantageous for blade tip thickness to be minimized for aerodynamic performance and for the blade material to be dictated by overall structural requirements, acceptable abradability requires achievement of a low density, preferably friable seal material. Unfortunately, this objective is in opposition to the other two major design considerations, erosion resistance and high temperature stability. The material choice for all abradable systems must provide an effective trade between durability and abradability, taking into account the engine rub history and operating environment — temperature, pressure, flow field, erosion climate and the time factor. Other factors which must be considered in the design of abradable blade tip seals include minimum cost, field refurbishment capability, a rotor/stator thermal response match and minimum weight.

Various material systems have been investigated for use as compressor abradables. For the high pressure stages of engine compression systems the oxidation or chemical stability limits of the material are important. To meet the more severe environment metallic seal systems are required. Use of such systems with conventional titanium and nickel base blade materials considerably aggravates one of the wear problems — that of softening and wearing of the compressor blade tips due to rub energy dissipation. The approach used for current generation high pressure compressor abradables has been to use oxidation resistant metals fabricated to form low strength bodies. The most successful systems have been formed by sintering metallic fibers or powders into porous structures which can be brazed to a compressor case or seal ring.

For porous metallic seal systems the desired material removal mechanism is fracture of the bonds between particles or fibers. In current seal systems this objective is only partially met. When bonds are not broken by the rub forces, the resulting deformation of the structure produces an increase in the heat generation within a very thin plastically deformed layer at the abradable surface. Subsequent blade interactions, in the form of high frequency loading and unloading, fatigue the smoothened seal surface developing both surface and underlying cracks, eventually flaking off sections of the thin surface layer. Under some circumstances repeated rubbing does not remove material, resulting in a further increase in surface densification and heat generation with attendant glazing. While substantial progress in improved abradability has been achieved by lowering the strength of the structure and improving its uniformity, consistent with maintaining the required erosion resistance, there is still ample impetus for continued development. To meet this need, development of a correlation which will define the boundaries between regions of favorable and unfavorable rub mechanisms is required. The problems which must be overcome are seen to vary with the different conditions and different materials used. In each case, however, rub induced problems are present which could be attacked with a suitable analytical model of the rub process. The key aspect of the problem is the rub energy. It has been observed that small variations in rub parameters can lead to large differences in rub energy dissipation. Rub energy is consequently an excellent measure of the mode of wear and an indicator of incipient change from one wear mechanism to another. The testing conducted in this program concentrated on measuring and providing rub energies, interface temperature and wear.

3.2 PROGRAM OVERVIEW

Because of the lack of an established criterion for the optimization of abradable seal systems for rub tolerance the extensive on-going abradable seal development programs being pursued by engine manufacturers and their suppliers must be guided by purely qualitative rub tolerance judgements and the results of comparative tests in rigs and engines. Crucial to the development of a suitable criterion is the requirement for rub energy data including heat splits to the blade, shroud and wear debris and interface temperatures under controlled rub conditions. Application of such data to thermal rub models is required to validate the model and identify areas for additional work.

Recent efforts at P&WA have established techniques for measurement of rub energy and blade temperature response under simulated engine tip seal rubbing conditions and for analysis of data to determine heat splits and interface temperatures. This program applied these techniques in measuring rub energies over a range of rub conditions, geometry variation and blade material variations. Data from the tests was analyzed for rub energy, heat splits and interface temperature and statistical analysis was completed to establish linear and interactive effects of the independent variables on rub energy and wear parameters. Metallographic analysis was conducted to identify microstructural changes on the rubbed surfaces, and shroud and blade wear measurements were taken.

In the initial series of tests a range of test conditions including variations of rub velocity, incursion rate, incursion depth, blade thickness and abradable density was investigated using a reference abradable and a single titanium blade. A statistical test plan employing twelve tests was used to permit establishment of the linear effect of each variable plus interactive effects between the critical variables on rub energy and wear. Based on the results of the initial tests, test conditions were established for a second series of tests in which the effects of multiple blades and an additional blade material were investigated.

4.0 TECHNICAL PROGRAM

4.1 TEST CONFIGURATION

In engine applications abrasible seal rubs generally occur as a result of radial deflection of the structure due to loads induced by such effects as aircraft maneuvers, gusts and gyros or as a result of radial growth of rotor structure due to dynamic and thermal effects. In compressor blade tip seal applications rubbing speeds of 244 m/sec (800 ft/sec) are typical. Incursion rates which vary depending upon the source of the deflection, range from about .0025 mm/sec (0.1 mils/sec) to 0.25 mm/sec (10 mils/sec). While small variations in blade length generally cause only part of the blades in any one stage to rub simultaneously, with metallic abrasible blade wear usually brings most or all of the blades in contact with the shroud sometime during the life of the engine. Spacing between actively rubbing blades therefore typically varies from about 25 mm (1 inch) which is typical of the circumferential distance between adjacent blades, up to 400 to 500 mm (15 to 20 inches). Rub length on the shroud varies from a few centimeters to the full circumference depending on the type and severity of the rub-producing effect. Other factors such as environmental conditions, blade tip geometry and abrasible and blade material properties also influence the behavior of the system under rubbing conditions.

In establishing an experimental facility to investigate engine rub phenomena, it was desired to model as many of these factors as possible. Because of cost factors it was desirable to work in a small scale rig. Comparative testing in small scale rigs and full scale rigs and engines was used to substantiate that rig size does not have a significant effect on the controlling rub phenomena. Environmental conditions which are often costly to reproduce in a rig appear to be of secondary importance except for the effect of temperature on material properties. For compressor seal rubbing, however, rub energy is often the dominant effect in determining the temperature in the rub zone so that ambient testing is justified for initial studies of compressor seal rub energetics. The remaining variables of known importance can all be simulated in the P&WA small scale abrasibility test rig facilities. A photograph of the rig used in this program is shown in Figure 1 and a schematic of the rig is shown in Figure 2.

In this rig the rotating disk is driven by an air turbine to achieve the desired rub velocities. Both governed operation, in which air flow to the turbine is controlled automatically by a speed controller to maintain constant wheel speed, and ungoverned operation, in which air supply pressure to the drive turbine is controlled by the operator, are available. Because the in-line torque meter can be damaged if excessive torque is delivered by the turbine, tests in which the meter is employed are generally run ungoverned.

The stationary test piece is mounted on a carriage which is supported on two rails by low friction bearings and which is driven toward the rotating disk by a pulley and weight system. Controlled incursion rates are achieved with a variable motor micrometer-feed system which acts to restrain the motion of the carriage. A load cell is incorporated in series with the micrometer-feed system to measure load; the normal rub force being the difference between the force of the carriage drive weights (generally 111 N (25 lbs.)) and the reading of the load cell. In order to achieve accurate control of the incursion depth and to prevent "spark-out" rubbing at the end of a test, which tends to alter the metallographic data on the rub surfaces, an automatic carriage withdrawal system was incorporated in the rig. The withdrawal force is provided by a pneumatic piston. Actuation of the piston is controlled by a limit switch which is adjustable to carriage position.

The standard test utilizes a static rubstrip segment which is translated at a controlled rate into a bladed rotor held at a constant surface speed. The rub occurs as a series of intermittent pulses as each blade contacts the shroud and, because of the high wheel speed and relatively short rub length, the duration of each rub is on the order of 10^{-4} seconds. This situation makes energy measurements, specifically force and blade temperatures, very difficult to obtain. To overcome these problems the basic rig setup for rub energy testing has been inverted. The rubstrip material is applied as a coating on the rim of a rotating disk and the blade or blades are affixed to a stationary holder which is translated at a controlled rate into the rotating disk to obtain the incursion rate desired. The rig disk designed for this contract included eight inserts equally spaced around the periphery of the disk to permit a shroud specimen at any of the insert locations to be removed for detailed metallographic analysis and replaced with new shroud material without sacrificing the entire disk.

Initial testing at P&WA with the inverted blade/disk setup utilized nickel graphite flame sprayed on the disk rim, as the abradable shroud material. Inconsistencies inherent in sprayed nickel graphite prompted a change to a sintered product to obtain more uniformity of density and tensile strength throughout the abradable material. Feltmetal® fibermetal was chosen because of its widespread use as an abradable shroud material in current engine high pressure compressors.

4.2 MEASUREMENT OF RUB ENERGY

The primary information desired from the tests is the total energy dissipated by rub, the energy split between the shroud abradable/blade/wear debris and the interface temperature. The methods employed to determine each of these quantities are discussed in the following paragraphs.

4.2.1 Total Rub Energy

The total energy at the rub zone is equal to the power expended in the rub zone. Although a small percentage (~1-4%) of the expended power is stored as elastic energy around dislocations newly generated by the rub, a compensating percentage of energy is drained from the lattice structure in the rub zone by thermal strains associated with the original mechanical heat dissipation. Thus, the total heat into the rub zone can be represented by

$$q_{\text{total}}(t) = T_{\text{rub}} \times \omega \quad (1)$$

where: $q_{\text{total}}(t)$ is the total heat load on the rub zone

T_{rub} is the rub torque

ω is the rotational speed

The rub torque is determined by a rotational equilibrium balance (see Figure 3) as follows:

$$\Sigma \tau = J \frac{d\omega}{dt} = \tau_{\text{turbine}} - \tau_{\text{rub}} - \tau_{\text{windage} + \text{friction}} \quad (2)$$

$$\text{or } \tau_{\text{rub}} = \tau_{\text{turbine}} - \tau_{\text{windage} + \text{friction}} - J \frac{d\omega}{dt} \quad (3)$$

Since an accurate measurement of angular acceleration ($d\omega/dt$) was not feasible, and the measured torque is not an extremely high frequency measurement, but a time averaged value, time averaging over a small time (Δt) was used, resulting in the following:

$$\begin{aligned} \tau_{\text{rub}} &= \frac{1}{\Delta t} \int_{\Delta t} \tau_{\text{rub}} dt \\ &= \frac{1}{\Delta t} \int_{\Delta t} \tau_{\text{turbine}} dt - \frac{1}{\Delta t} \int_{\Delta t} \tau_{\text{windage} + \text{friction}} dt - J \frac{\omega_{t+\Delta t} - \omega_t}{\Delta t} \end{aligned} \quad (4)$$

and similarly

$$\tilde{q}_{\text{total}} = \frac{1}{\Delta t} \int_{\Delta t} \tau_{\text{turbine}} \cdot \omega \cdot dt - \frac{1}{\Delta t} \int_{\Delta t} \tau_{\text{windage} + \text{friction}} \cdot \omega \cdot dt - \frac{J}{2\Delta t} (\omega_{t+\Delta t}^2 - \omega_t^2) \quad (5)$$

where: \tilde{q}_{total} is the time average of the total heat load on the rub zone over a time increment Δt ;

τ_{turbine} is the torque exerted on the disk by the turbine;

$\tau_{\text{windage} + \text{friction}}$ is the frictional resistance torque;

J is the rotational inertia

To evaluate the first term of the total heat load expression τ_{turbine} was measured with an optical torquemeter and recorded as a continuous trace on the oscillograph. Speed (ω) was sampled by an electronic counter system at small time increments (Δt) chosen small enough to insure a smooth curve of total heat load on the rub zone vs. time. The second term, bearing and windage frictional resistance, was determined by setting \dot{q}_{total} equal to zero (operation at a no rub condition) and measuring τ_{turbine} as a function of ω . The third term includes J , the rotational inertia, which was calculated for the disk and the entire rotor system.

The instrument used to measure the turbine torque was a Vibrac Corporation in-line optical transducer which provides the capability to measure rotational torque accurately without slip rings. The Vibrac torque transducer uses adjacent slotted disks to detect rotation of one end of the calibrated torque bar relative to the other. Torque bar twist alters the "window area" of the slotted disks set between lamps and photocells which develop an output current proportional to torque.

In this unit the photocells operate the torque display meter directly thus eliminating any electronic amplification. In addition, the optical coupling between moving and stationary components requires no slip rings or AC carrier techniques to produce a signal. The particular model used was developed specifically for the P&WA seal rigs. This meter has a range of minus 1.13 Nm (10 in.-lb.) to plus 1.13 Nm with an accuracy of approximately ± 0.011 Nm and a frequency response of 400 Hz. This response and the 40 Hz torsion natural frequency of the combined disk, shaft and torque meter system were well in excess of the 10 Hz requirement for data reduction. Output of the torque meter was fed into a conditioning circuit which allowed a continuous oscillograph trace of the torque.

Having selected the optical torquemeter for turbine torque measurements, a system of obtaining angular speed variation was desired which would permit resolution of total heat load on the rub zone to the limits of the torque meter. Using a magnetic speed pip system, already mounted inside the turbine drive to provide an electrical pulse at the end of every 1/6th of a revolution of the disk, an electronic counter was selected which measured the time between ten speed pip pulses (1-2/3 revolutions of the disk). The counter, which used an internal frequency generator producing 10^7 Hz, together with a digital printer having a maximum printing speed of 10 lines/sec was used to record elapsed time between 10 speed pip pulses to 5 significant figures. The combined uncertainty in the speed measurement of this system was then $\pm 0.005\%$ or ± 1.5 rpm. For the minimum dwell time, as dictated by the printing speed, this translates to an error in total rub energy which is approximately one half the error caused by the uncertainty in measured turbine torque.

The electronic counter provided a command to the printer to record a value following a pre-selected dwell time. The counter was modified such that this signal was also traced on the oscillograph as a square wave, thus providing for synchronization of the speed recordings with time and all the other measurements.

4.2.2 Blade Heating and Interface Temperature

In order to determine the fraction of the rub energy going into the blade tip and the interface temperature as a function of time through the test, transient measurement of an array of

thermocouples was used in conjunction with a one dimensional conduction analysis of the blade. The thermocouple array consisted of six, 0.08 mm diameter platinum-platinum/10% rhodium thermocouples, located on the blade tip as shown in Figure 4. Although calibration of these thermocouples can be carried out up to 1920°K, titanium alloys with platinum at a lower temperature. Because of this each blade was first sputtered with a 0.05 mm thick layer of molybdenum to prevent alloying of the two materials.

The thermocouple junctions were formed by laser welding, and then were resistance welded to the molybdenum layer. The 0.08 mm wires were routed down the length of the blade, off onto the blade holder, and then held in place with a layer of ceramic cement. Copper-Copper/Nickel extension wires were resistance welded to the 0.08 mm lead wires, and strapped down to the holder. They were then connected to a signal conditioning circuit which fed into the oscillograph for continuous recording during each test.

4.2.3 Heat to Abradable and Wear Debris

To provide an indication of the abradable material heat-up and temperature decay, optical pyrometers were focused at two positions on the disk O.D. — 30° from the rub zone, in the direction of disk rotation, and 180° from the rub zone. The optical pyrometer at the 30° position was a silicon detector unit which has a low temperature threshold of 980°K. The pyrometer at the 180° position was a Vanzetti lead sulfide unit which has a threshold of 590°K. As noted in Table V, the silicon detector pyrometer was subsequently replaced by a Vanzetti lead sulfide detector unit with a 750°K threshold temperature when it was determined that the 980°K threshold was too high. The response time of the Vanzetti's was 25 K Hz.

While it was not possible to measure the heat fraction to the wear debris directly, the interface temperatures determined for the blade and abradable were felt to be representative of the temperature of the debris leaving each surface. While oxidation of the wear debris is evident from the sparking which occurs during most tests, post-test analysis of the wear debris can provide some additional insight into the thermal energy carried in the rub debris.

4.2.4 Supplementary Instrumentation

Dynamic strain gages were used on three Task I, single bladed tests in order to obtain an indication of the number of rubs/revolution, and change with time of this quantity. Strain gages on each blade of the two Task III multi-bladed tests were intended to show, also, how often each of the blades rubbed. The 1.6 mm wide gages were connected as close to the holder as possible, and then covered with ceramic cement, following routing of the thermocouple lead wires. Maximum response of the strain gages was limited by the response of the galvanometers to 6000 Hz.

A certified time code generator, capable of indicating time to 0.001 secs, was used as the reference time trace for each test. Its output was traced on the two oscillographs required for this testing, synchronizing one with the other.

4.2.5 Convective "h" Determination

One of the independent variables required for determination of heat load to the blade is the average convective heat transfer coefficient for the air pumped over the blade by the rotating disk. Although some correlations of heat transfer coefficients are available in the literature for flow over bluff bodies in a constant velocity air-stream, the effect of the flow field produced by the disk and the effect of blade angle made use of these correlations questionable. Consequently, a simple experimental test to measure the average heat transfer coefficient over the blade was conducted.

The basic test apparatus used consisted of an electrically heated blade specimen which was placed in the standard blade holder and mounted in the rig in close proximity to the disk rim. The blade specimen was fabricated from low conductivity material (Micarta®) to approximately the same dimensions as the thick test blades. A 0.08 mm thick nichrome foil heater strip was fabricated by EDM and bonded to the blade specimen as shown in Figure 5. The ends of the heater element which were routed around to the rear of the blade for connection to copper lead wires and insulated with zirconia cement were sized to minimize the heat conducted away from the face of the test specimen. A low voltage, high current A.C. variable power supply was used to control the electrical power to the heater.

The power dissipated from the heater face was determined from an $I^2 R$ calculation, the current being measured with a shunt/millivoltmeter system in series with the heater element and the resistance being determined ahead of time with a wheatstone bridge circuit. Temperature measurement of the face of the heater element was made using an optical pyrometer, the emissivity of the heater surface being fixed by painting the strip with high temperature "black" paint.

Testing to determine the heat transfer coefficient on the upstream face of the blade was carried out with the rig setup in the same manner as for the rub tests. Measurement of the heat transfer coefficient on the downstream face was made by running the drive turbine in reverse.

Analysis of the data was performed using the equation:

$$h = \frac{I^2 R}{A (T_s - T_a)} - U \quad (6)$$

where: h = average convective heat transfer coefficient
 I = current to strip
 R = resistance of strip (corrected for temperature)
 A = area within the perimeter of the strip
 T_s = measured surface temperature
 T_a = measured ambient temp. in vicinity of strip
 U = overall heat loss conductance through blade to air at back surface of blade.

The heat loss conductance term which was kept small by the use of the low conductivity Micarta® blade material, was estimated using published values of Micarta® conductivity and approximate values of the back side heat transfer coefficient. Analysis of the data for both forward and reverse testing resulted in the smooth curve of average h vs disk speed shown in Figure 6. For multi-bladed tests, the h was found to be identical to single bladed tests. A photograph of this set-up is shown in Figure 7.

4.3 STATISTICAL TEST MATRIX

In this test program the independent variables were blade thickness, abradable density, rub velocity, rub depth and incursion rate. Each of these parameters were assigned two operation levels except the incursion rate which was assigned three levels. These levels reflect engine operating conditions in the compressor and the blade/seal geometry variations in that area. A test program which would test all possible combinations of the five independent variables at the levels chosen would require at least 48 tests. Because of the large cost of conducting such a program, it was decided to employ statistical test planning techniques to minimize the number of tests required. With the objective of identifying the significant variables and establishing the linear main effects of the five independent variables on rub energy and wear, it was determined that eight tests were required. Two additional tests were included in the test matrix to determine the degree of repeatability over the range of the test conditions chosen. Variation in the repeatability of these two tests must be smaller than effects from changes in the significant independent variables to enable valid conclusions to be made from the data. The final two tests included in the fundamental rub interaction test program were chosen after the first ten tests were completed. The first of these, test 11, was used to replicate test 6 of the statistical test matrix because excessive speed drop occurred during the original test and the second, test 12, was used to further explore a region of high rub energy in which ignition of the titanium blade was thought to have occurred during the ten-test series. Table I shows the test matrix for the first twelve tests.

4.4 METHOD OF TEST

Rub tests were conducted in accordance with the sequence and test conditions established in the statistically designed experiment. The Feltmetal® fibermetal specified for the test was cut to size, cleaned, primed and coated with epoxy. The accompanying disk O.D. seal surface was grit blasted, cleaned and primed. The fibermetal abradable was bonded to the disk, cured and final machined to obtain the correct abradable thickness. This assembly was balanced and installed in the dynamic abradability rig. The blade was processed as explained in section 4.2.2 to provide six high temperature, high response thermocouples on the back face of the blade. For tests requiring strain gages the gages were cemented to the base of the blade prior to cementing the thermocouple leads in place. The rub specimen was then installed in the rig mounting fixture and the lead wires connected to the conditioning circuits feeding the oscillograph.

The start of the specified incursion depth was set by moving in the blade/holder/carriage assembly until the disk just touched the blade. The disk was then removed from the rig and carriage assembly was accurately moved in the specified incursion depth. With the carriage at this position the limit switch that triggers the pneumatic carriage withdrawal piston was

moved in until it would be actuated by the carriage. This setup ensured that the scheduled interaction depth would be obtained. In the past this has been difficult to achieve, especially for tests having high incursion rates and shallow depths.

A rheostat was used to control the drive motor for the carriage micrometer-feed system to achieve the predetermined incursion rate. Calibration of the feed system was accomplished prior to each test using the oscillograph. A certified time code generator provided timing lines every 0.001 seconds on the oscillograph trace. The feed system was used to move the carriage assembly through the previously set incursion depth and the start and stop of motion was indicated on the oscillograph by a displacement transducer. The rheostat was then adjusted to achieve drive motor speed required for the desired incursion rate.

The disk was then bolted to the drive spindle and two optical pyrometers were mounted to view the disk abrable surface at the 30° and 180° positions after the rub zone. Each unit was positioned using an external light source to set the correct focal length.

The timing interval between speed readings was set on the oscillograph using the time code generator. Selection of the timing interval was made to obtain the optimum number of speed readings for each test. The speed reading intervals varied from 0.1 seconds to 2 seconds, corresponding to the test duration range of 2 seconds to 400 seconds.

The debris catcher was set in place after all rig adjustments and calibrations were completed. The catcher consisted of a flat plate coated with petroleum jelly in which the particles could easily penetrate and not be blown away by disk windage. This form of particle entrapment could be easily transferred to slides or filtered for size distribution analysis.

A television camera and associated lighting was set up and connected to a video tape recording system to document each test. In addition, high speed motion pictures were taken for several selected tests. When the lighting requirements interfered with pyrometer response shielding was provided.

Just prior to test start a thorough pre-test check list was followed. All test instrumentation and settings were checked, including those required to operate the rig. The turbine air pressure was increased slowly to bring the disk to speed while the rig bearing system was monitored for temperature and vibration. After setting the test speed a windage plus friction resistive torque was measured. The test was then conducted following a set procedure and ended when the carriage was withdrawn by the pneumatic piston, after which the rig was stopped.

During initial Task I testing the turbine drive system was set in the ungoverned operation mode for the test in order to avoid over-torquing the optical torque meter. Prior to conducting test 6 this type of operation was satisfactory as the speed drop never exceeded 11.5%. During test 6, however, high rub torque was encountered which completely stalled the rotor near the end of the incursion. Since the observed rub torque at the desired test speeds had always been substantially less than the 1.1 Nm torque meter limit, subsequent tests were programmed to be run governed to assure that test rub velocities would be maintained.

Operation of this rig has a particular windage plus friction resistive torque associated with each speed level. To accurately measure rub energy the value for this torque was required for each test speed. Prior to starting Task I testing a representative disk and blade assembly was operated in close proximity, without rubbing, over the applicable speed range. A windage plus friction torque vs. speed curve was generated and is shown in Figure 8.

4.5 FUNDAMENTAL RUB INTERACTION TESTS

Each of the twelve Task I Fundamental Rub Interaction Tests were conducted as described in Section 4.4. Subsequent to testing the magnetic tape TV records were reviewed, wear measurements were taken on the blades and abradable material and the hardware was subjected to metallographic analysis.

The review of the TV records produced a synopsis of the visual activity during each test as related below. After each test number title the test conditions are listed in an abbreviated form in the following sequence: incursion rate, rub velocity, blade thickness, rub depth, abradable density, and test duration.

Test 1 (i = .25 mm/sec, v = 213 mps, b = 1.78 mm, δ = 1.0 mm, ρ = 19% — 4 sec)

An intense glow and shower of sparks was visible during the entire test. The glow and sparking was constant but did vary in intensity. The recorded blade temperature rose continually through the test reaching a maximum of 1220°K.

Test 2 (i = .0025 mm/sec, v = 213 mps, b = .53 mm, δ = 0.5 mm, ρ = 19% — 3 min, 20 sec)

Extremely light intermittent sparking and even more intermittent blade tip glowing was visible during the test. The peak blade temperatures were approximately 810°K for most of the test. Just prior to the end of the test, however, the intermittent temperature peak reached 1115°K.

Test 3 (i = .25 mm/sec, v = 152 mps, b = .56 mm, δ = 0.5 mm, ρ = 16% — 2 sec)

Blade tip glowing started almost immediately upon contact. The glow increased rapidly in intensity becoming so bright it masked over any sparking that occurred. The temperature recorded rose continuously reaching a maximum of 1420°K.

Test 4 (i = .025 mm/sec, v = 213 mps, b = 1.74 mm, δ = 0.5 mm, ρ = 16% — 20 sec)

Intermittent sparking that seemed to glow was visible from the test start. This condition continued for approximately 16 seconds into the test. At this time the sparking began glowing intensely but remaining intermittent for the remainder of the test. The maximum temperatures recorded by the blade thermocouples showed a peak of 920°K 5 seconds into the test, settled down to 700°K through the middle of the test and, beginning at 15 seconds into the test started rising, reaching 1100°K just before the end of the test.

Test 5 ($i = .25$ mm/sec, $v = 213$ mps, $b = 1.74$ mm, $\delta = 1.0$ mm, $\rho = 19\% - 4$ sec)

An intense glow with sparking was visible for the first half of the test, dying down to a very light glow and light sparking for the remainder. The highest recorded temperature of 1105°K occurred 0.6 seconds into the test, following which it dropped off to 935°K and then rose slowly to 990°K , at the end of the test.

Test 6 ($i = .025$ mm/sec, $v = 152$ mps, $b = .51$ mm, $\delta = 1.0$ mm, $\rho = 19\% - 40$ sec)

Light sparking and light blade tip glowing were visible at the test start, remaining relatively constant but varying in intensity for the first 25 seconds. At that time the blade tip glow became very intense remaining at that level for 13 seconds. At that point the disk, which had been continuously decelerating throughout the test, stopped rotating altogether (38 seconds into the 40 second test). The maximum recorded temperature was 1480°K .

Test 7 ($i = .0025$ mm/sec, $v = 152$ mps, $b = 1.75$ mm, $\delta = 1.0$ mm, $\rho = 16\% - 6$ min, 40 sec)

No visible indication of a rub was evident until approximately 20 seconds into the test, at which time extremely light sparking was visible. At approximately one minute or 0.15 mm inches into the rub an intense glow was noted on the blade but there was no increase in the amount of sparking. This glowing occurred periodically, every 10 to 20 seconds, for the duration of the test as did the light sparking. The maximum recorded temperature during one of the intermittent peaks was 1270°K .

Test 8 ($i = .25$ mm/sec, $v = 213$ mps, $b = .56$ mm, $\delta = 1.0$ mm, $\rho = 16\% - 4$ sec)

A moderately intense glow with very little sparking was visible during the entire test. The glow grew in intensity for the first three seconds, then dying down for the last second. At the height of the glow, 1.3 seconds into the rub, the maximum temperature recorded was 1180°K .

Test 9 ($i = .25$ mm/sec, $v = 152$ mps, $b = 1.75$ mm, $\delta = .5$ mm, $\rho = 19\% - 2$ sec)

Sparking and glowing of the blade tip started immediately upon contact. The glowing increased in intensity very rapidly becoming so bright that it blotted out the blade and some of the adjacent disk. The recorded temperature began oscillating 1.2 seconds into the rub but continued rising steadily to a maximum of 1690°K at the end of the test.

Test 10 ($i = .0025$ mm/sec, $v = 213$ mps, $b = 0.52$ mm, $\delta = 0.5$ mm, $\rho = 19\% - 3$ min, 20 sec)

Sparking was extremely light and intermittent during the entire test. No blade tip glowing was noted. The maximum temperature recorded during an intermittent rub was 770°K .

Test 11 ($i = .025$ mm/sec, $v = 152$ mps, $b = 0.56$ mm, $\delta = 1.0$ mm, $\rho = 19\% - 40$ sec)

Sparking, followed quickly by blade tip glowing was noted at the test start. The blade tip glow and sparking reached a peak approximately 2 seconds into the rub as the recorded blade temperature reached a maximum of 1055°K . For the remainder of the test intermittent blade tip glowing and sparking of slightly less intensity was noted. The maximum temperature recorded during the intermittent operation varied between 1000°K and 1035°K .

Test 12 ($i = .25$ mm/sec, $v = 152$ mps, $b = 0.61$ mm, $\delta = 1.0$ mm, $\rho = 19\% - 4$ sec)

Very intense glowing and sparking was visible almost immediately upon contact, wavering slightly in intensity and lasting the entire test. The recorded temperature rose quickly to a maximum of 1700°K in 0.8 seconds and then oscillated rapidly, as low as 1370°K , the remainder of the test.

4.5.1 Wear Analysis

A shadow-graph technique, enlarging the seal or blade rub surface between 20X and 30X, was used to document post test seal and blade wear. In cases where the rub mechanism changed from a wear to transfer phenomenon, covering the entire blade tip, the original wear surface was located by dislodging a small area of transfer from the blade tip. Also, when necessary, the shadowgraph measurements were substantiated by sectioning and mounting the hardware for photomicrographs. In most transfer tests the transferred wear material was not evenly deposited on the blade tip in either the axial or circumferential direction. To account for this a representative section was taken through the 6.35 mm (.250 inch) blade width and the profile of the transfer height was measured and averaged. Photomicrographs of these cases were required because the shadowgraph technique identifies only the highest points of transfer. In many tests both the blade and seal rub surfaces were either rough, ridged or canted. These conditions required taking many measurements which were averaged.

The basic blade and seal wear measurements for the Task I tests are summarized in Table II. Included in the table are "measured incursion", which uses the measured values of seal and blade wear and transfer, and "carriage incursion", which was determined from accurate time/carriage travel traces for the test. Comparing the two numbers shows that agreement was achieved to within 0.1143 mm (0.0045 inches). This discrepancy can be accounted for by measurement errors and the identification of the exact time when rubbing began in each test. In particular, local high spots, which were used to set the test start point, were measured to be as much as 0.076 mm (0.003 inches) on some abrasable rotors which accounts for a significant part of the discrepancy in some tests.

Wear results for the Task I tests are summarized in Table III. The data are presented in terms of two parameters, "Adjusted Blade Wear Plus Transfer" and "Volume Wear Ratio". The "adjusted blade wear" term normalizes all wear to a 0.508 mm (0.020 inch) thick blade based on volume of blade material lost and directly adds in the average height of transfer on the blade tip. This factor was selected to provide an all inclusive term which contained both blade wear and transfer, which reflected the overall severity of the rub and which would be useful as a dependent variable in the statistical analysis of the data.

"Volume Wear Ratio" (VWR) has long been used as an indication of the abrasability of a blade/seal system; the smaller the number the more abrasable the system. The volume wear ratio is the volume of material worn off the blade tip during the rub divided by the volume of the seal material grooved out by the blade. Under ideal rub conditions the blade grooves the seal without glazing and the majority of wear occurs on the seal, resulting in a very low VWR. Under other operating conditions high rub energy results in localized plasticity at the rub interface which produces a thin glazing on the seal rub surface. Continued rubbing at

these conditions does not necessarily disrupt the glaze which continues to thicken at the expense of blade wear, resulting in the high VWR's. Under still other conditions the plasticity at the rub interface can preferentially occur on the seal and when the blade tip is cooler it becomes a ready depository for transfer of softened abradable material. This change in mechanism makes it difficult to clearly define the VWR when the blade tip is covered with transfer. In this program the VWR was calculated as though transfer initiated at the end of the planned incursion. Thus, the measured groove depth was reduced by the height of the transfer for the calculation of VWR. This assumption yields a lower limit value of VWR for the tests in which transfer occurred.

Volume wear ratios have been calculated on high compressor seal systems in low time audit engines (approximately 10 hours of operation). Depending on the density/tensile strength of the seal material and engine operating conditions rubbed seal appearance varied from a clean to a glazed rub. The VWR's for these situations for Feltmetal® seals varied from 1.0×10^{-4} to 10.0×10^{-4} . The values of VWR shown for the 12 fundamental rub interaction tests in Table III generally are within the range of that measured for Feltmetal® engine seal systems and their physical appearance is also the same as noted on the engine seals. The two exceptions are tests 9 and 12 which exhibited a completely different rub mechanism with correspondingly high VWR's. Extremely high interface temperatures were experienced in these tests soon after the interaction began. In addition, examination of the torque data indicated that when interface temperatures reached 1480°K during the titanium blade rub its strength was reduced to nearly zero. This situation allowed easy removal of the soft blade tip by the cooler, stronger seal surface. The results of this rub mechanism have been observed with Feltmetal® in isolated stages of service engines, evidenced by excessive blade wear and associated heavily glazed/transferred seals. The good agreement between the rig and engine data gives credence to the use of single blade/rotating abradable testing to simulate engine rub behavior with fibermetal. Further work is required to identify the causes of the occurrence of the severe wear and high energy rub mode and to develop improved seal systems for its elimination.

4.5.2 Metallographic Analysis

Metallographic analysis was completed on selected blades and all abradable seals from Task I testing to identify changes in material structure and to determine the presence and constituents of any material transfer. Figures 9, 10, 11 and 12 show post test cross sections of all twelve Task I test seals. Visual inspection of the abradable rub surfaces showed that they varied from a cleanly machined to a highly smeared or glazed surface as shown in Figure 13. The representative cleanly rubbed surface in this figure was the fibermetal from test 10 and representative highly glazed surface shown was from test 9. These figures clearly show the difference in surface densification between the clean rub and glazed rub surface. In addition, X-Ray Emission Spectroscopy (XES) analysis revealed the presence of titanium material on the glazed seal surface of test 9, transferred from the titanium blades. Glazing or rub surface densification was noted on the seals from all tests conducted at the 0.25 mm/s incursion rate. At lower incursion rates the densification was noted on the rub surface of seals run at only one other test condition; test 6 and its repeat, test 11, run at the 0.025 mm/s incursion rate. Test 6 exhibited densification of the same magnitude as the high incursion rate tests while test 11 had less. During the running of test 6 the rub torque had gradually increased in value until it reduced abradable disk seal speed to zero rpm. Low speed opera-

tion had been found, from prior testing, to promote densification at the seal surface; thus the highly glazed condition was expected. Test 11 was a repeat of test 6 except that provisions were made to minimize the speed drop. The resulting surface glazing was not as severe as test 6 but was more extensive than the other 0.025 mm/s tests and all the 0.0025 mm/s tests.

Wear measurements of the twelve Task I tests indicated that tests 1, 4, 5, 8, 11 and 12 exhibited transfer on the blade tips at the end of the test. Of these, four (tests 1, 5, 8 and 12) were tests conducted at .25 mm/s incursion rate, two (tests 4 and 11) were conducted at .025 mm/s and none were conducted at .0025 mm/s. The test 11 blade was chosen to be sectioned and metallurgically examined as a representative transfer specimen. XES analysis identified the bulk of the built-up material as Hastelloy X fibermetal seal material and the dark particles mixed in as SermeTel AP-1, the cement used in instrumenting the blades. Figure 14 shows a transverse section of test 11 blade tip. This particular section shows the transfer increasing from nothing at the leading edge to a thickness of 0.1 mm at the trailing edge. The transfer in each test was extremely rough and wavy with gross striations in the direction of the rub as vividly shown in Figure 15, a top view of the blade from test 1.

Metallographic examination was also used to verify rub interface temperatures above 1300°K and determine if any evidence of titanium burning was present. This was accomplished by studying the microstructure of the blade tip. The normal AMS 4916 titanium microstructure is a blocky α grain structure below temperatures of 1300°K, which is the $(\alpha + \beta)/\beta$ transus temperature. Prior temperatures above 1300°K are identified by the presence of α -platelets which are coarse when the titanium is cooled slowly through the transus temperature and take on a fine martensitic appearance when the titanium is rapidly cooled. Areas such as the blade tip that reach temperatures well in excess of 1300°K have many elongated α -platelets. Evidence of titanium ignition and burning, if any was present at the rub interface, would be identified by cratering of the surface and by the presence of titanium oxide and alpha case or platelet structure.

A study of the TV monitor and blade thermocouples indicated that rub interface temperatures during test 9 had approached ignition conditions, although any evidence of possible burning/melting on the blade tip surface had been removed by subsequent rubbing. The metallographic examination of the blade identified the presence of many fine elongated α -platelets at the rub surface in a martensitic type alignment (Figure 16), indicating that the blade tip temperature had been well in excess of 1300°K and was subsequently rapidly cooled. The rub testing for this program incorporated a pneumatic carriage/blade retraction system which provided for rapid withdrawal and thus rapid blade cooling at test completion. No evidence of recast structure or pitting which are indicative of melting or burning was noted but the extreme blade wear together with the α -platelet structure suggested the possibility of incipient ignition of the blade.

A metallographic analysis was also conducted on the blade from test 12 which had been chosen to provide a test point that approached the severity of test 9. Visual observations made during and after test 12 substantiated the postulation that this test would provide additional data in the high rub energy, severe wear regime. The maximum temperature recorded by a blade thermocouple during the test was 1720°K. Post test blade wear measure-

ments identified that two distinct wear modes had occurred during the test. One fourth of the blade wore 0.323 mm, grooving the seal 0.757 mm. The remaining three fourths of the blade averaged 0.787 mm wear while grooving the seal only 0.153 mm. Figure 17 is a section through the blade showing both the high and low wear areas. The lesser wear area is covered with transfer containing, as in test 11, Hastelloy X seal material and SermeTel AP-1 cement, used to hold thermocouples on the back side of the blade. The presence of elements of SermeTel AP-1 in the transfer suggest that they were first transferred to the rotating disk from the back side of the blade and subsequently transferred from the rubstrip to the blade tip. Again, as in test 9, the microstructure of blade 12 indicated that the tip had exceeded 1300°K but no evidence of melting remained.

4.6 DATA REDUCTION AND ANALYSIS

As the Task I tests were being completed, data reduction was initiated to determine total rub energy, interface temperature, and the heat split between blade, abradable and wear debris. Upon completion of the Task I tests, energy and wear parameters were selected for statistical analysis and correlation. The specific objective of the statistical analysis was to determine the linear main effects and primary interactive effects of the independent variables on rub energy and wear. Upon conclusion of the analysis a plan was developed and recommendations made for tests to extend the range of the investigation, as called for in Task III. Details of the analysis performed and the results and conclusions of the work are presented in the following paragraphs.

4.6.1 Total Rub Energy

As developed in Section 4.2.1, the rub torque and the total rub energy are determined from equations 4 and 5 which are repeated here:

$$\tau_{\text{rub}} = \frac{1}{\Delta t} \int^{\Delta t} \tau_{\text{turbine}} dt - \frac{1}{\Delta t} \int^{\Delta t} \tau_{\text{windage} + \text{friction}} dt - J \frac{\omega_{t+\Delta t} - \omega_t}{\Delta t} \quad (4)$$

$$\tilde{q}_{\text{total}} = \frac{1}{\Delta t} \int^{\Delta t} \tau_{\text{turbine}} \cdot \omega \cdot dt - \frac{1}{\Delta t} \int^{\Delta t} \tau_{\text{windage} + \text{friction}} \cdot \omega \cdot dt - \frac{J}{2\Delta t} (\omega_{t+\Delta t}^2 - \omega_t^2) \quad (5)$$

Selection of the integration time, Δt , for each test was made in such a manner as to resolve the variations in rub energy visible in the oscillograph traces. In each case an even multiple of the time between speed readings was used to enable precise values of speed to be acquired for the last term in the equation. Integration of the first term made use of piecewise linear integration of the oscillograph turbine torque trace together with the average value of rotor speed over the time increment, speed changes being less than 0.5% for any integration. Integration of the second term, employed the average rotor speed and the windage and friction curve (Figure 8) generated in the zero-rub tests described in Section 4.4. In making this calculation, the windage calibration check taken just prior to each test was used to adjust the level of the windage and friction for minor variations. Since repeated windage tests showed the variation of windage and friction with speed to be highly repeatable, this procedure permitted acquisition of accurate rub torque and total energy values without

time consuming steps to resolve static friction effects which made exact zeroing of the torquemeter very difficult. To facilitate calculation and plotting of the rub torque and total rub energy, a small computer program was written which performed these operations, calculated the time average value of total heat load for use in the statistical analysis, and provided plots of the results as a function of time throughout the test. These plots are presented for the Task I tests in Figures 18 through 25, and 29 through 31. Tabulated values of the peak total rub energy which occurred during the test and the average total rub energy for the test are presented in Table IV for all of the Task I tests.

4.6.2 Rub Heat Into the Blade

Blade heating and interface temperature were computed from the blade thermocouple data using a simple, one-dimensional, fin model as shown schematically in Figure 26. The governing differential equation for heat transfer in the blade is given by:

$$\frac{\partial^2 T}{\partial y^2} + \frac{G C_p}{k} \frac{\partial T}{\partial y} - \frac{hP}{kS} (T - T_a) = \frac{1}{\alpha} \frac{\partial T}{\partial t} \quad (7)$$

where T is the local blade temperature, y is the distance from the rub interface, G is the mass flux of blade material due to wear at the interface, C_p , k and α are, respectively, the specific heat, thermal conductivity and thermal diffusivity of the blade material, h is the convection coefficient on the surface of the blade, P and S are, respectively, the perimeter and cross-sectional area of the blade and T_a is the ambient air temperature surrounding the blade. An order of magnitude study of the terms in this equation showed that, for the wear rates experienced in this program, the influence of the wear induced convective term was negligible. Consequently, this term was dropped which permitted ready solution of the equation with a transient heating boundary condition at the blade tip using Laplace transforms and superposition. The Laplace transform solution for a step change in heat input, Δq , at the blade tip, assuming ambient initial temperature and ambient temperature far from the blade tip, yields:

$$T(y, t) = T_a + \Delta q f(h, y, t) \quad (8)$$

$$\text{where } f(h, y, t) = \frac{1}{2 k S \sqrt{\nu}} \left\{ e^{-\sqrt{\nu} y} \operatorname{erfc} \left(\frac{y}{2 \sqrt{\alpha t}} - \sqrt{\nu \alpha t} \right) - e^{\sqrt{\nu} y} \operatorname{erfc} \left(\frac{y}{2 \sqrt{\alpha t}} + \sqrt{\nu \alpha t} \right) \right\}$$

$$\text{and } \nu = \frac{hP}{kS}$$

Applying superposition over n incremental time steps, each of duration Δt , yields:

$$T(y, n\Delta t) = T_a + \sum_{k=0}^{n-1} (q_{k+1} - q_k) \cdot f[h, y, (n-k) \Delta t] \quad (9)$$

where $q_{k+1} - q_k$ is the $(k+1)^{th}$ step change in heat input.

Upon rearrangement, the instantaneous heat load on the blade tip is given by:

$$q(n\Delta t) = q[(n-1)\Delta t] + \frac{[T(y, n\Delta t) - T_a] - \sum_{k=0}^{n-2} (q_{k+1} - q_k) \cdot f[h, y, (n-k)\Delta t]}{f[h, y, \Delta t]} \quad (10)$$

In order to solve equation (10) for heat load to the blade tip, numerical integration was used. For each time step starting at the outset of the test, the value of temperature at the end of a time step of the thermocouple closest to the tip was used to calculate the change in heat load at the beginning of the time step. The tip heat loads so calculated were then stored and used in the summation term for later steps. The value of h required for the calculation was taken from the curve presented in Figure 6 which was obtained experimentally as explained in Section 4.2.5. Since the distance y from the tip to the thermocouple position varied through the test with blade wear and/or transfer, an estimate of wear rate was required for the solution. To this end it was assumed that all wear occurred first followed by transfer, if any, and that the wear and transfer rates were both constant and equal to each other. This assumption was modified for those tests that experienced extremely high interface temperatures. The occurrence of sustained high temperatures produced blade tip softening and the subsequent wear rate during this period was assumed equal to the incursion rate. In addition to blade heating, interface temperature was computed using the blade heat transfer model. Equation (8) evaluated at $y = 0$ yields the interface temperature directly:

$$T(0, n\Delta t) = T_a + \sum_{k=0}^n (q_{k+1} - q_k) \cdot f[h, 0, (n-k)\Delta t] \quad (11)$$

The heat load terms required for the calculation are the same ones generated in the solution of equation (10).

To facilitate the data analysis, a computer program was written to perform the calculations, to calculate the time average value of blade heat load for use in the statistical analysis, and to plot heat load to the blade tip and interface temperature as a function of time through the test. These plots are included in Figures 18 through 25 for the Task I tests except those conducted at an incursion rate of 0.0025 mm/s.

As a check of the assumptions involved in the analysis for these tests, a second computer program was written to calculate blade temperature at any distance from the blade tip as a function of blade tip heat load. Input of the calculated heat loads was then used to predict blade temperatures at locations of other blade thermocouples. The resulting temperature/time curves were found to agree with the actual measured temperatures to within 10%.

The method of determining the heat load on the tip and the blade tip temperature, as described above, is very sensitive to a steep gradient in the input thermocouple data. To adequately represent a quickly rising thermocouple response requires recording a large number of temperature points. The cyclic nature of the thermocouple response for the slow incursion rate (0.0025 mm/s) tests, as typified by Figure 27, made continuous analysis of thermocouple data from all three of these tests (2, 7 and 10) untenable. To reduce data reduction time with little loss in accuracy, an averaging method was used to determine both heat load on the blade tip and interface temperature. Each thermocouple data cycle was characterized, based on its peak temperature, as one of two or three typical cycles. Input of these typical cycles into the blade heat transfer model then provided the interface temperature and the average heat load on the blade tip for each characteristic cycle. The thermocouple temperature cycles shown in Figure 28 for test 7 are representative of the data cycles recorded for that test. The value of average blade heat load for the entire test was then determined by summing the contribution of each cycle as follows:

$$\bar{q} = \frac{\sum_{i=1}^j n_i \bar{q}_i \Delta t_i}{\text{Total test time}} \quad (12)$$

where: j is the number of different characteristic cycles used

n_i is the number of i^{th} characteristic cycles in the test

\bar{q}_i is the average heat load for the i^{th} characteristic cycle

Δt_i is the duration of the i^{th} characteristic cycle

To check the accuracy of this method, test 7 data was reduced on a continuous basis, and agreed well with the results of the above approach (blade heat load results shown in Figure 28 compare with the averaged results shown in Figure 30) for the continuous approach.

Interface temperature cycles shown in Figures 29, 30, and 31, for three slow incursion rate tests (0.0025 mm/s), are representative of the characteristic thermocouple cycles from which they were evaluated. The number of thermocouple data cycles at each characteristic level and the time of occurrences of each cycle is also shown in these figures and is used for determining the average value of heat load on the blade tip for each test.

Tabulated values of the maximum interface temperatures which occurred during each test as well as the peak and average blade heat load are presented in Table IV for the Task I tests.

4.6.3 Rub Heat Into the Disk and Debris

The difference between the total heat load on the rub zone and the heat load on the blade tip is the heat conducted into the disk and that carried away by both the blade and seal debris. A method of obtaining the heat load due to each of these components was established.

The heat lost to blade debris was determined by calculating the amount of heat stored in the material that is worn from the blade tip, as follows:

$$q_{bd} = \frac{1}{t} \int_0^t G C_p (T_i - T_a) dt \quad (13)$$

where t is the test duration, G is the mass flux of blade material due to wear at the interface, C_p is the specific heat and T_i is the interface temperature.

The highest value of heat loss to blade debris for the task I tests was calculated for test #9 to be 5.67 watts or less than 1.7% of the total heat load on the rub zone.

Because the seal surface is porous and the seal material removal process involves subsurface fracture of the fiber bonds, the instantaneous contact area between blade tip and the seal material is only a small fraction of the blade tip area and the bulk temperature of the seal debris is significantly less than the interface temperature. For this reason, the approach selected for determining the heat to the disk and the heat to the seal debris employed both a first law analysis of the total system and a transient conduction analysis of the disk surface. From the first law analysis it is seen that the combined heat to the disk and the seal debris is the difference between the total rub energy and the sum of the heat conducted into the blade and that lost in the blade debris. Measurements of the seal surface temperature at two angular positions provided the basis for calculating the heat being conducted into the disk. Due to the low conductivity of the abrasible material, optical pyrometry, as discussed in Section 4.2.3, was the only viable technique for measurement of the abrasible surface temperature.

In order to determine the heat flow into the disk from the abrasible surface temperature data, simple one-dimensional transient heat conduction into a semi-infinite body was utilized. Because of the low thermal diffusivity of the Feltmetal® ($\sim 2.5 \times 10^{-7} \text{ m}^2/\text{s}$) the penetration of heat into the abrasible in one revolution of the disk is only about 0.13 mm. At the same time, the analysis shows that the surface temperature effect due to rub energy, which is a maximum just where the abrasible leaves contact with the blade, decays to 15 percent of this maximum in one half a revolution and to only 4 percent of the maximum in a full revolution just due to conduction into the abrasible. The conclusion then is that within a few mils below the surface the abrasible undergoes a relatively steady temperature rise which is unaffected by the periodic effect of the disk rotation and that the surface temperature measurements on the disk at 180° position relative to the rub are representative of the temperature rise of the disk surface with the periodic effects averaged out.

As shown in Table V surface temperatures were obtained in only three tests. During all of the other tests the rub surface temperature remained below the threshold limit of the pyrometers. It is interesting to note, however, that these three tests, (tests 1, 3 and 9) were among the highest in average total rub energy and interface temperature and were the highest tests in peak total rub energy.

In order to estimate the average heat into the disk, the pyrometer data at the 180° position was assumed to be the result of uniform one-dimensional constant heating on the periphery of the disk (i.e. the periodic effects of disk rotating were averaged out as explained above). The thickness of the abradable was taken as its final value and the disk under the abradable was assumed to remain at its initial temperature. Based on these assumptions, Carslaw and Jaeger (ref. 7) gives the temperature in the abradable as:

$$T = T_0 + \frac{q_0 x}{k} - \frac{8q_0 \delta_a}{k \pi^2} \sum_{n=0}^{\infty} \frac{(-1)^n}{(2n+1)^2} e^{-\frac{\alpha(2n+1)^2 \pi^2 t}{4\delta_a^2}} \sin(2n+1) \frac{\pi x}{2\delta_a} \quad (14)$$

where T_0 is the initial disk temperature, q_d is the heat flow into the abradable, x is the distance from the abradable bond interface, δ_a is the abradable thickness, t is the duration of rub heating and k and α are, respectively, the thermal conductivity and thermal diffusivity of Feltmetal®. Rearranging and solving gives the average heat into the disk.

$$q_d = (T_s - T_0) \frac{k}{\delta_a} \left[1 - \frac{8}{\pi^2} \sum_{n=0}^{\infty} \frac{1}{(2n+1)^2} e^{-\frac{\alpha(2n+1)^2 \pi^2 t}{4\delta_a^2}} \right] \quad (15)$$

where T_s is the measured surface temperature. Applying this equation to the Task I pyrometer and wear data yields the disk conduction results shown in Table V.

As a final step, the heat lost in the wear debris is estimated by summing the remaining component terms (heat to the blade and blade debris, heat to the disk and convection from the disk surface) and subtracting the sum from the total rub energy. For this computation the heat transfer coefficient on the disk surface was estimated to be 600 w/m² °K for the 152 mps rub velocity and 770 w/m² °K for the 213 mps rub velocity using correlations given by Kreith (ref. 8) for heat transfer from rotating disks and cylinders. The resulting numbers for tests 1, 3 and 9 are reported in Table V. The occurrence of negative temperatures for tests 3 and 9 is indicative that additional energy was being supplied to the rub interface which was not accounted for in the total rub energy measurement. In view of the very high interface temperature (1583°K for test 3 and 1747°K for test 9) and the high heat of combustion titanium alloys it appears reasonable that this excess energy is coming from oxidation of the titanium.

As can be seen from the wide variation in calculated rub debris temperature and the lack of correlation of this temperature with either the interface temperature or the abradable surface temperature at the 30° position, the accuracy of the pyrometer data and data reduction procedure are inadequate to permit resolution of the fraction of the rub energy going into the seal debris. While the total rub energy and blade heating have been obtained using quite accurate measuring techniques and data analysis procedures, significant improvements in both instrumentation and data analysis will be required to permit reasonably accurate determination of heat lost in the abradable debris.

4.6.4 Statistical Analysis of the Data

One of the primary objectives of the program was to correlate rub energy and wear parameters with the independent variables. In order to accomplish this it was necessary to select parameters which were single valued for each test and which represented the important characteristics of the energy or wear for that test. The following parameters were selected for the analysis:

Average Total Rub Energy	— The time average of total rub energy for the test
Peak Rub Energy	— The maximum value of rub energy which occurred during the test
Average Heat to the Blade	— The time average of blade heat load for the test
Peak Heat to Blade	— The maximum value of blade heat load which occurred during the test
Maximum Blade Temperature	— The maximum value of interface temperature which occurred during the test
Adjusted Blade Wear Plus Transfer	— Wear plus transfer computed as described in Sec. 4.4.1

To develop the prediction equations for each of these dependent parameters with the independent test variables, linear regression analysis was employed using the principle of least squares. Prior to performing a regression analysis it is necessary to formulate a mathematical model expressing the ways in which the independent variable might be functionally related to the dependent variable. The general model takes the form:

$$\hat{Y} = A + B_1 X_1 + B_2 X_2 + \dots + B_i X_i \quad (17)$$

where \hat{Y} is the predicted value of the dependent variable, the X 's are specified functions uniquely related to the independent variables and the values of the A and the B 's are to be determined by the regression analysis to achieve the best fit of the data to the model, based on the least squares criterion. Figure 32 is a generalized illustration. The term to be minimized in the least squares method is:

$$v^2 = \sum_{i=1}^N (Y_i - \hat{Y}_i)^2 \quad (18)$$

where N is the sample size.

Upon completion of the regression the multiple correlation coefficient, which is defined by the equation:

$$r = \sqrt{\frac{\sum (\hat{Y}_i - \bar{Y})^2}{\sum (Y_i - \bar{Y})^2}} \quad (19)$$

where $\bar{Y} = \frac{1}{N} \sum_{i=1}^N Y_i$ is computed. This quantity shows the degree of association between Y and X as represented by the model with a value of 1.0 being a perfect fit. Its square, the coefficient of determination (r^2), is a measure of the proportion of the variation of the dependent variable which is accounted for by the model. Since the correlation coefficient can rather obviously be increased for a given set of data by increasing the number of terms in the model, additional statistical tests must be applied to determine the confidence level associated with the result. The final statistical quantity calculated is the standard error of estimate (SEE) which is a measure of the magnitude of the error in predicting the dependent variable and is computed by the equation:

$$SEE = \sqrt{v^2 / (N - K)} \quad (20)$$

where K is the number of degrees of freedom of the model (i.e. the number of coefficients, $A + B_i$'s). In the initial statistical analysis of the data a simple linear dependence upon each of the independent test parameters was assumed for the X 's in equation (17). Inspection of the results indicated, as would be expected from past experience in abrasability testing, that a logarithmic dependency upon incursion rate would provide better correlation. In addition, since one of the primary objectives was to establish the significance of the several independent variables, it was decided to normalize each one so as to represent the test range by the band -1 to +1. The resulting transformed variables are shown in Table VI and the corresponding form of the model used becomes:

$$\begin{aligned} \hat{Y} = & A + B_i \frac{\log i \text{ (mm/s)} - \log 0.025}{\log 10} + B_\delta \frac{2\delta \text{ (mm)} - 1.5}{0.5} + B_V \frac{2V \text{ (mps)} - 365}{61} \\ & + B_b \frac{2b \text{ (mm)} - 2.29}{1.27} + B_\rho \frac{2\rho \text{ (\%)} - 35}{3} \end{aligned} \quad (21)$$

or, in terms of the normalized independent variables:

$$\hat{Y} = A + B_i i' + B_\delta \delta' + B_v v' + B_b b' + B_\rho \rho' \quad (22)$$

Since the ranges of the variables were chosen, as much as possible, to be representative of engine rubs, use of the normalized formulation allows the relative influence of each of the independent variables upon the dependent variable to be seen through direct comparison of the magnitude of the coefficients in the regression expression. The sign of each coefficient indicates the direction of the trend.

The regression analysis for each of the rub energy and wear parameters was carried out in two different ways for the Task I data. The results of these analyses are presented in terms of the regression coefficients in Table VII and as plots in Figures 33 through 43. The second regression analysis was done because, as a result of the rub energy data being recorded continuously, it was recognized that additional data points could be gained by treating the first half of a 1.0 mm incursion test as an 0.5 mm incursion test. While this approach was able to provide a second correlation for the energy and temperature parameters, it obviously could not be used for correlation of the wear data. In the tabulated regression coefficients presented in Table VII the starred (*) items indicate that these variables are statistically important at the 95% confidence level. The question mark (?) terms are marginally important at that confidence level. The remaining terms are of little importance in explaining the variation in the dependent variables, at least for the models selected.

In addition to the regression coefficients, statistics for each prediction model are presented in Table VII. Comparison of the coefficient of determination, r^2 , with standard "table" values which depend upon the number of test points and the number of degrees of freedom in the model, permits the significance of the correlation to be assessed. Since the table values, based on 95% confidence, are 56.9% for 11 test points and 30.6% for 17 test points it is evident that all of the correlations were significant with total rub energy being the best, blade heating in the middle and blade temperature and blade wear the poorest. A comparison of the standard error of estimate, S.E.E. with the repeatability error factor, σ , permits an assessment to be made of the cause of a high S.E.E. value. The σ values reported in Table VII were calculated from the replicated test pairs, test 1/test 5 and test 2/test 10. In the average total rub energy and peak heat to the blade correlations the high value of σ relative to S.E.E. together with the high r^2 indicates that most of the error is due to experimental error. The lower relative values of σ and/or lower r^2 values for the other two energy parameter correlations suggest that a greater number of tests might be useful for defining additional functional relationships to improve the correlation. The comparable values of σ and S.E.E. with lower values of r^2 suggest that basic effects, such as stability factors which govern the occurrence of transfer, may be lacking from the model and the data.

In general, the results of the statistical test plan and regression models are seen to be very successful. A ranking of the significance of the individual independent variables is presented in Table VIII. The numbers shown in the table are derived from the percent of variation of the dependent variables attributed to an independent variable as calculated from the coefficients in Table VII using the equation:

$$\Delta_i (\%) = 100X B_i / \sum_{j=1}^5 B_j \quad (23)$$

Throughout the correlations incursion rate is seen to be the strongest factor in the rub phenomenon. Disk rim speed and blade thickness are substantially lower in influence but still show a significant effect, the effect of disk speed on interface temperature and possibly blade wear being particularly noticeable. Incursion depth and abradable density were found to have minimal effect except for the influence of abradable density on blade wear. Of particular interest is the relatively minor change in the coefficients which resulted from including extra 0.5 mm data points from the deep rub tests. This rather large change in the sample size would have had a significant impact on the equations had the data been of lower quality. Examination of the interactive effects of two combined variables was completed, and none were found significant. It should be noted, however, that the lack of importance of these two-factor interactions may be due to an insufficient number of tests.

4.6.5 Summary of Task I Test Results

From the results of Task I tests the primary variable effecting rub energy and wear is seen to be incursion rate. The observed rub modes ranged from clean rubs with very low rub energy, relatively low blade tip temperatures and low blade wear for the 0.0025 mm/s incursion rate to high rub energy, extreme blade tip temperatures and high blade wear or transfer of seal material from the disk to the blade tip for the 0.25 mm/s incursion rate. At the intermediate incursion rate of 0.025 mm/s the blade wear was low but transfer occurred on both tests. At the high incursion rate (0.25 mm/s) tests either high wear or transfer or a combination of the two occurred on every test.

Rub velocity was found to be a significant factor in rub phenomena, although substantially less influential than incursion rate. The strongest dependency was seen in the effect of disk rim speed upon interface temperature where the regression analysis exhibited approximately 320°K higher peak temperatures for the 152 mps rub velocity than for the 213 mps rub velocity. Blade wear and transfer showed a corresponding increase with decreased rub velocity.

Blade thickness proved to be a significant term, of the same order of importance as rub velocity, but with the effect comparatively high in the rub energy terms and very low in the interface temperature and blade wear plus transfer terms. Since the wear term used blade volume rather than blade length, the regression equation yields less loss in blade length for the thick blades than the thin ones, for rub conditions which are the same in other respects.

Both incursion depth and abradable density produced no significant effects on rub energy or interface temperature but an increase in blade wear plus transfer was observed for the higher density abradable.

4.7 DETAILED INVESTIGATION OF SIGNIFICANT PARAMETERS

The objective of this final portion of the test program was to further explore the most significant parameters identified in the statistically planned, fundamental rub interaction tests and to extend the range of investigation, if possible, to include the effect of compressor steel blade materials and multiple blades. The high degree of confidence which was realized from the statistical test portion enabled all five Task III tests to be used to explore the effects of these two variables. Because of the high rub energy, interface temperature and wear which occurred at the high (.25 mm/s) incursion rate and low rub velocity condition (tests 9 and 12), emphasis was placed on determining the effect of blade material and number of blades on the rub phenomena at these conditions. In addition, two tests with compressor steel blade materials were selected at conditions corresponding to those in which seal material had transferred to the blade tips during initial testing to determine whether a change in blade material would affect the occurrence of such transfer. Because of the added information made possible by conducting the test to the deeper incursion depth all five tests were chosen to be run with a 1.0 mm maximum incursion depth. The resulting program, consisting of three tests run with Incoloy 901 blade material and two with multiple (3) 8-1-1 titanium blades, is presented in Table IX together with the Task I test array.

4.7.1 Energy Measurements and Test Methods

The methods employed to determine the energy dissipation and interface temperature and the test procedure for Task III testing were very similar to that for Task I. The variations are described as follows. High temperature thermocouple installations for Task I testing used a 0.05 mm thick layer of molybdenum sputtered to the titanium to prevent alloying of the platinum thermocouple leads with the titanium blade during resistance welding of the thermocouples to the blade. This method replaced the use of tack welded molybdenum foil which, in previous testing, exhibited a thermocouple survival rate of approximately 50%. As Task I testing progressed it was noted that thermocouple malfunctioning had been reduced to 7% using the sputtered molybdenum. Therefore, the number of thermocouples required to record temperature data could be substantially reduced. Figure 44 shows the Task III thermocouple locations; three per blade for the single blade tests and two per blade for the multi-bladed tests. Since verification of the thermal analysis was already carried out in reducing Task I data, the thermocouple location furthest from the blade tip (i.e. the 0.91 mm location) was felt to be unnecessary and was eliminated.

Strain gage data acquired during Task I testing did not succeed in providing an indication of the rub frequency because the signal to noise ratio was too small. To overcome this problem in the Task III multi-blade tests, amplifiers of higher quality and gain were obtained, a higher strain gage translator excitation voltage was used and the calibration was carried out beyond the range of the gage. These improvements provided a signal strong enough to identify the rub period and even to differentiate between several levels of rub severity.

The multi-bladed tests each contained 3 blades located approximately 10° apart and oriented 45° from the rub direction (see Figure 45). Prior to cementing the strain gages and thermocouple leads to the blade and holder the blades were accurately positioned against the test disk and locked into place. The tip of each blade was located within 0.05 mm of the initial true rubbing position for that test. As in the Task I testing a thorough pretest calibration and check list was followed to insure that the rig and instrumentation would operate and record satisfactorily.

4.7.2 Visual Test Results

Each of the five Task III tests were conducted as described in Sections 4.4 and 4.7.1. As in the Task I testing schedule a post-test review of the magnetic tape TV records was made, wear measurements were taken on the blades and abradable material and the hardware was metallographically analyzed.

The review of the TV records and high speed motion pictures of the Task III tests yielded a synopsis of the visual activity during each test which is related below. After each test number title the test conditions are listed in an abbreviated form in the following sequence: number of blades, blade material, incursion rate, rub velocity, blade thickness, rub depth, abradable density, test duration.

Test 13 (1, Ni, $i = .25$ mm/sec, $V = 213$ mps, $b = .48$ mm, $\delta = 1.0$ mm, $\rho = 16\% - 4$ sec)

An intense continuous blade tip glowing accompanied by very light sparking was visible the entire test. The highest thermocouple reading rose steadily to a maximum of 965°K approximately 1 second into the test. The temperature oscillated over a range of 45°K for the remainder of the test with the maximum values declining slowly to 840°K at the end of the test.

Test 14 (3, Ti, $i = .25$ mm/sec, $V = 152$ mps, $b = .55$ mm, $\delta = 1.0$ mm, $\rho = 19\% - 4$ sec)

Light sparking and blade tip glowing were visible for the first second of the test followed by very heavy, rapid intermittent sparking with intense blade tip glowing for the remainder of the test. Blades 1 and 2 had similar maximum recorded temperature traces rising steadily, after an early dip at test start, for the first 2.5 seconds and then oscillating, with amplitudes as large as 280°K , reaching a maximum of 1810°K at the end of the test. The maximum recorded temperature for blade 3 rose to a maximum of 1280°K in 0.8 seconds and remained steady until the thermocouples stopped functioning, approximately 1.5 seconds into the test.

Test 15 (1, Ni, $i = .025$ mm/sec, $V = 213$ mps, $b = 1.70$ mm, $\delta = 1.0$ mm, $\rho = 16\% - 40$ sec)

No visible blade tip glowing or sparking was noted during this test. The maximum recorded temperature rose to a maximum of 920°K in 2.75 seconds and then fell to 560°K , staying essentially constant for the remainder of the test.

Test 16 (3, Ti, $i = .25$ mm/sec, $V = 152$ mps, $b = 1.71$ mm, $\delta = 1.0$ mm, $\rho = 19\%$ – 4 sec)

Very intense blade tip glowing was visible from the start of the test. Light sparking was noted for the first 1/2 second becoming extremely bright and severe even though it was intermittent for the remainder of the test. Thermocouple readings rose to a maximum of 1965°K 2.5 seconds into the rub. Approximately 1.5 seconds into the rub oscillations in temperature, as large as 500°K , began, lasting the remainder of the test.

Test 17 (1, Ni, $i = .25$ mm/sec, $V = 152$ mps, $b = 1.68$ mm, $\delta = 1.0$ mm, $\rho = 19\%$ – 4 sec)

A bright glowing of the blade tip was noted almost from the start of the test accompanied by extremely light sparking. This continued throughout the test except at one point large pieces of debris left the rub zone and hit the pyrometer shield slowing down a sufficient amount to become visible. Thermocouples reached a maximum of 1530°K near the end of the test.

4.7.3 Wear Analysis

Wear measurements for Task III tests 13, 14, 15, 16 and 17 were taken with the shadow-graph and photomicrograph techniques used in Task I. The blade and seal wear measurements for the Task III tests are summarized in Table X. Included are the data for the parameters "Adjusted Blade Wear Plus Transfer" and Volume Wear Ratio" (VWR). These terms are discussed in detail in Section 4.5.1. The VWR's of tests 14, 16 and 17 were significantly higher than those normally expected for Feltmetal® seal systems and can be compared to tests 9 and 12 in Task I which also exhibited extremely high VWR's.

As previously noted, the test conditions for tests 9 and 12 provided data in the high rub energy, severe wear regime. Test 14 was a multiple blade test chosen to operate at the same conditions as test 12 to determine the effect of multiple blades on a high energy rub. It was anticipated that the multiple blades, by reducing the effective incursion rate (i.e. depth of cut), might lower the total rub energy and reduce the peak interface temperatures. However, the number of blades did not reduce the work per blade and, as in test 12, high interface temperatures resulted in soft blade tips and correspondingly high blade wear and VWR's. Tests 16 and 17 were chosen to operate at the same conditions (except for incursion depth) as test 9 which had experienced high rub energy and severe wear. Test 16 was to determine the effect of multiple blades on a high energy rub and test 17 was to determine the effect of a blade material change (titanium to Incoloy 901) on a high energy rub. Both of these effects were anticipated to have a tendency to reduce rub energy and wear; the multiple blades for the reason given above and the blade material because of the less reactive nature of nickel based alloy relative to titanium. Again, contrary to expectations, neither of these changes reduced the high rub energy, high interface temperature and both resulted in high blade wear and VWR's. Further work is required to identify the causes of this severe blade wear and high rub energy mode.

4.7.4 Metallographic Analysis

Metallographic analysis was completed on selected blades and all the Feltmetal® seals from Task III testing to identify changes in material structure and to determine the presence and constituents of any material transfer. Figures 46 and 47 show 25X cross sections of the seals from tests 13, 14, 15, 16 and 17. As in Task I the seals from the high incursion rate tests were distinguished by surface densification. Test number 15, run at 0.025 mm/second, was the only test operated at an incursion rate other than 0.25 mm/second. The seal from this test was not densified and as Figure 48 indicates there was no surface smearing or glazing. The seal from one other test, number 13, did not have surface smearing or glazing (Figure 49). This seal, although densified, did not exhibit the plasticity and eventual glazing that was prone to occur with the high incursion rate tests. A review of the rub energy, temperatures and physical wear for this test indicated that the total rub energy, heat into the blade and blade wear were all noticeably less than for the other Task III high incursion rate tests.

Metallographic examination of the three nickel alloy Incoloy 901 blades was conducted. The condition of the surface material structure was representative of the amount of energy associated with the rub. The least severe rub, test 15, showed no heat affected area at the blade rub interface, Figure 50. The test of intermediate severity (#13) exhibited sections of recrystallization at the blade rub surface (Figure 51). These localized transition areas reached a temperature of approximately 1300°K. Test 17 experienced the most severe rub and a cross section (Figure 52) through its 1.68 mm thickness shows a large area near the surface indicating a decomposition of the original grain structure with surrounding grain boundaries that are broad, indicating that melting had taken place. Taking the short test duration into account (4 seconds), melting probably occurred in the 1560°K to 1590°K temperature range. The Feltmetal® seal in test 17 exhibited the heaviest surface glazing (Figure 53) of all tests. The smearing and glazing was continuous except for isolated locations of spallation. In addition the blades in tests 13 and 15 experienced seal material transfer. Figure 54 shows a cross section through blade 13's 0.48 mm thickness at approximately the point of maximum transfer (0.20 mm). The amount of transfer varied considerably along the blade width and averaged 0.122 mm high. As in Test 11 and Task I the bulk of the transfer was Hastelloy X seal material. The lighter gray areas mixed in with the Hastelloy X are SermeTel AP-1, the cement used to hold the thermocouple leads in place. The transfer on blade 15 was similar in structure and material constituents as that on blade 13.

The first multi-bladed titanium test ran with the thinner blades, 0.55 mm thick, and experienced very high temperatures. A post test visual examination, Figures 55, 56 and 57, noted that the Test 14 blade tips had gross rough rub striations and a mushy molten appearance. The leading edge of each blade had a large plastically deformed burr of titanium material while the trailing edge had a burr that was generally a mixture of titanium, molybdenum and thermocouple cement (Figure 58). The rub surfaces had several areas of spallation and the appearance of gross mixing. Figure 59 shows a section of a rub surface area where mixing apparently took place. X-ray Emission Spectroscopy identified the top layer as basically titanium with traces of Hastelloy X, the next layer (darker in appearance) as a mixture of titanium and Hastelloy X and the substrate as the titanium blade alloy.

Figure 60 shows another blade tip area where a distinct surface layer is present and has been identified as titanium with traces of Hastelloy X. All figures of the rub surface indicate the presence of the many fine elongated α -platelets in a martensitic type alignment indicating a blade tip temperature in excess of 1300°K. In addition, molten titanium debris was visible in several areas of the trailing edge burr material indicating that the titanium had at least reached its softening temperature. All the metallography completed on test 14's blades could not identify any evidence of melting or burning remaining.

Although the photomicrograph of the Beltmetal® rubstrip for test 14 showed densification at the rub surface a plan view of the rubstrip indicated that the rub varied from fairly clean with no glazing to heavy glazing in some areas. The glazing generally appeared as both localized and discrete circumferential striations (Figure 61).

Test conditions for test 16 were the same as those for test 14 except test 16 blades were three times as thick. A post test visual examination, Figures 62, 63 and 64, was also conducted on the blade tips of test 16. The surfaces had gross rough rub striations and a mushy appearance but did not exhibit the molten condition that test 14 blades did. The leading edge of each blade had a burr which was more pronounced on each succeeding blade. The material in the burr, Figure 65, was identified as Hastelloy X seal material mixed with SermeTel AP-1 thermocouple cement. Material generated from the rub was also pushed off the trailing edge of the blade some of which adhered to the thermocouple cement. There was also molten titanium debris visible in spherical shapes on the trailing edge. The rub surface of each blade also had irregular areas of a thin light colored film adhering to the surface. This white film appears to be titanium oxide which, in some areas, had flaked off revealing the start of further oxidation which appears as shades of blue and purple. SEM probe corroborated this observation but could not identify elements below an atomic number of 11 and thus could not identify oxygen. Oxidation is a time/temperature phenomenon and to form during the short time duration between blade passes and remain at the end of a rub the interface temperatures must be extremely high. Test 16 had a maximum recorded blade temperature of nearly 1980°K which was the highest for all the tests. The metallographic sections of the first blade did not evidence any areas of recast structure or pitting indicative of titanium melting or burning in the blade itself but did note the presence of many fine, elongated α -platelets, indicating temperatures in excess of 1300°K. A plan view of the Beltmetal® from test 16 (Figure 66) showed mostly discrete heavily glazed circumferential striations with some localized glazed areas. This condition existed on the entire rubstrip, exhibiting more glazing than the seal from test 14.

Rub debris from all the Task III tests were collected in petroleum jelly and filtered for size distribution. Table XI lists the percentage of particles for each size range for tests 13, 14, 15, 16 and 17. For all tests except test 13 the quantity of particles was inversely proportional to their size, the majority of the particles being below 10 microns in size. Representative particles from test 14 were viewed and analyzed on the SEM. The majority of the particles were thin and flake-like in appearance as shown in Figure 67. An elemental analysis indicated that the majority of the debris was Hastelloy X with traces of titanium. This information gives credence to the postulation that one form of seal wear, or removal of abradable debris,

occurs as localized spallation or flaking of highly plasticized, flattened seal fibers. Repeated rubbing plastically deforms and flattens the fibers which are also rapidly cooling between blade hits. This sequence continues during blade incursion, which is approximately 0.025 microns per blade pass, until the bonds holding the flake are fractured and it is dislodged as rub debris. Particles can also be dislodged nearly intact during a rub as indicated by Figure 68 which shows a Hastelloy X abradable seal fiber. The number of these particles was very small compared to the flake-like particles.

4.7.5 Data Reduction and Analysis

The methods used to reduce the energy and blade temperature data were identical to the Task I procedures which were described in detail in sections 4.6.1 and 4.6.2. Blade heating and interface temperature were computed for each of the three blades in the multiple titanium blade tests and strain gage readings were analyzed to determine the occurrence and intensity of rubbing for each blade. The results of the analysis are presented as plots of the energy and temperature terms as a function of time throughout the tests in Figures 69 through 73 and in terms of average and peak values of the energy and temperature terms in Table XII. Strain gage results for the multiple titanium blade tests are presented in Figures 74 and 75.

4.7.6 Summary of Task III Test Results

From a qualitative point of view the Task III test results were very similar to the Task I results. Magnitudes of the energy, temperature and wear terms were comparable but with several striking differences. The following paragraphs present comparisons of each of the Task III tests with the corresponding Task I tests, noting similarities and differences between the tests, and finally, a comparison is made between the Task III results and the predictive models developed in Task II from the Task I data.

The first Task III test, test 13, was run at all the same conditions as test 8 of Task I except with Incoloy 901 blade material in place of 8-1-1 titanium (AMS 4916). As in test 8, the rub produced considerable transfer and resulted in a densified abradable surface. The blade wear prior to transfer was the same for both materials. The peak interface temperature was over 222°K lower for the nickel material but the rub energy and heat splits were comparable. Since one of the primary objectives of this test was to examine the effect of blade material upon the occurrence of transfer, the close similarity between the tests with respect to wear and transfer was of particular interest.

Test 14 was conducted at the same conditions as Task I test 12 except that three blades were used in place of one. In spite of the fact that the three blades might have been expected to divide up the abradable "cutting," to produce an effectively 3x lower incursion rate for test 14 than for test 12, the total rub energies were remarkably similar. As shown in Figure 74, within 0.3 seconds of the 4 second test all three of the blades were actively rubbing and they all continued rubbing at varying intensities throughout the balance of the test.

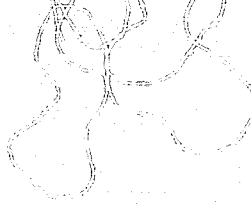
Since prior experience at moderate incursion rates has typically exhibited intermittent rubbing with the longest blades rubbing first and thermal growth effects producing the periodic effects, this result was somewhat unexpected. On a per blade basis the rub energy was less for the multiple blade configuration and the maximum blade temperature was 250°K lower than for the single blade test, but the total energy for test 14 was slightly higher and the total volume of blade material lost was considerably greater. While this result was at first surprising, analysis of the data indicated clearly that the close spacing of the blades prevented the abrasible from cooling between blades so that heating effects were intensified. In a normal engine rub where blades rubbing in concert are probably much more widely spaced such an effect could be expected to be greatly diminished.

Test 15 was conducted at the same conditions as test 4 except for Incoloy 901 blade material in place of 8-1-1 titanium and utilization of a 1.0 mm rub depth rather than 0.5 mm. Again the primary objective was to examine the effect of blade material in a region where transfer had occurred. For these tests the incursion rate was 0.025 mm/s rather than the 0.25 mm/s used in tests 8 and 13, the other transfer tests. The nickel base blade material was seen to produce transfer as did the titanium blade, both after minimum blade wear had occurred. In this case rub energy was considerably less for the nickel blade and the abrasible exhibited less glazing and densification than seen with the titanium blade. As in the prior comparison the nickel alloy blade yielded a lower maximum interface temperature, by 190°K in this instance.

Test 16 duplicated the conditions of test 9 except for utilization of three blades rather than one and an increase in rub depth to 1.0 mm. Although the interface temperatures and heat into each blade were similar for the two tests the total energy was higher for the multiple blade test. Again the expected reduction of rub energy due to distribution of cutting between the three blades did not occur and, as shown in Figure 75, all three blades again participated in the rub throughout the test after an initial start-up transient. Heavier abrasible glazing, which occurred for the multiple blade test, was attributed to the greater rub depth.

The final test, test 17, was also conducted at the same conditions as test 9 except this time with Incoloy 901 blade material in place of the titanium and, again, the 1.0 mm rub depth rather than the 0.5 mm depth. In view of the extreme wear and high interface temperature of test 9, which had been attributed to ignition of the titanium blade material, this test produced very surprising results -- the nickel based blade wore as severely as the titanium blade. Rub energy was much higher for the nickel blade and interface temperature lower, corresponding to the lower melting temperatures of the nickel alloy. Blade heating was somewhat lower, undoubtedly due to the lower interface temperature. The abrasible glazing which occurred for test 17 was the most severe of any test. This test was strong evidence that the excessive wear of the titanium alloy blade in test 9 was due to a reduction in blade material strength and not ignition.

Although the changes in blade material and number of blades incorporated in Task III would be expected to have a significant effect on most, if not all, of the observed rub phenomena, it is interesting to compare the results of the Task III tests with the predictive models developed from the statistical analysis of the Task I test data. Figures 76 through 81 are reproductions of the Y_{calc} versus Y_{obs} plots of section 4.6.4 which include the Task III



data points. Since all of the Task III tests are conducted to 1.0 mm rub depth, points for both 0.5 mm and 1.0 mm incursion depths are presented in each of the energy and temperature plots; the 0.5 mm points being derived from analysis of the first half of the tests and the 1.0 mm points from analysis of the entire test.

A review of the plots shows that for both the transfer mode tests (tests 13 and 15) the Incoloy 901 material yielded lower total rub energy and interface temperature but about the same blade heating as the titanium blades. Since Incoloy 901 has higher thermal conductivity than 8-1-1 titanium but about the same thermal diffusivity, the lower interface temperature coupled with a minimal difference in blade heating is understandable. The lower total rub energy with the Incoloy 901 appears to relate to the reduced interface temperature and somewhat lesser degree of abradable densification and glazing.

While the transfer mode tests with Incoloy 901 resulted in lower total rub energy than predicted by the Task I model, test 17, with the Incoloy 901 at conditions producing high rub energy and wear in Task I, resulted in substantially higher total rub energy than the Task I model predicts. This coincides with the extreme amount of abradable densification and glazing and blade wear which occurred on this test. In spite of the high rub energy and blade wear, this test showed the same reduced interface temperature and congruent blade heating effect, relative to the Task I models, as did the other Incoloy 901 tests. The degree of blade wear was particularly noteworthy in that the rapid blade wear mode observed in Task I is confirmed as a system problem rather than just a blade material problem.

The two multiple blade tests (tests 14 and 16), both conducted at conditions which produced high rub energy and blade wearing during Task I testing, exhibited somewhat higher total energies than the corresponding Task I tests but not a factor of three as would have been the case had the per blade rub force remained constant. Blade heating, on a per blade basis, and maximum blade temperature are seen in Figures 78, 79 and 80 to be in general agreement with the Task I findings. Blade wear, on an average per blade basis, ranged from moderate wear, close to the prediction model, for test 14 with thin blades to severe blade wear for test 16 with the thick blades. The extreme difference in wear between the normal wear mode and the severe wear mode is clearly seen in Figure 81.

REFERENCES

1. Mahler, F.H., "Advanced Seal Technology," PWA-4372, 1972 (AD-739922).
2. Ludwig, L.P., "Gas Path Sealing in Turbine Engines," NASA TM-73890, 1978.
3. Shiembob, L.T., "Development of Abradable Gas Path Seals," NASA Cr-134689, 1974.
4. Shiembob, L.T., "Development of a Plasma Sprayed Ceramic Gas Path Seal for High Pressure Turbine Applications," NASA CR-135183, 1977.
5. Bill, R.C. and Shiembob, L.T., "Friction and Wear of Sintered Fiber-Metal Abradable Seal Materials," NASA TM X-73650, 1977.
6. Bill, R.C. and Wisander, D.W., "Friction and Wear of Several Compressor Gas Path Seal Materials," NASA Technical Paper 1128, 1978.
7. Carslaw, H.S. and Jaeger, J.C., "Conduction of Heat in Solids," 2nd Ed., Oxford Press, 1959, p. 83.
8. Kreith, F., "Principles of Heat Transfer," 3rd Ed., International Textbook Co., 1973, pp. 404, 405.

SYMBOLS

A	Constant in regression equations or area within the perimeter of the strip
B	Coefficient in regression equations
b	Blade thickness
C_p	Specific heat
G	Mass flux of blade material due to wear at the interface
h	Convective heat transfer coefficient
I	Current to strip
i	Incursion rate
J	Rotational inertia
K	Number of degrees of freedom of the model
k	Thermal conductivity
N	Sample size
P	Perimeter of blade
q	Heat load
q_{bd}	Heat load to blade debris
q_d	Heat load to the abradable
q_{total}	Total rub heat load
\bar{q}_{total}	Time average of total rub heat load over time increment Δt
R	Resistance of strip
r	Multiple correlation coefficient
r^2	Coefficient of determination
S	Cross-sectional area of the blade
SEE	Standard error of estimate
T	Temperature
T_a	Ambient air temperature
T_i	Interface temperature
T_o	Initial disk temperature
T_s	Measured surface temperature
t	Time
U	Overall heat loss conductance
V	Rub velocity
v^2	Sum of unexplained variation
VWR	Volume wear ratio
X_i	Specified function uniquely related to i^{th} independent variable

SYMBOLS (Cont'd)

x	Distance from abradable bond interface
Y	Predicted value of dependent variable
y	Distance from the rub interface
α	Thermal diffusivity
δ	Rub depth
δ_a	Abradable thickness
ρ	Abradable density
σ	Repeatability error factor
τ	Torque
ω	Rotational speed

ORIGINAL PAGE IS
OF POOR QUALITY

TABLE I
STATISTICAL TEST MATRIX FOR TASK I

Blade Thickness — mm (in)	Abradable Density — %	Rub Velocity — m/s (ft/sec)	0.5 (0.020)			1.0 (0.040)			Rub Depth — mm (in)	Incursion Rate — mm/s (in/sec)
			0.0025 (0.0001)	0.025 (0.001)	0.25 (0.010)	0.0025 (0.0001)	0.025 (0.001)	0.25 (0.010)		
0.5 (0.02)	16	152 (500)			③*					
		213 (700)						⑧		
	19	152 (500)					⑥ ⑪	⑫		
		213 (700)	② ⑩							
1.8 (0.07)	16	152 (500)				⑦*				
		213 (700)		④						
	19	152 (500)			⑨*					
		213 (700)						① ⑤		

* These tests were instrumented with a blade strain gage.

**ORIGINAL PAGE IS
OF POOR QUALITY**

TABLE II

WEAR MEASUREMENTS FOR THE TASK I TESTS

Test No.	Programmed Incursion	Carriage Incursion	Measured Wear (Avg)		Measured Incursion
	mm (in)	mm (in)	Seal mm (in)	Blade ^(a) mm (in)	mm (in)
1	1.0 (.040)	1.087 (.0428)	1.112 (.0438)	.086 / .051T (.0034/.0020T)	1.147 (.0452)
2	0.5 (.020)	0.538 (.0212)	0.478 (.0188)	.038 (.0015)	0.516 (.0203)
3	0.5 (.020)	0.513 (.0202)	0.396 (.0156)	.079 (.0031)	0.475 (.0187)
4	0.5 (.020)	0.564 (.0222)	0.635 (.0250)	.005 / .069T (.0002/.0027T)	0.571 (.0225)
5	1.0 (.040)	1.128 (.0444)	1.143 (.0450)	.010 / .127T (.0004/.0050T)	1.026 (.0404)
6	1.0 (.040)	0.965 (.0380)	0.635 (.0250)	.198 (.0078)	0.832 (.0328)
7	1.0 (.040)	1.036 (.0408)	1.031 (.0406)	.005 (.0002)	1.036 (.0408)
8	1.0 (.040)	0.991 (.0390)	1.112 (.0438)	.005 / .152T (.0002/.0060T)	0.965 (.0380)
9	0.5 (.020)	0.539 (.0212)	0.279 (.0110)	.239 (.0094)	0.518 (.0204)
10	0.5 (.020)	0.483 (.0190)	0.508 (.0200)	.058 (.0023)	0.566 (.0223)
11	1.0 (.040)	0.991 (.0390)	1.194 (.0470)	.051 / .140T (.0020/.0055T)	1.105 (.0435)
12	1.0 (.040)	0.991 (.0390)	0.757 (.0298)	.323 / .107T (.0127/.0042T)	0.973 (.0383)
			(b) 0.152 (.0060)	.787 (.0310)	0.939 (.0370)

^a In tests where transfer occurred following wear, wear is tabulated first and the amount of transfer is followed by a "T".

^b Test 12 had two different distinct wear modes occur at two different areas of the blade tip.

TABLE III
WEAR RESULTS FOR THE TASK I TESTS

Test No.	Blade Thickness mm (in)	Seal mm (in)	Measured Wear (Avg) Blade (a) mm (in)	Adjusted Blade Wear & Transfer mm (in)	Vol Wear Ratio (b) (X 10 ⁻⁴)
1	1.78 (.0700)	1.112 (.0438)	.086 / .051T (.0034/.0020T)	.353 (0.0139)	5.4
2	0.53 (.0210)	.478 (.0188)	.038 (.0015)	.041 (0.0016)	1.4
3	0.56 (.0220)	.396 (.0156)	.079 (.0031)	.086 (0.0034)	3.8
4	1.74 (.0685)	.635 (.0250)	.005 / .069T (.0002/.0027T)	.086 (0.0034)	0.6
5	1.74 (.0685)	1.143 (.0450)	.010 / .127T (.0004/.0050T)	.163 (0.0064)	0.6
6	0.51 (.0200)	.635 (.0250)	.198 (.0078)	.198 (0.0078)	5.5
7	1.75 (.0690)	1.031 (.0406)	.005 (.0002)	.018 (0.0007)	0.3
8	0.56 (.0220)	1.112 (.0438)	.005 / .152T (.0002/.0060T)	.158 (0.0062)	0.1
9	1.77 (.0695)	.279 (.0110)	.239 (.0094)	.838 (0.0330)	52.2
10	0.52 (.0205)	.508 (.0200)	.058 (.0023)	.061 (0.0024)	2.1
11	0.56 (.0220)	1.194 (.0470)	.051 / .140T (.0020/.0055T)	.196 (0.0077)	1.0
12	0.62 (.0245)	.757 (.0298)	.323 / .107T (.0127/.0042T)	.503 (0.0198)	9.8
		.152 (.0060)	.787 (.0310)	.965 (0.0380)	103.8

^a In tests where transfer occurred following wear, wear is tabulated first and the amount of transfer is followed by a "T".

^b Volume Wear Ratio (VWR) = $\frac{\text{volume of blade wear}}{\text{volume of seal groove}}$

TABLE IV

TASK I TEST CONDITIONS, WEAR AND DATA ANALYSIS RESULTS

Test No.	Blid Th (mm)	Rub Vel (m/s)	Rub Dpt (mm)	Inc Rate (mm/s)	Seal Den (%)	Measured Seal (mm)	Wear Blade(a) (mm)	Peak Tot Engy (kw)	Ave Tot Engy (kw)	Max Inter Temp (°K)	Avg Q Into Blade (kw)	Peak Q Into Blade (kw)	Heat Split (%)
1	1.78	213	1.0	0.25	19	1.112	.086/ .051T	1.50	0.954	1323	0.033	0.070	3.4
2	0.53	213	0.5	0.0025	19	0.478	.028	0.04	0.013	1234	0.003	0.020	21.8
3	0.56	152	0.5	0.25	16	0.396	.079	1.81	0.507	1582	0.027	0.044	5.4
4	1.74	213	0.5	0.025	16	0.635	.005/ .069T	1.48	0.411	1179	0.018	0.037	4.2
5	1.74	213	1.0	0.25	19	1.143	.019/ .127T	1.37	0.680	1230	0.031	0.095	4.4
7	1.75	152	1.0	0.0025	16	1.031	.005	0.33	0.144	1337	0.017	0.047	11.4
8	0.56	213	1.0	0.25	16	1.112	.005/ .152T	1.00	0.660	1323	0.017	0.033	2.6
9	1.77	152	0.5	0.25	19	0.279	.239	1.93	0.346	1746	0.080	0.131	23.2
10	0.52	213	0.5	0.0025	19	0.508	.058	0.06	0.006	851	0.003	0.010	50.0
11	0.56	152	1.0	0.025	19	1.194	.051/ .041T	0.56	0.234	1142	0.010	0.113	4.4
12	0.62	152	1.0	0.25	19	0.757	.323/ .107T (b) 0.152 .787	1.18	0.585	1941	0.036	0.066	6.1

^a In tests where transfer occurred following wear, wear is tabulated first and the amount of transfer is followed by a "T".

^b Test 12 had two different distinct wear modes occur at two different areas of the blade tip.

ORIGINAL PAGE IS
OF POOR QUALITY

TABLE IVa

TASK I TEST CONDITIONS, WEAR AND DATA ANALYSIS RESULTS

Test No.	Blade Th (in)	Rub Vel (fps)	Rub Dpt (in)	Inc Rate (ips)	Seal Den (%)	Measured Seal (in)	Wear Blade ^(a) (in)	Peak Tot Engy (BTU/Sec)	Ave Tot Engy (BTU/Sec)	Max Inter Temp (°F)	Avg Q Into Blade (BTU/Sec)	Peak Q Into Blade (BTU/Sec)	Heat Split (%)
1	.0700	700	.040	0.0100	19	.0438	.0034/ .0020T	1.42	0.905	1922	0.031	0.066	3.4
2	.0210	700	.020	0.0001	19	.0138	.0015	0.04	0.012	1762	0.003	0.019	21.8
3	.0220	500	.020	0.0100	16	.0156	.0031	1.72	0.481	2389	0.026	0.042	5.4
4	.0685	700	.020	0.0010	16	.0250	.0002/ .0027T	1.40	0.390	1663	0.017	0.035	4.2
5	.0685	700	.040	0.0100	19	.0450	.0004/ .0050T	1.30	0.645	1754	0.029	0.090	4.4
7	.0690	500	.040	0.0001	16	.0406	.0002	0.31	0.137	1947	0.016	0.045	11.4
8	.0220	700	.040	0.0100	16	.0438	.0002/ .0060T	0.95	0.626	1922	0.016	0.031	2.6
9	.0695	500	.020	0.0100	19	.0110	.0094	1.83	0.328	2684	0.076	0.124	23.2
10	.0205	700	.020	0.0001	19	.0200	.0023	0.06	0.006	1073	0.003	0.009	50.0
11	.0220	500	.040	0.0010	19	.0470	.0020/ .0055T	0.53	0.222	1596	0.010	0.107	4.4
12	.0245	500	.040	0.0100	19	.0298	.0127/ .0042T (b) .0060 .0310	1.12	0.555	3035	0.034	0.063	6.1

^a In tests where transfer occurred following wear, wear is tabulated first and the amount of transfer is followed by a "T".

^b Test 12 had two different distinct wear modes occur at two different areas of the blade tip.

ORIGINAL PAGE IS
OF POOR QUALITY

TABLE V

PYROMETER READINGS AND CALCULATED BULK TEMPERATURES

Test	Location 30° From Rub Zone		Location 180° From Rub Zone		Calculated Value Of Heat Conducted Into The Disk kw (BTU/Sec)	Calculated Bulk Temperature of Seal Debris °K (°F)
	Type of Optics Used	Maximum Recorded Temperature ^(a) °K (°F)	Type of Optics Used	Maximum Recorded Temperature ^(a) °K (°F)		
1	Silicon	Below 975 (1300)	Lead Sulfide	790 (960)	0.228 (0.216)	750 (890)
2	Silicon	Below 975 (1300)	Lead Sulfide	Below 590 (600)		
3	Silicon	Below 975 (1300)	Lead Sulfide	660 (730)	0.246 (0.233)	-11 (-480)
4	Silicon	Below 975 (1300)	Lead Sulfide	Below 590 (600)		
5	Lead Sulfide	Below 750 (900)	Lead Sulfide	Below 590 (600)		
7	Lead Sulfide	Below 750 (900)	Lead Sulfide	Below 590 (600)		
8	Lead Sulfide	Below 750 (900)	Lead Sulfide	Below 590 (600)		
9	Lead Sulfide	880 (1130)	Lead Sulfide	690 (780)	0.231 (0.219)	-2660 (-5250)
10	Lead Sulfide	Below 750 (900)	Lead Sulfide	Below 590 (600)		
11	Lead Sulfide	Below 750 (900)	Lead Sulfide	Below 590 (600)		
12	Lead Sulfide	Below 750 (900)	Lead Sulfide	Below 590 (600)		
13	Lead Sulfide	Below 750 (900)	Lead Sulfide	Below 590 (600)		

14 - 17 Pyrometers did not function properly.

^a The values tabulated with the word "Below" are the lower threshold temperature limit of the pyrometer.

TABLE VI
**BASIC INDEPENDENT PARAMETERS AND THEIR NUMERICAL
AND CODED VALUES**

<u>Independent Parameters</u>	<u>Level</u>	<u>Coded Value</u>
Incursion Rate — mm/s (inch/sec)	.0025, .025, .25 (.0001), (.0010), (.0100)	—1, 0, +1
Incursion Depth — mm (inch)	.5, 1.0 (.020), (.040)	—1, +1
Rub Velocity — mps (ft/sec)	152, 213 (500), (700)	—1, +1
Blade Thickness — mm (inch)	.5, 1.8 (.02), (.07)	—1, +1
Abradable Density (%)	16, 19	—1, +1

TABLE VII
REGRESSION EQUATION COEFFICIENTS
 $Y = A + B_1 X_1 + B_2 X_2 + \dots + B_5 X_5$

Y \ X	Avg Total Energy (kw)		Peak Total Energy (kw)		Avg Heat To Blade (kw)		Peak Heat To Blade (kw)		Max Blade Temperature (°K)		Adjusted Blade Wear (mm)
	Task I	Task I Expanded (a)	Task I	Task I Expanded	Task I	Task I Expanded	Task I	Task I Expanded	Task I	Task I Expanded	Task I
Constant (A)	.336	.380	.908	.795	.0217	.0193	.0461	.0428	1311	1300	.192
Incursion Rate (B ₁)	.265*(b)	.302*	.677*	.621*	.0151*	.0148*	.0218*	.0221*	178*	185*	.176?(c)
Incursion Depth (B ₂)	.083?	.018	-.233*	-.097	-.0070	-.0045*	-.0063	-.0075	-42	-6	-.033
Rub Velocity (B ₃)	.083?	.093*	-.090	-.074	-.0090*	-.0065*	-.0097	-.0022	-150	-160*	-.127
Blade Thickness (B ₄)	.037	.064?	.221*	.202*	.0097*	.0095*	.0218*	.0206*	19	6	.032
Abradable Density (B ₅)	-.027	-.015	-.077	-.057	.0059	.0037	.0114	.0089?	0	-14	.149?
STATISTICS											
Sample Size	11	17	11	17	11	17	11	17	11	17	12
S.E.E.	.119	.157	.121	.246	.0109	.0097	.0182	.0165	208	200	.247
r ² - %	92.1	84.1	98.4	88.3	87.5	81.6	87.4	82.5	71.6	62.5	67.5
Repeatability Error (σ)	±.137		±.066		±.0013		±.0137		±162		±.140

^a The expanded equations include all 1.0 mm incursion depth tests evaluated at both 0.5mm incursion and 1.0mm incursion.

^b The coefficients denoted by an asterisk (*) are statistically important at the 95% confidence level.

^c The coefficients denoted by a question mark (?) are marginally important at the 95% confidence level.

TABLE VIIa

REGRESSION EQUATION COEFFICIENTS

$$Y = A + B_1 X_1 + B_2 X_2 + \dots + B_5 X_5$$

X \ Y	Avg Total Energy (BTU/Sec)		Peak Total Energy (BTU/Sec)		Avg Heat To Blade (BTU/Sec)		Peak Heat To Blade (BTU/Sec)		Max Blade Temperature (°F)		Adjusted Blade Wear (mils)
	Task I	Task I Expanded ^(a)	Task I	Task I Expanded	Task I	Task I Expanded	Task I	Task I Expanded	Task I	Task I Expanded	Task I
Constant (A)	.319	.360	.861	.754	.0206	.0183	.0437	.0406	1900	1880	7.54
Incursion Rate (B ₁)	.251 ^(b)	.286*	.642*	.589*	.0143*	.0140*	.0207*	.0210*	320*	334*	6.94 ^(c)
Incursion Depth (B ₂)	.079?	.017	-.221*	-.092	-.0066	-.0043*	-.0060	-.0071	-75	-10	-1.30
Hub Velocity (B ₃)	.079?	.088*	-.085	-.070	-.0085*	-.0062*	-.0092	-.0021	-271	-289*	-5.00
Blade Thickness (B ₄)	.035	.061?	.210*	.192*	.0092*	.0090*	.0207*	.0195*	35	11	1.26
Abradable Density (B ₅)	-.026	-.014	-.073	-.054	.0056	.0035	.0108	.0084?	0	-26	5.85?
STATISTICS											
Sample Size	11	17	11	17	11	17	11	17	11	17	12
S.E.E.	.113	.149	.115	.233	.0103	.0092	.0173	.0157	374	360	9.70
r ² - %	92.1	84.1	98.4	88.3	87.5	81.6	87.4	82.5	71.6	62.5	67.5
Repeatability Error (σ)	±.130		±.063		±.00125		±.0130		±292		±5.51

^aThe expanded equations include all 40 mil incursion depth tests evaluated at both 20 mils incursion and 40 mils incursion.

^bThe coefficients denoted by an asterisk (*) are statistically important at the 95% confidence level.

^cThe coefficients denoted by a question mark (?) are marginally important at the 95% confidence level.

ORIGINAL PAGE IS
OF POOR QUALITY

ORIGINAL PAGE IS
OF POOR QUALITY

TABLE VIII

SIGNIFICANCE OF TERMS - % OF VARIATION ACCOUNTED FOR
BY INDEPENDENT VARIABLE

Controlled Variable	Avg of Energy, Temp and Wear Eqns ^(a)	Avg of Energy Eqns ^(a)	Interface Temp Eqn ^(a)	Wear Eqn	Number of *'s	Number of *'s and ?'s
Incursion Rate (<i>i</i>)	46	48	50	34	5	6
Incursion Depth (δ)	7	9	1	6	1	1
Rub Velocity (<i>v</i>)	19	12	43	25	3	3
Blade Thickness (<i>b</i>)	16	22	2	6	3	4
Abradable Density (ρ)	11	8	4	29	0	1

^a Expanded equations used for energy and interface temperature

Conclusion:

- i* - Very important
- v* - Moderate importance
- b* - " "
- δ - Low importance
- ρ - " "

TABLE IX

TEST MATRIX FOR TASKS I AND III

mm Blade Thickness — (in)	Abradable Density — %	m/s Rub Velocity — (ft/sec)	0.5 (0.020)			1.0 (0.040)			Rub Depth — mm (in)	Incursion Rate — m/s (in/sec)
			0.0025 (0.0001)	0.025 (0.001)	0.25 (0.010)	0.0025 (0.0001)	0.025 (0.001)	0.25 (0.010)		
0.5 (0.02)	16	152 (500)			3*					
		213 (700)						8 13		
	19	152 (500)					6 11	12 14*		
		213 (700)	2 10							
1.8 (0.07)	16	152 (500)				7*				
		213 (700)		4			15			
	19	152 (500)			9*			16* 17		
		213 (700)						1 5		

* These tests were instrumented with blade strain gage.

* These tests were instrumented with a blade strain gage.

NOTES:




- The numbers and letters encircled in the matrix are the test numbers. Numbers 1 through 12 are Task I tests. Numbers 13 through 17 are Task III tests.
- 's denote single 8-1-1 titanium blades; 's denote single Incoloy 901 blades, 's denote multiple (3) 8-1-1 titanium blades.

TABLE X

TASK III TEST CONDITIONS AND WEAR RESULTS

Test No.	No. Blds	Bld Matl	Bld Th mm (in)	Seal Den (%)	Rub Vel m/s (ft/sec)	Rub Dpt mm (in)	Inc Rate mm/s (in/sec)	Measured Wear		Vol Wear Ratio(b) (X 10 ⁻⁴)	Adjusted Blade Wear & Transfer mm (in)
								Seal mm (in)	Blade(a) mm (in)		
13	1	Inco 901	.48 (.0190)	16	213 (700)	1.0 (.040)	.25 (.0100)	1.161 (.0457)	.005 / .122 (.0002/.0048T)	0.08	.127 (0.0050)
14	3	Ti	.55 (.0215)	19	152 (500)	1.0 (.040)	.25 (.0100)	.427 (.0168)	.502 (.0198) .490 (.0193) .470 (.0185)	66.4	1.572 (0.0619)
15	1	Inco 901	1.70 (.0670)	16	213 (700)	1.0 (.040)	.025 (.0010)	1.181 (.0465)	.002 / .112 (.0001/.0044T)	0.14	.119 (0.0047)
16	3	Ti	1.71 (.0673)	19	152 (500)	1.0 (.040)	.25 (.0100)	.254 (.0100)	.752 (.0296) .739 (.0291) .638 (.0251)	508	7.155 (0.2817)
17	1	Inco 901	1.68 (.0660)	19	152 (500)	1.0 (.040)	.25 (.0100)	.206 (.0081)	.815 (.0321)	236	2.692 (0.1060)

^a In tests where transfer occurred following wear, wear is tabulated first and the amount of transfer is followed by a "T".

^b Volume Wear Ratio (VWR) = $\frac{\text{volume of blade wear}}{\text{volume of seal groove}}$

ORIGINAL PAGE IS
OF POOR QUALITY

TABLE XI

PERCENT OF DEBRIS PARTICLES FOUND WITHIN A GIVEN SIZE RANGE

Test	Particle Size Range					Total (%)
	5-10 μ	10-25 μ	25-50 μ	50-100 μ	> 100 μ	
	0.2-0.4 mils (%)	0.4-1.0 mils (%)	1.0-2.0 mils (%)	2.0-4.0 mils (%)	> 4.0 mils (%)	
13	17.5	26.0	17.1	28.3	11.1	100.0
14	42.1	30.3	13.8	9.6	4.3	100.1
15	40.3	35.0	12.9	10.7	1.1	100.0
16	59.7	24.1	9.5	4.8	2.0	100.1
17	51.6	29.6	10.6	6.5	1.8	100.1

ORIGINAL PAGE IS
OF POOR QUALITY

TABLE XII
TASK III TEST CONDITIONS, WEAR AND DATA ANALYSIS RESULTS

Test No.	Blade No.	Blade Matl	Th (mm)	Seal Den (%)	Rub Vel (m/s)	Rub Dpt (mm)	Inc Rate (mm/s)	Measured Wear Seal (mm)	Measured Wear Blade ^(a) (mm)	Peak Tot Engy (kw)	Avg Tot Engy (kw)	Max Inter Temp (°K)	Peak Q Into Blade (kw)	Avg Q Into Blade (kw)	Heat Split (%)
13	1	Inco 901	0.48	16	213	1.0	0.25	1.161	.005/ .122T	0.89	0.589	1083	0.031	0.017	5.2
14	3	Ti	0.55	19	152	1.0	0.25	0.427	.503 .490 .470	1.36	0.896	1690	0.036 0.042 0.054	0.019 0.016 0.018	2.1 1.8 2.0
15	1	Inco 901	1.70	16	213	1.0	0.025	1.181	.002/ .112T	0.56	0.224	990	0.048	0.012	5.2
16	3	Ti	1.71	19	152	1.0	0.25	0.254	.752 .739 .638	2.59	1.006	1792	0.096 0.146 0.144	0.060 0.056 0.057	6.0 5.5 5.6
17	1	Inco 901	1.68	19	152	1.0	0.25	0.206	.815	2.31	0.920	1443	0.102	0.059	6.5

^a In tests where transfer occurred following wear, wear is tabulated first and the amount of transfer is followed by a "T".

TABLE XIIa

TASK III TEST CONDITIONS, WEAR AND DATA ANALYSIS RESULTS

Test No.	No.	Blade Matl	Th (in)	Seal Den (%)	Rub Vel (fps)	Rub Dpt (in)	Inc Rate (ips)	Measured Wear		Peak Tot Engy (BTU/Sec)	Avg Tot Engy (BTU/Sec)	Max Inter Temp (°F)	Peak Q Into Blade (BTU/Sec)	Avg Q Into Blade (BTU/Sec)	Heat Split (%)	
								Seal (in)	Blade ^(a) (in)							
13	1	Inco 901	.0190	16	700	.040	.0100	.0457	.0002/.0048T	0.84	0.559	1491	0.029	0.016	5.2	
14	3	Ti	.0215	19	500	.040	.0100	.0168	.0198 .0193 .0185	1.29	0.850	2583	0.034 0.040 0.051	0.018 0.015 0.017	2.1 1.8 2.0	5.9
15	1	Inco 901	.0670	16	700	.040	.0010	.0465	.0001/.0044T	0.53	0.212	1323	0.046	0.011	5.2	
16	3	Ti	.0673	19	500	.040	.0100	.0100	.0296 .0291 .0251	2.46	0.954	2767	0.091 0.139 0.137	0.057 0.053 0.054	6.0 5.5 5.6	
17	1	Inco 901	.0660	19	500	.040	.0100	.0081	.0321	2.19	0.873	2139	0.097	0.056	6.5	

^a In tests where transfer occurred following wear, wear is tabulated first and the amount of transfer is followed by a "T".

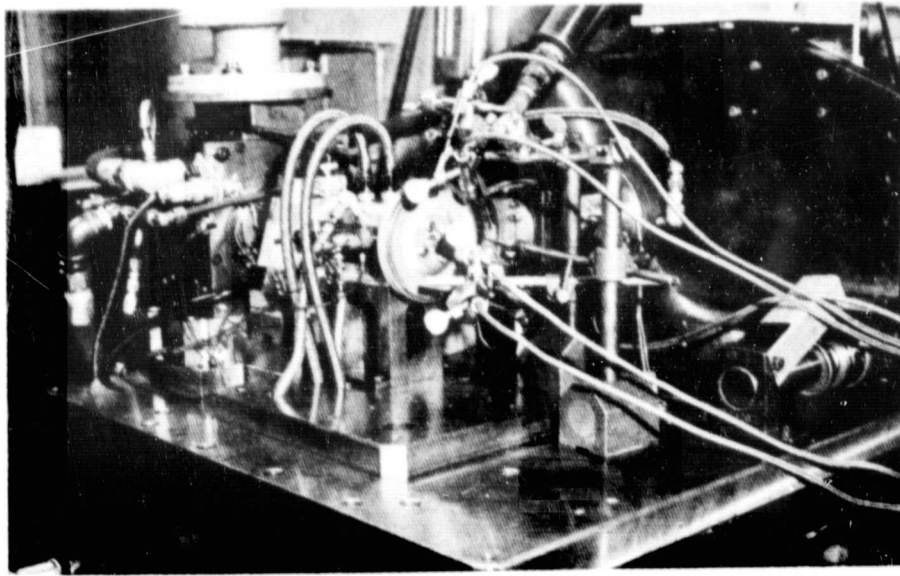


Figure 1. Test Rig Setup for Rub Energy Test

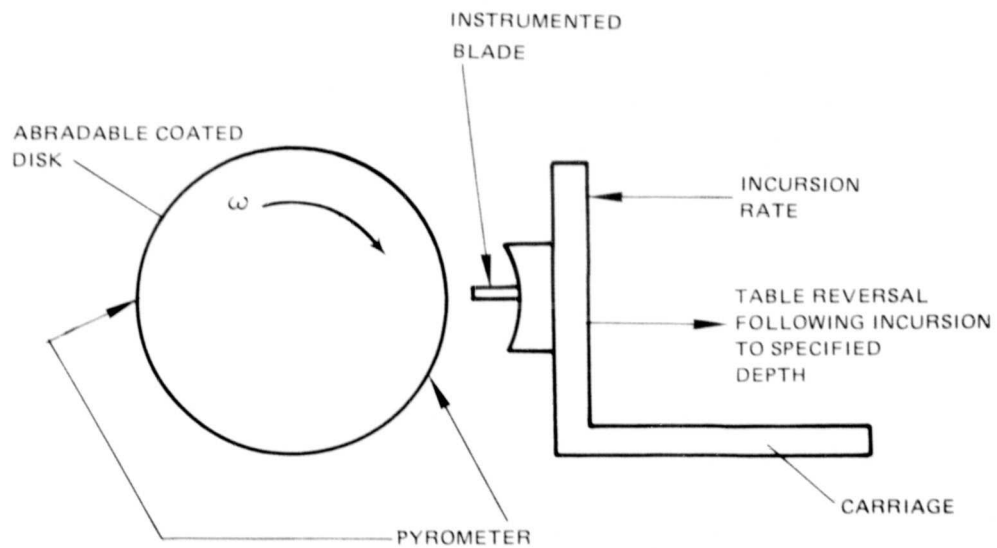


Figure 2. Schematic of Test Setup

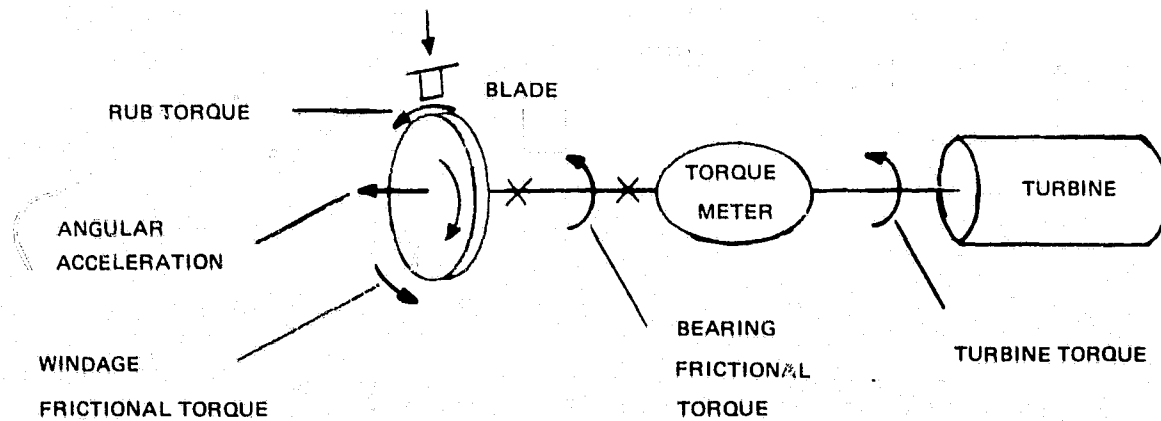


Figure 3. Schematic of Rotor System

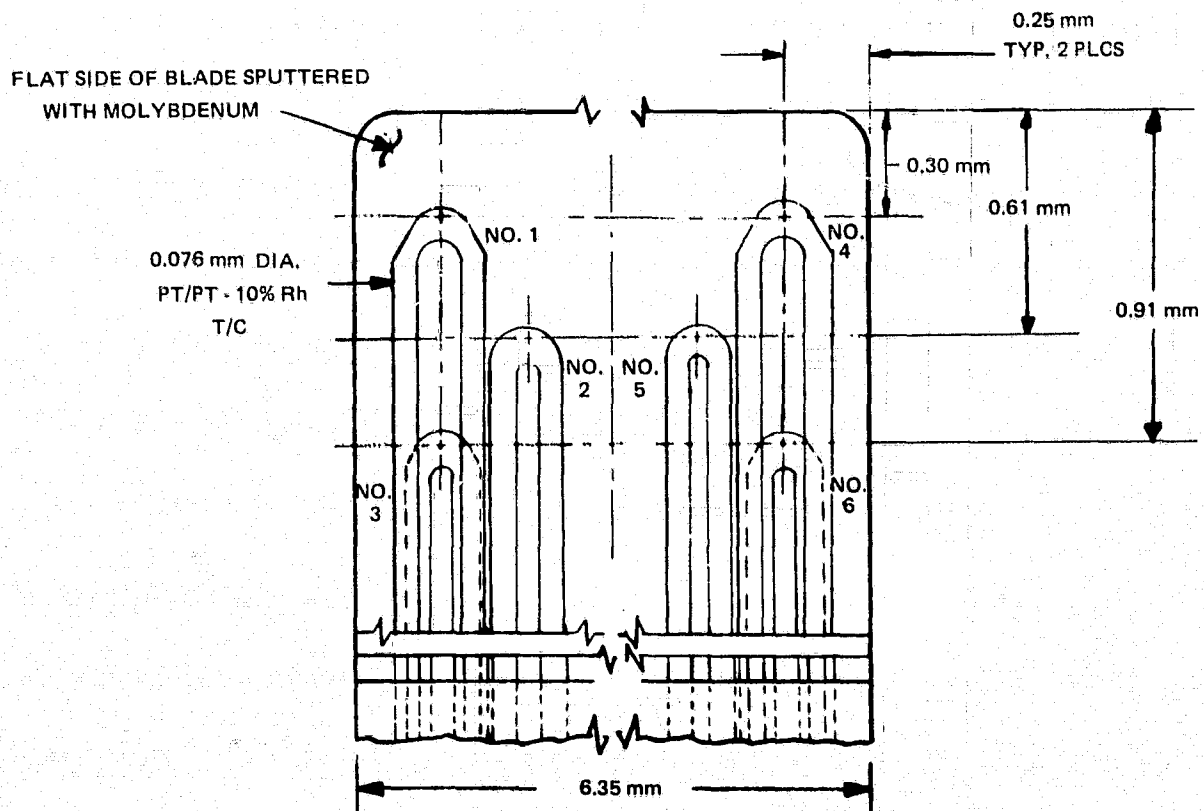


Figure 4. Instrumented Rub Test Blade

ORIGINAL PAGE IS
OF POOR QUALITY

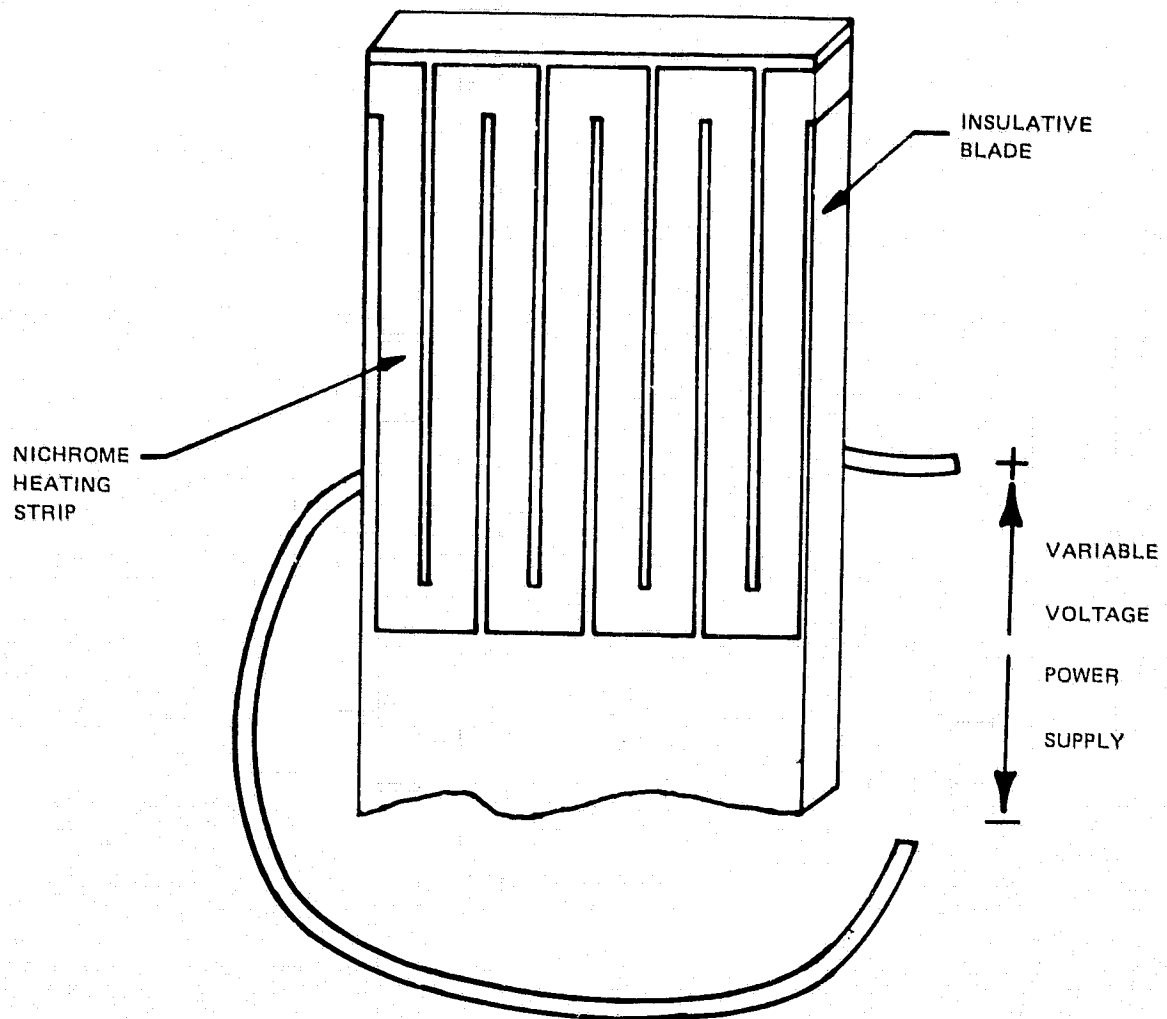


Figure 5. Specimen for Convective Heat Transfer Coefficient Evaluation Testing

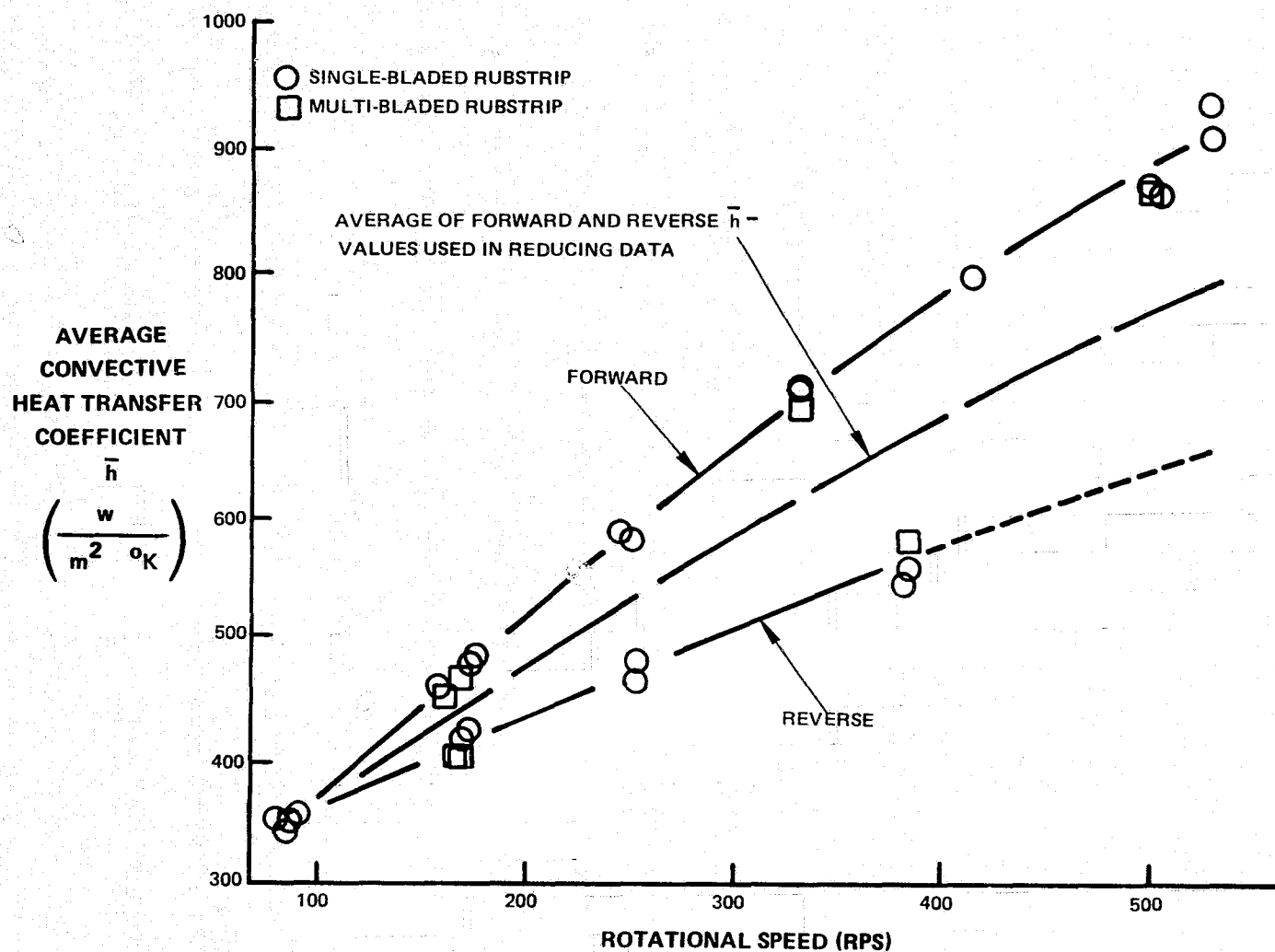


Figure 6. Results of Convective Heat Transfer Coefficient Evaluation

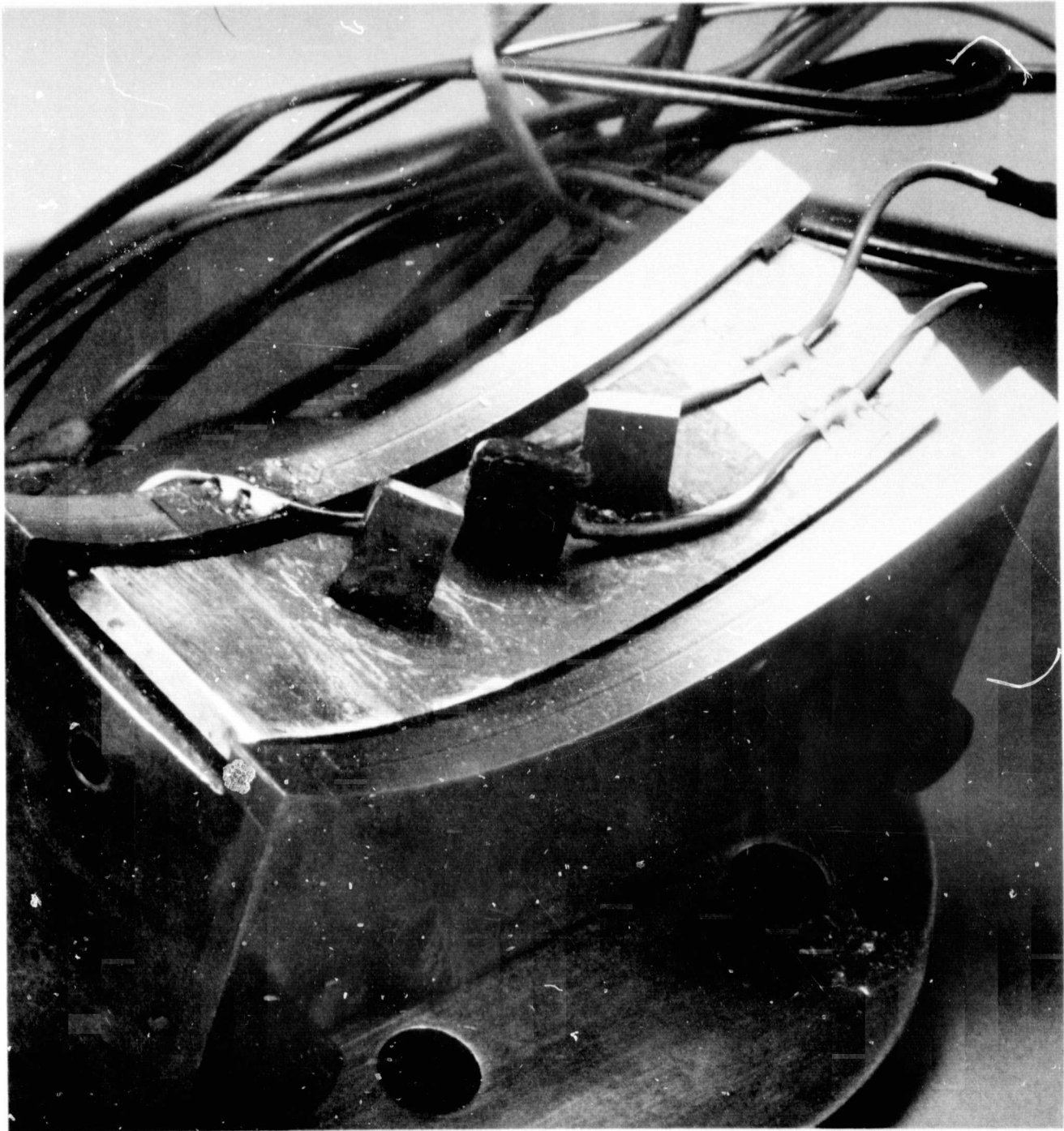


Figure 7. Setup to Determine Multiple Blade Heat Transfer Coefficients

FRICTIONAL RESISTANCE TORQUE IS THE SUM OF
BEARING TORQUE AND WINDAGE TORQUE

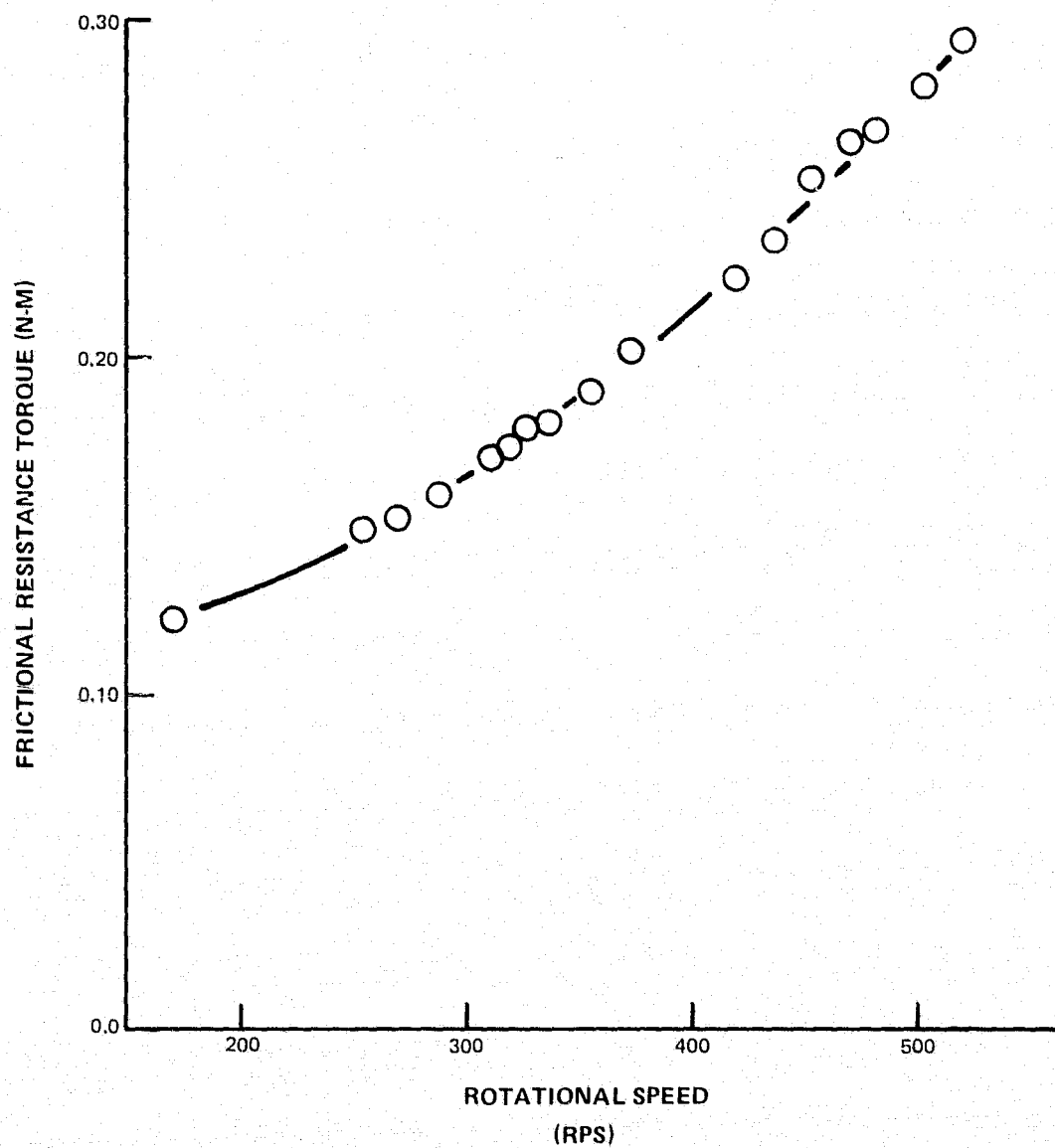
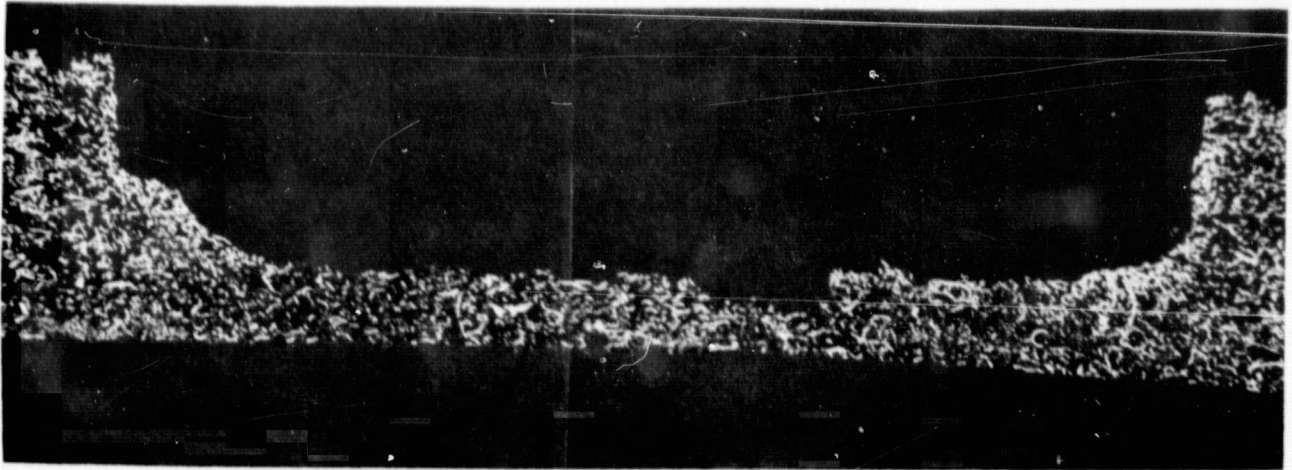
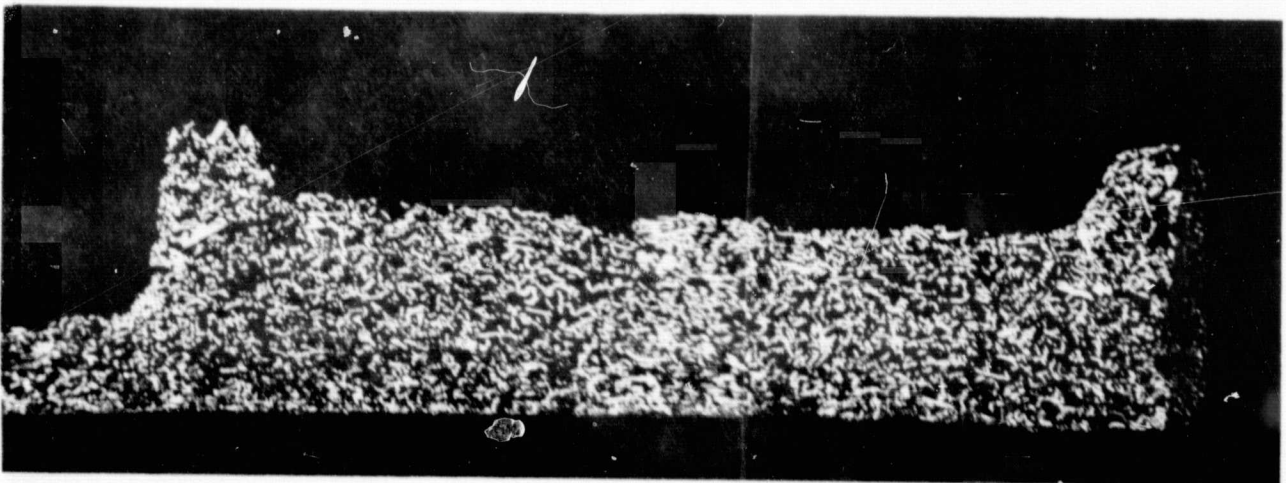


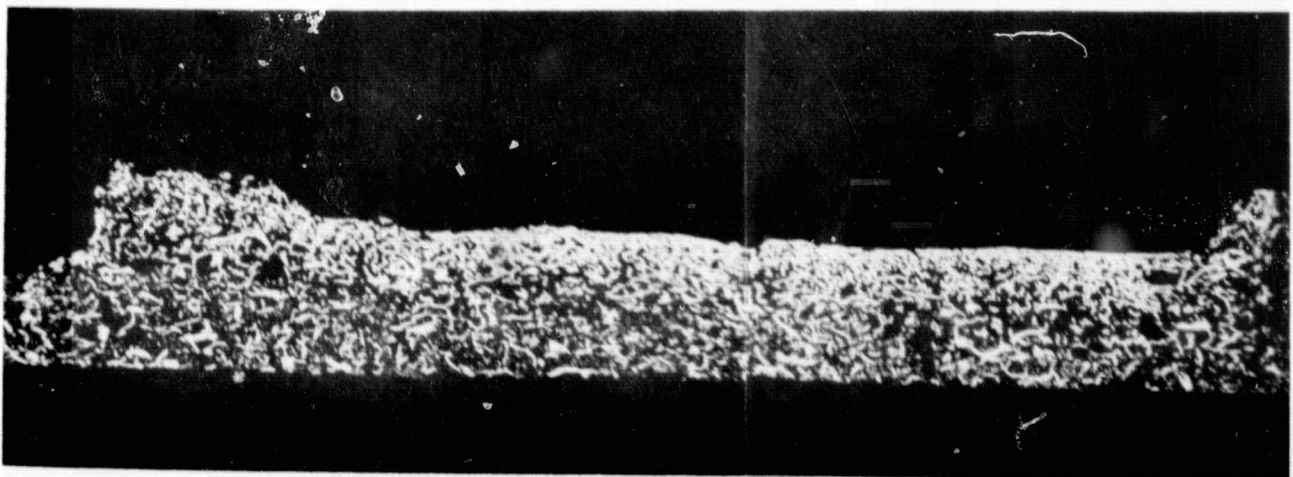
Figure 8. Results of Testing to Determine Frictional Resistance Torque



Test 1 ($i = 0.25$ mm/sec, $v = 213$ mps, $b = 1.78$ mm, $\delta = 1.0$ mm, $\rho = 19\%$)

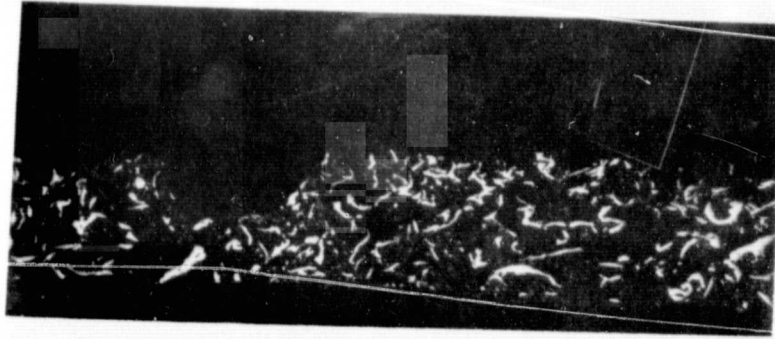


Test 2 ($i = 0.0025$ mm/sec, $v = 213$ mps, $b = 0.53$ mm, $\delta = 0.5$ mm, $\rho = 19\%$)

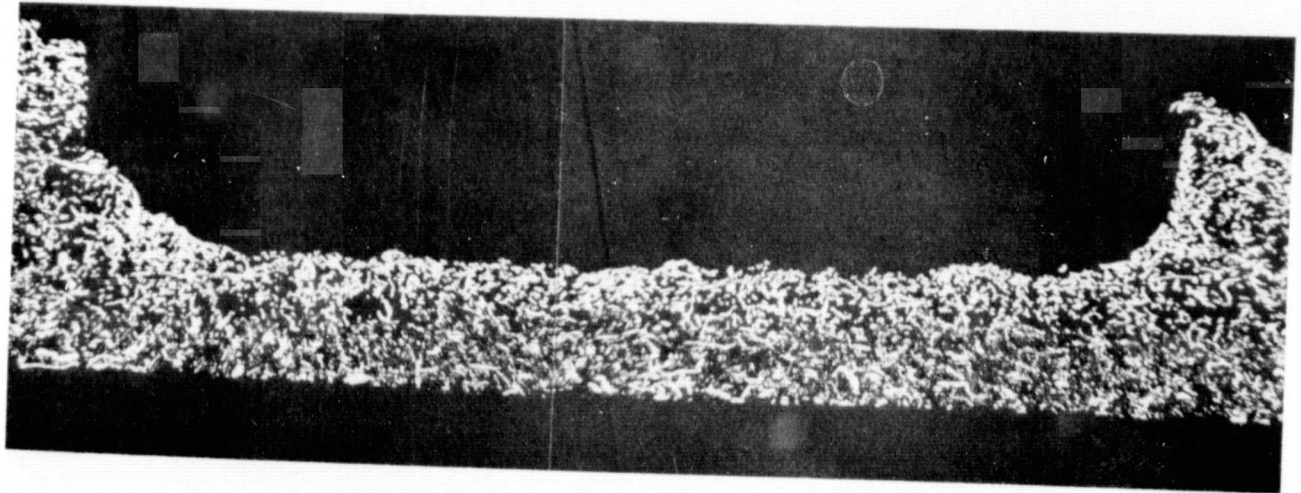


Test 3 ($i = 0.25$ mm/sec, $v = 152$ mps, $b = 0.56$ mm, $\delta = 0.5$ mm, $\rho = 16\%$)

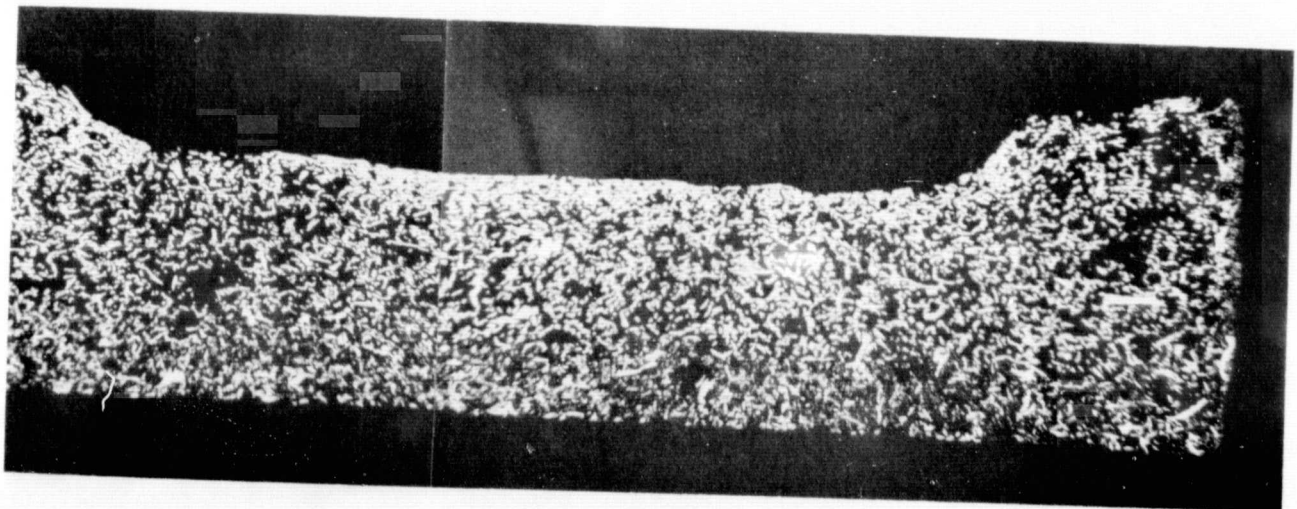
Figure 9. Post Test Cross-sections of Task I Test Seals (Mag: 25x)



Test 4 ($i = 0.025$ mm/sec, $v = 213$ mps, $b = 1.74$ mm, $\delta = 0.5$ mm, $\rho = 16\%$)

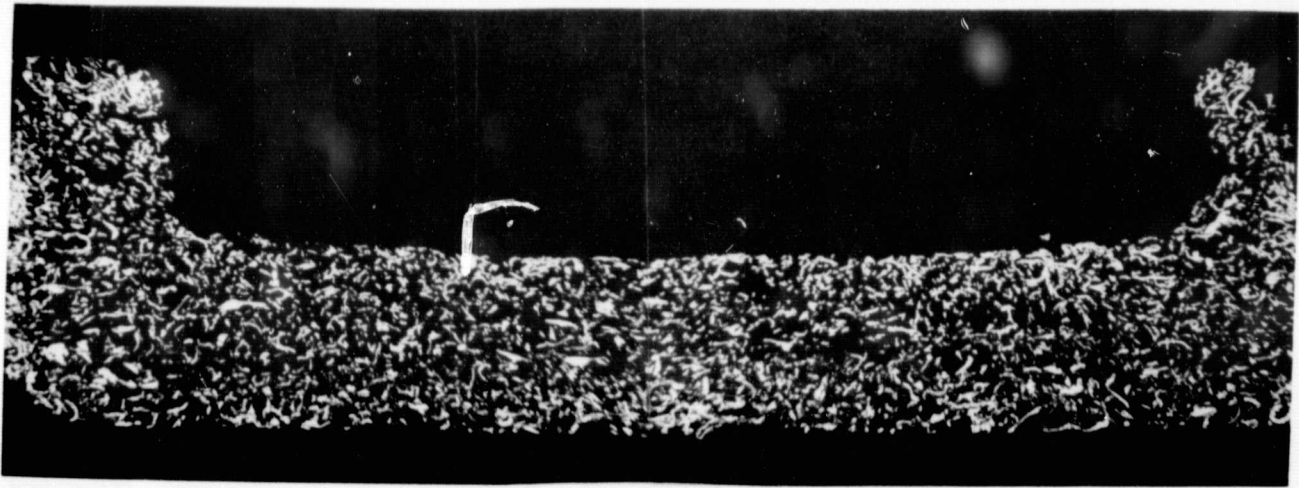


Test 5 ($i = 0.25$ mm/sec, $v = 213$ mps, $b = 1.74$ mm, $\delta = 1.0$ mm, $\rho = 19\%$)

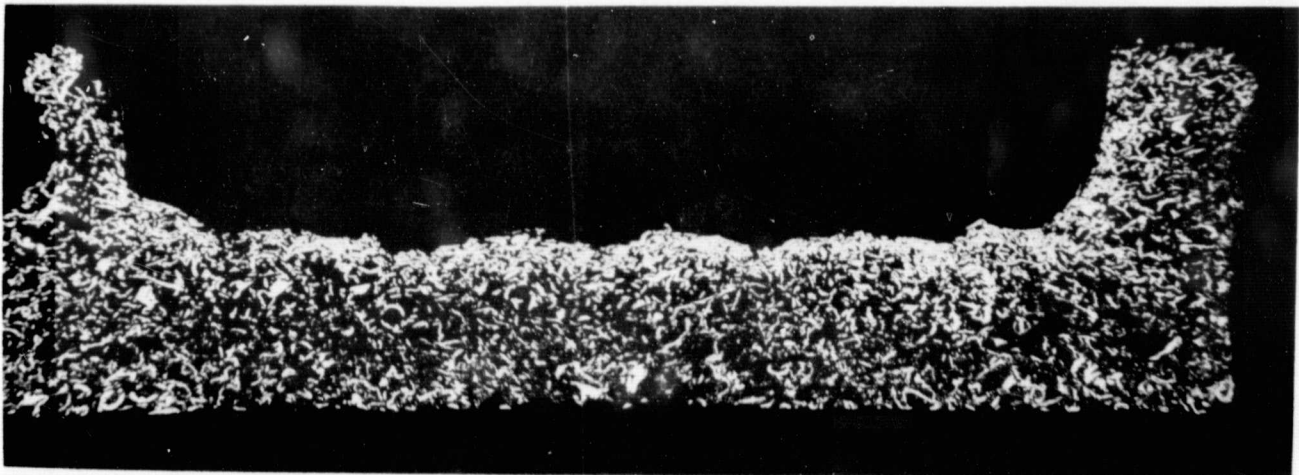


Test 6 ($i = 0.025$ mm/sec, $v = 152$ mps, $b = 0.51$ mm, $\delta = 1.0$ mm, $\rho = 19\%$)

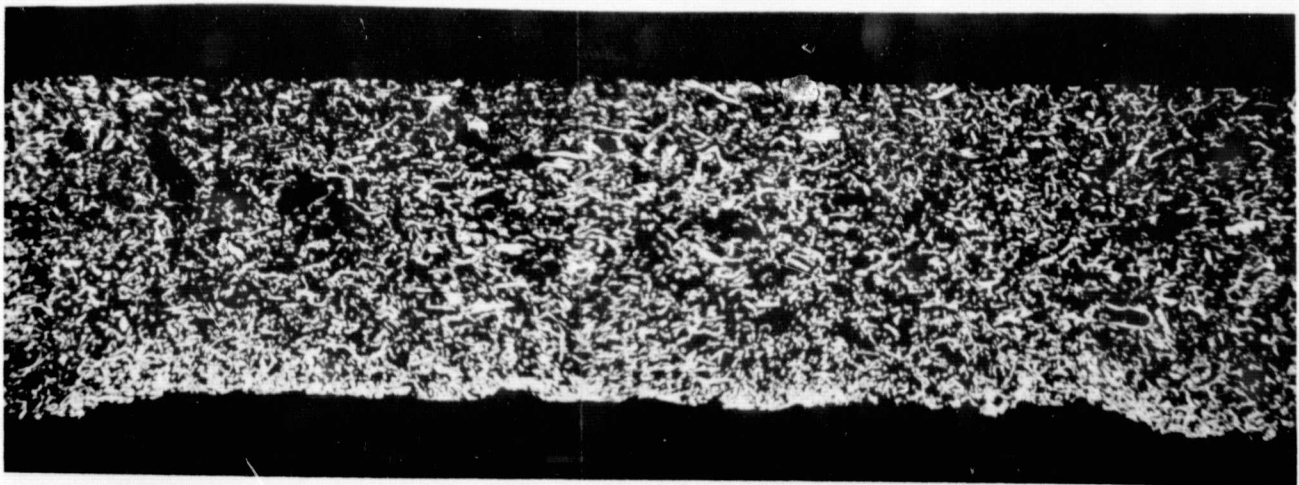
Figure 10. Post Test Cross-sections of Task I Test Seals (Mag: Top 50x, Center and Bottom 25x)



Test 7 ($i = 0.0025$ mm/sec, $v = 152$ mps, $b = 1.75$ mm, $\delta = 1.0$ mm, $\rho = 16\%$)

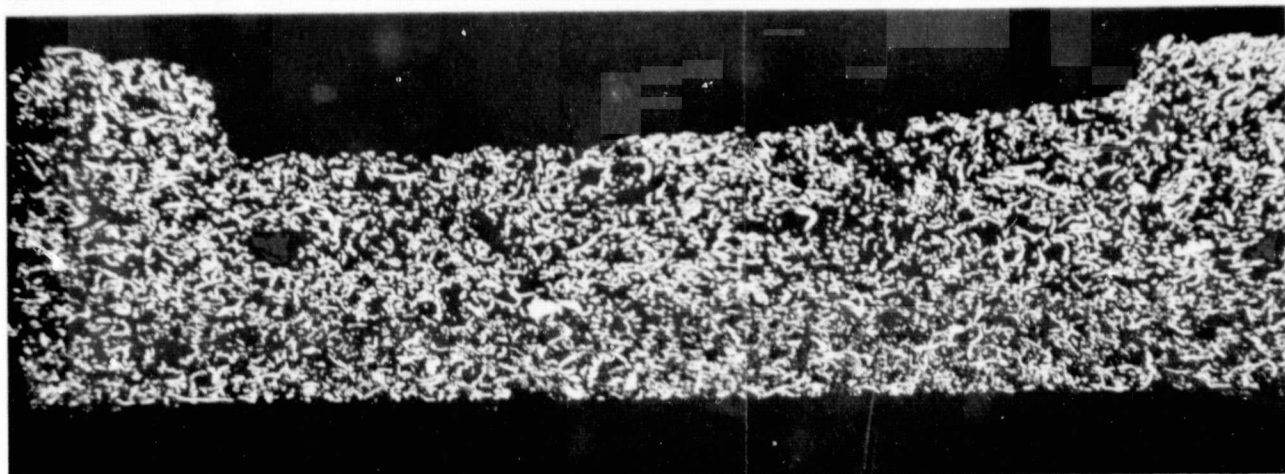


Test 8 ($i = 0.25$ mm/sec, $v = 213$ mps, $b = 0.56$ mm, $\delta = 1.0$ mm, $\rho = 16\%$)

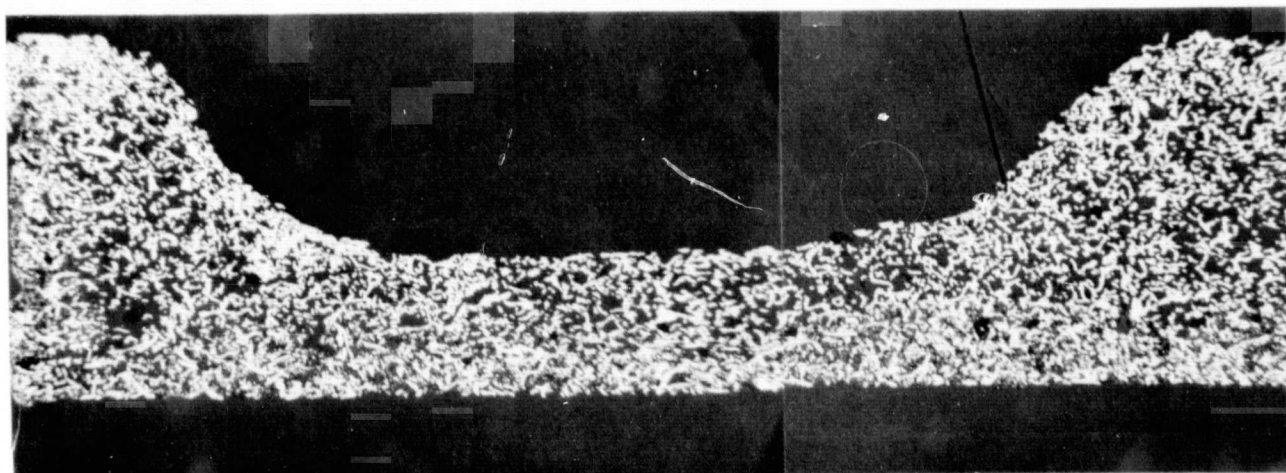


Test 9 ($i = 0.25$ mm/sec, $v = 152$ mps, $b = 1.75$ mm, $\delta = 0.5$ mm, $\rho = 19\%$)

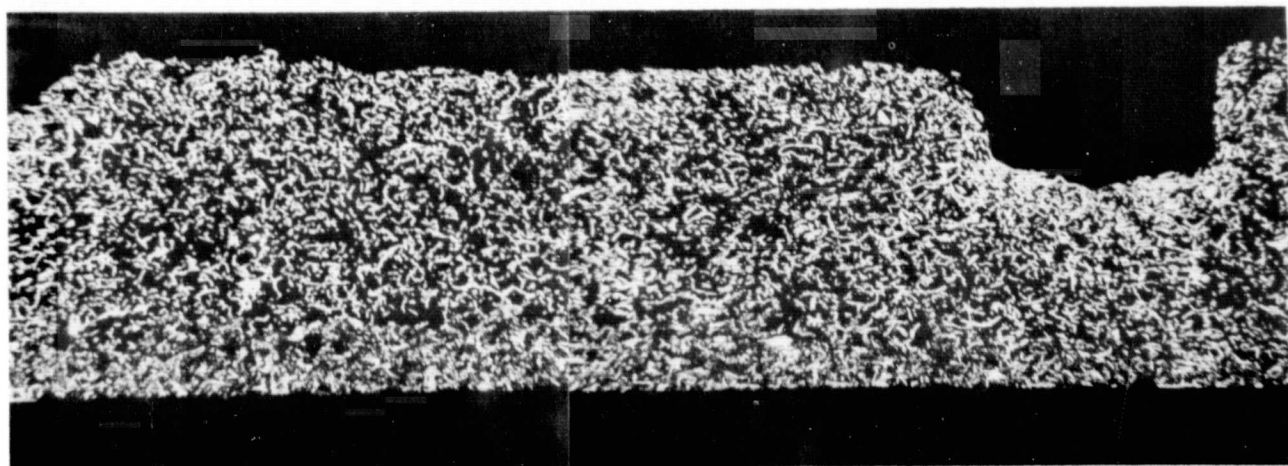
Figure 11. Post Test Cross-sections of Task I Test Seals (Mag: 25x)



Test 10 ($i = 0.0025$ mm/sec, $v = 213$ mps, $b = 0.52$ mm, $\delta = 0.5$ mm, $\rho = 19\%$)

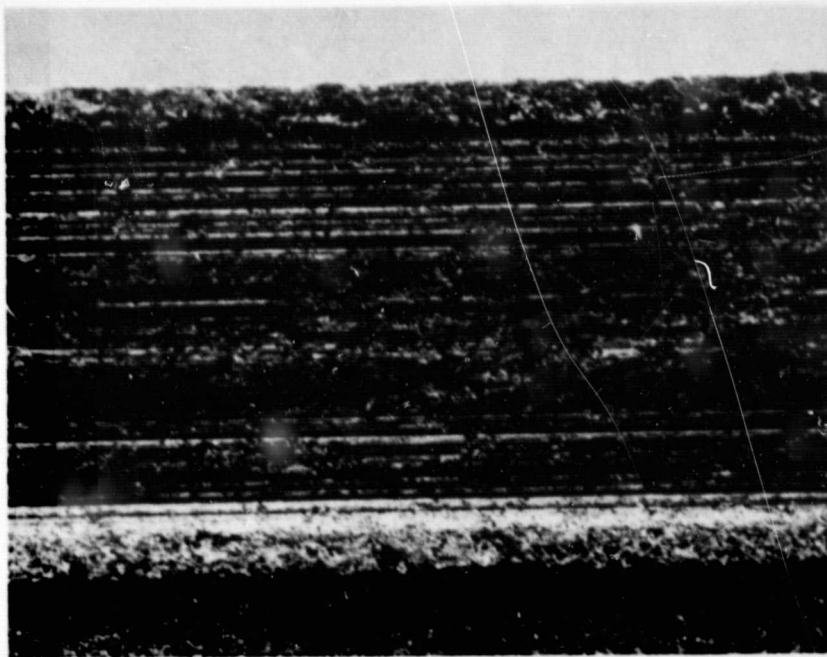


Test 11 ($i = 0.025$ mm/sec, $v = 152$ mps, $b = 0.56$ mm, $\delta = 1.0$ mm, $\rho = 19\%$)



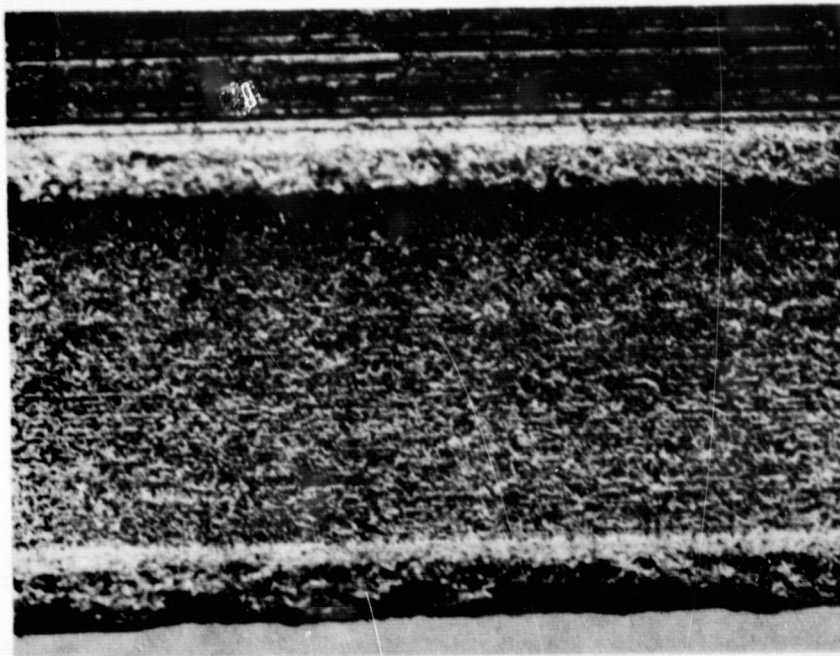
Test 12 ($i = 0.25$ mm/sec, $v = 152$ mps, $b = 0.61$ mm, $\delta = 1.0$ mm, $\rho = 19\%$)

Figure 12. Post Test Cross-sections of Task I Test Seals (Mag: 25x)



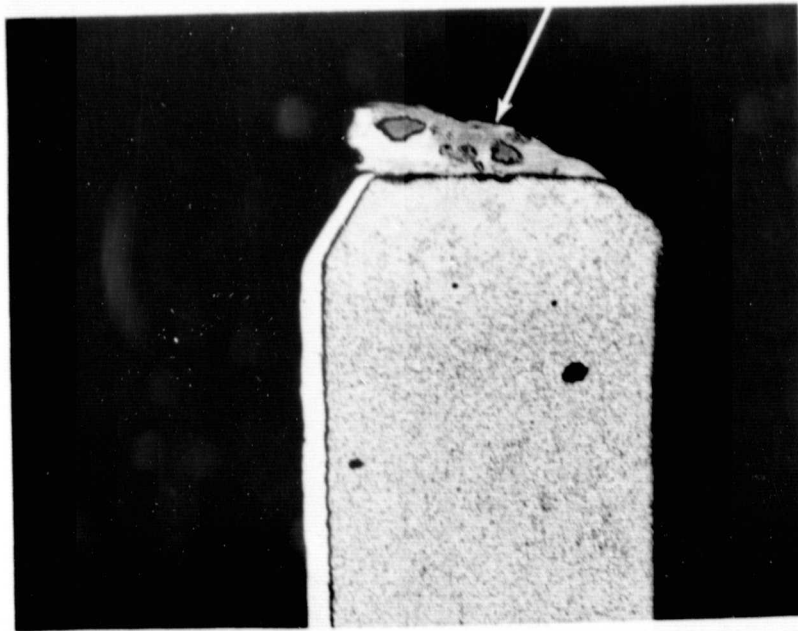
ORIGINAL PAGE IS
OF POOR QUALITY

Test 9 ($i = 0.25$ mm/sec, $v = 152$ mps, $b = 1.75$ mm, $\delta = 0.5$ mm, $\rho = 19\%$)



Test 10 ($i = 0.0025$ mm/sec, $v = 213$ mps, $b = 0.52$ mm, $\delta = 0.5$ mm, $\rho = 19\%$)

Figure 13. Photographs of Hastelloy X Fibermetal Abradable Seals Showing Typical Rub Surface Condition After Rub Interaction With PWA 1204 Blades. Note the smeared appearance and deep grooves on the seal from Test 9 (Mag: 10x)



100X

Test 11 ($i = 0.025$ mm/sec, $v = 152$ mps, $b = 0.56$ mm, $\delta = 1.0$ mm, $\rho = 19\%$)

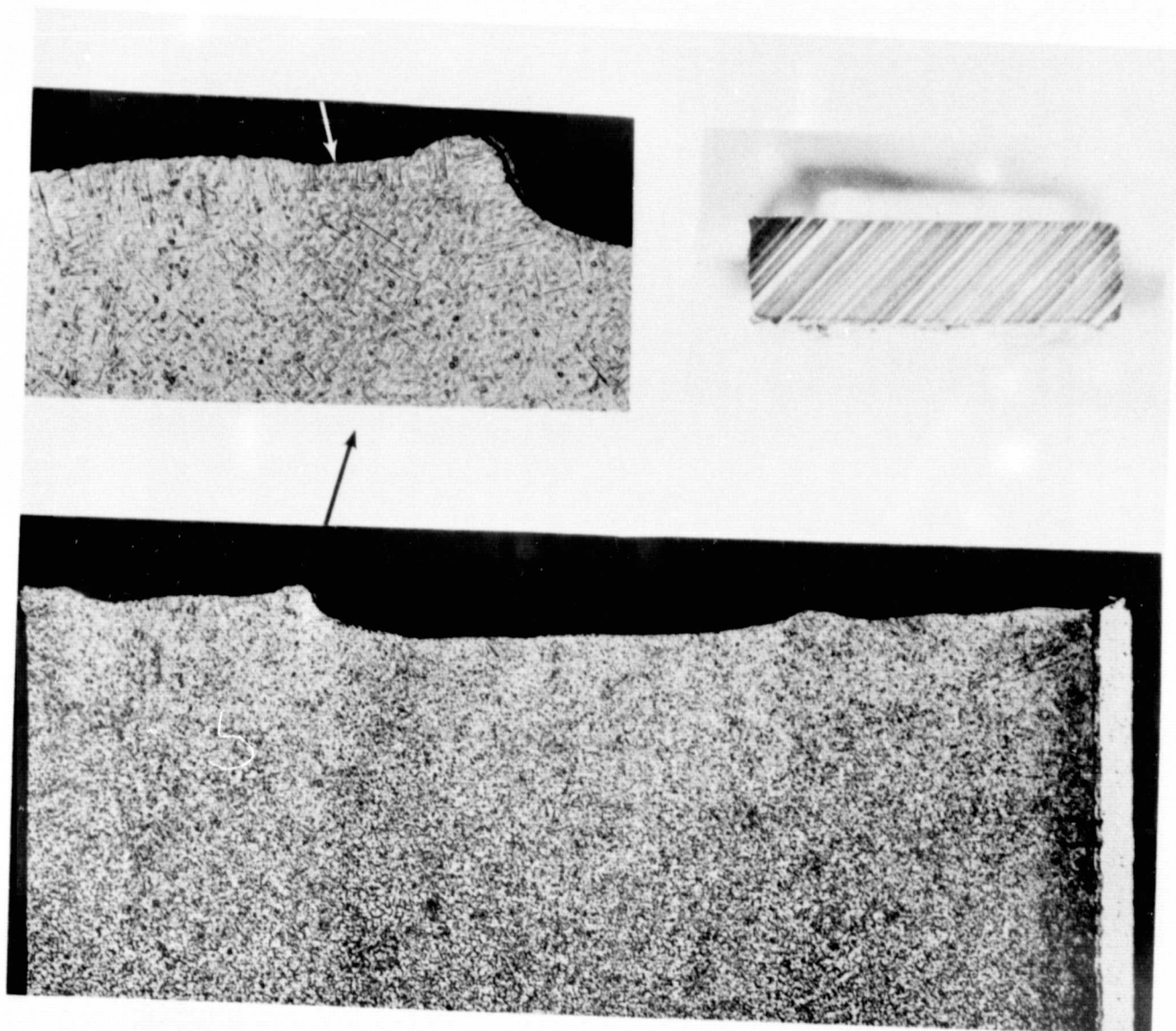
Figure 14. Transverse Section Through Test Blade #11 Showing Transfer (Mag: 100x)

ORIGINAL PAGE IS
OF POOR QUALITY



Test 1 ($i = 0.25$ mm/sec, $v = 213$ mps, $b = 1.78$ mm, $\delta = 1.0$ mm, $\rho = 19\%$)

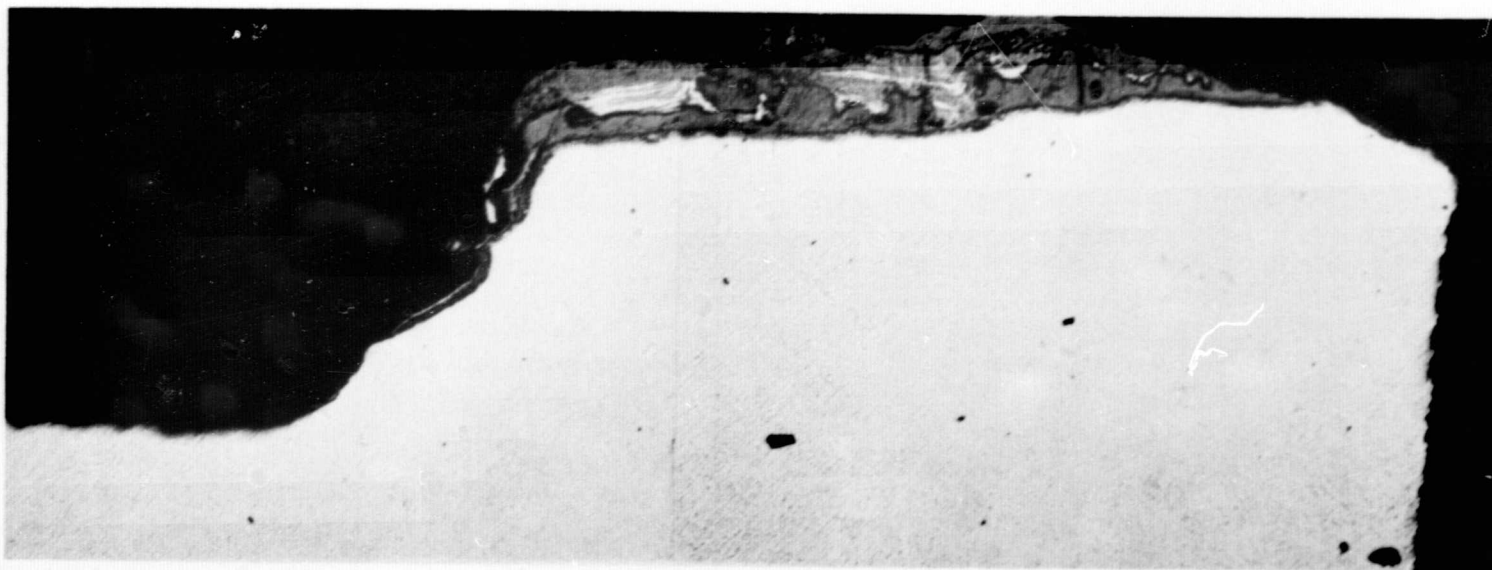
Figure 15. Top View of Test Blade #1 Showing Transfer



Test 9 ($i = 0.25$ mm/sec, $v = 152$ mps, $b = 1.75$ mm, $\delta = 0.5$ mm, $\rho = 19\%$)

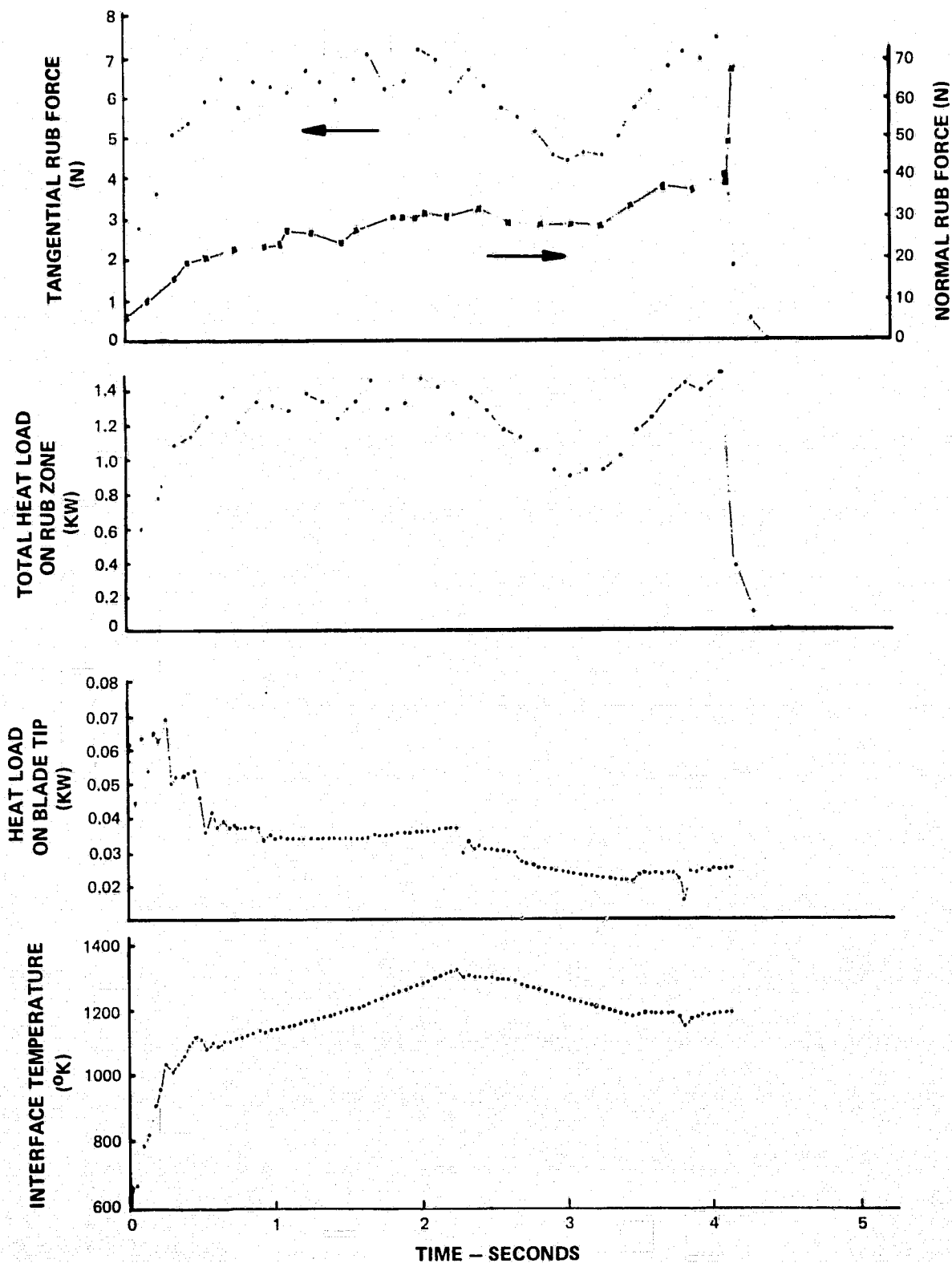
Figure 16. Transverse Section Through Tip of PWA 1204 Blade from Test 9 (Mag: Top Left 250x, Top Right 10x, Bottom 100x)

ORIGINAL PAGE IS
OF POOR QUALITY



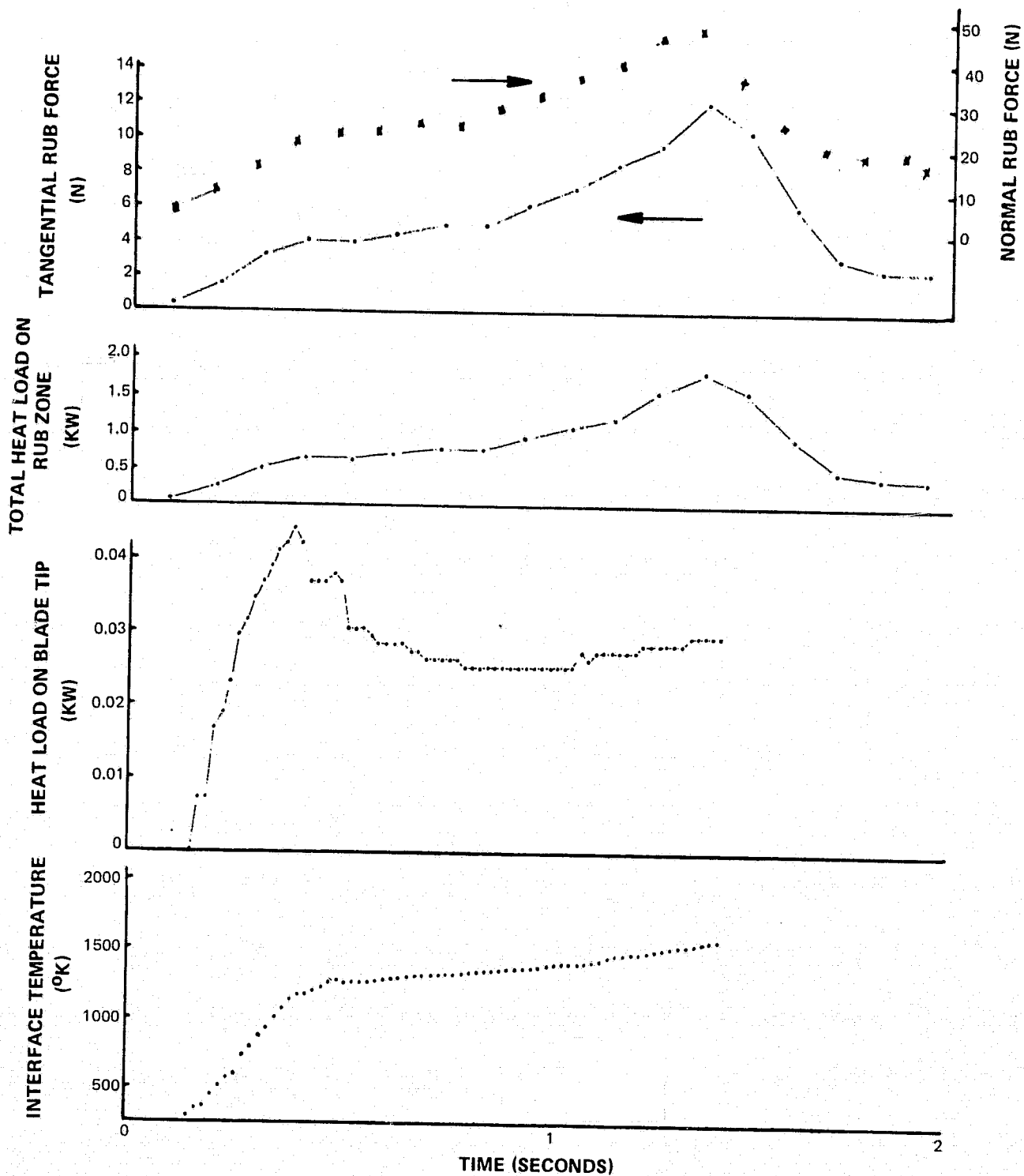
Test 12 ($i = 0.25$ mm/sec, $v = 152$ mps, $b = 0.61$ mm, $\delta = 1.0$ mm, $\rho = 19\%$)

Figure 17. Longitudinal Section Through Tip of PWA 1204 Blade from Test 12 (Mag: 100x)



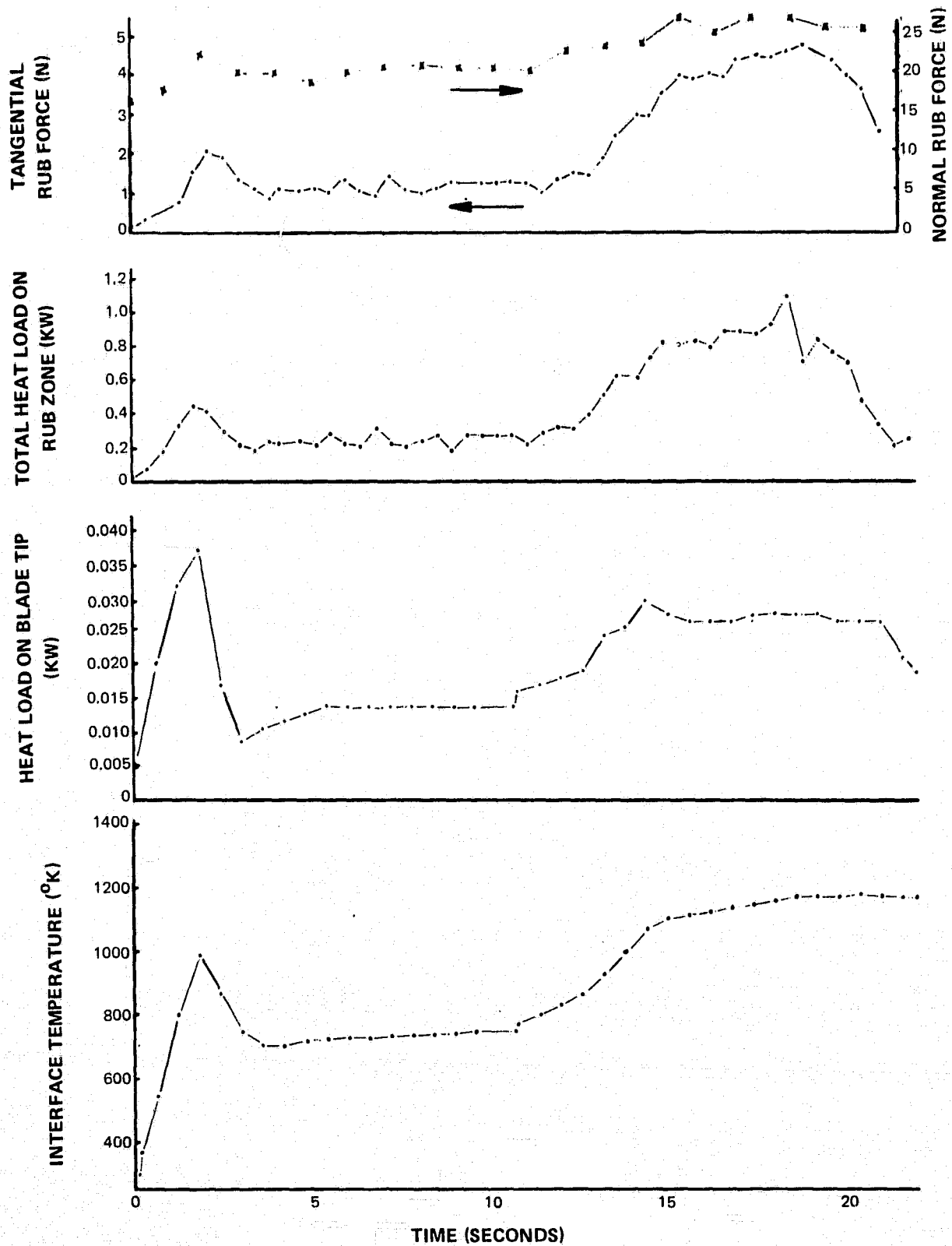
Test 1 ($i = .25$ mm/sec, $v = 213$ mps, $b = 1.78$ mm, $\delta = 1.0$ mm, $\rho = 19\%$)

Figure 18. Task I Test 1 Data Reduction Results



Test 3 ($i = .25$ mm/sec, $v = 152$ mps, $b = .56$ mm, $\delta = 0.5$ mm, $\rho = 16\%$)

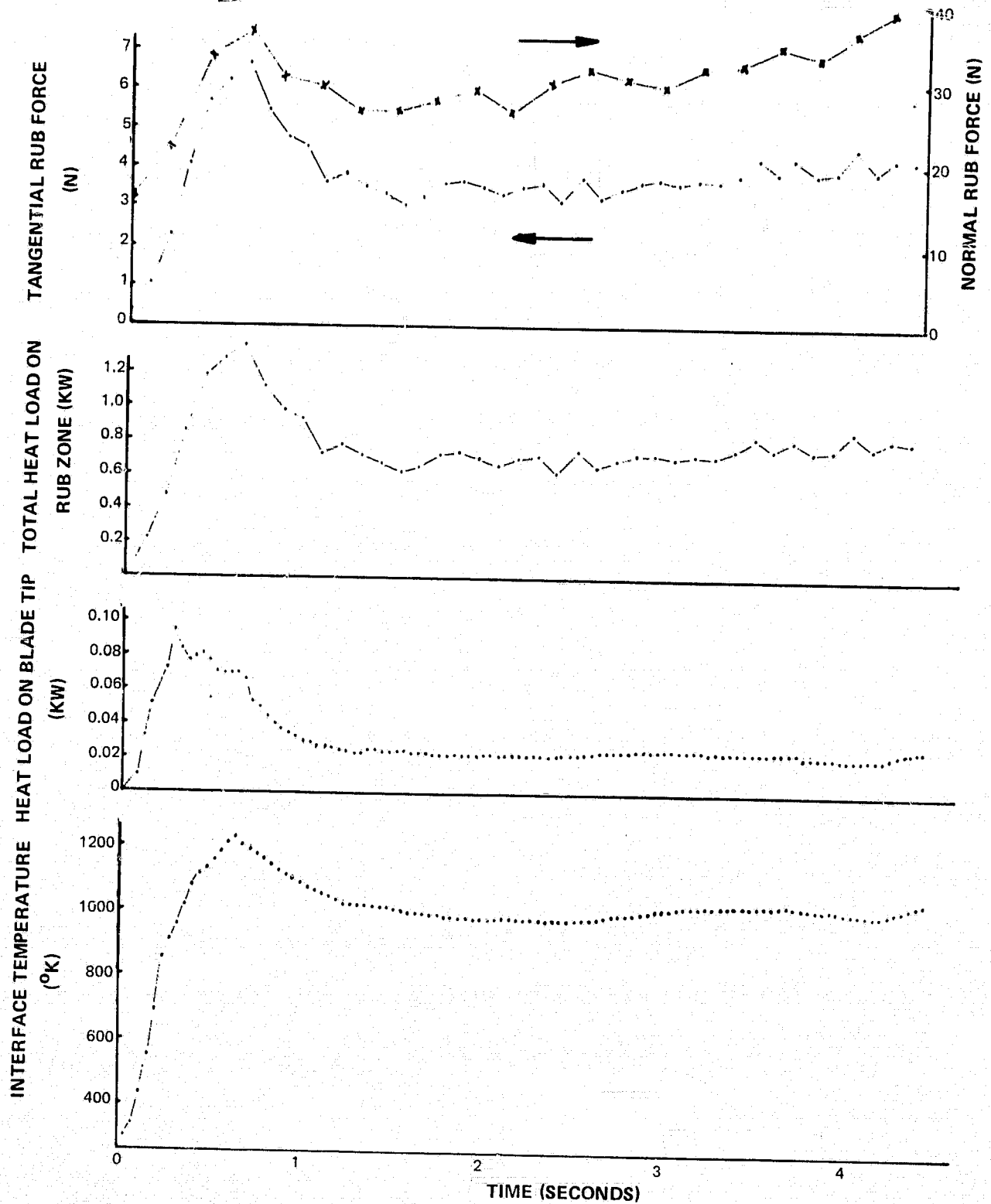
Figure 19. Task I Test 3 Data Reduction Results



Test 4 ($i = .025$ mm/sec, $v = 213$ mps, $b = 1.74$, $\delta = 0.5$ mm, $\rho = 16\%$)

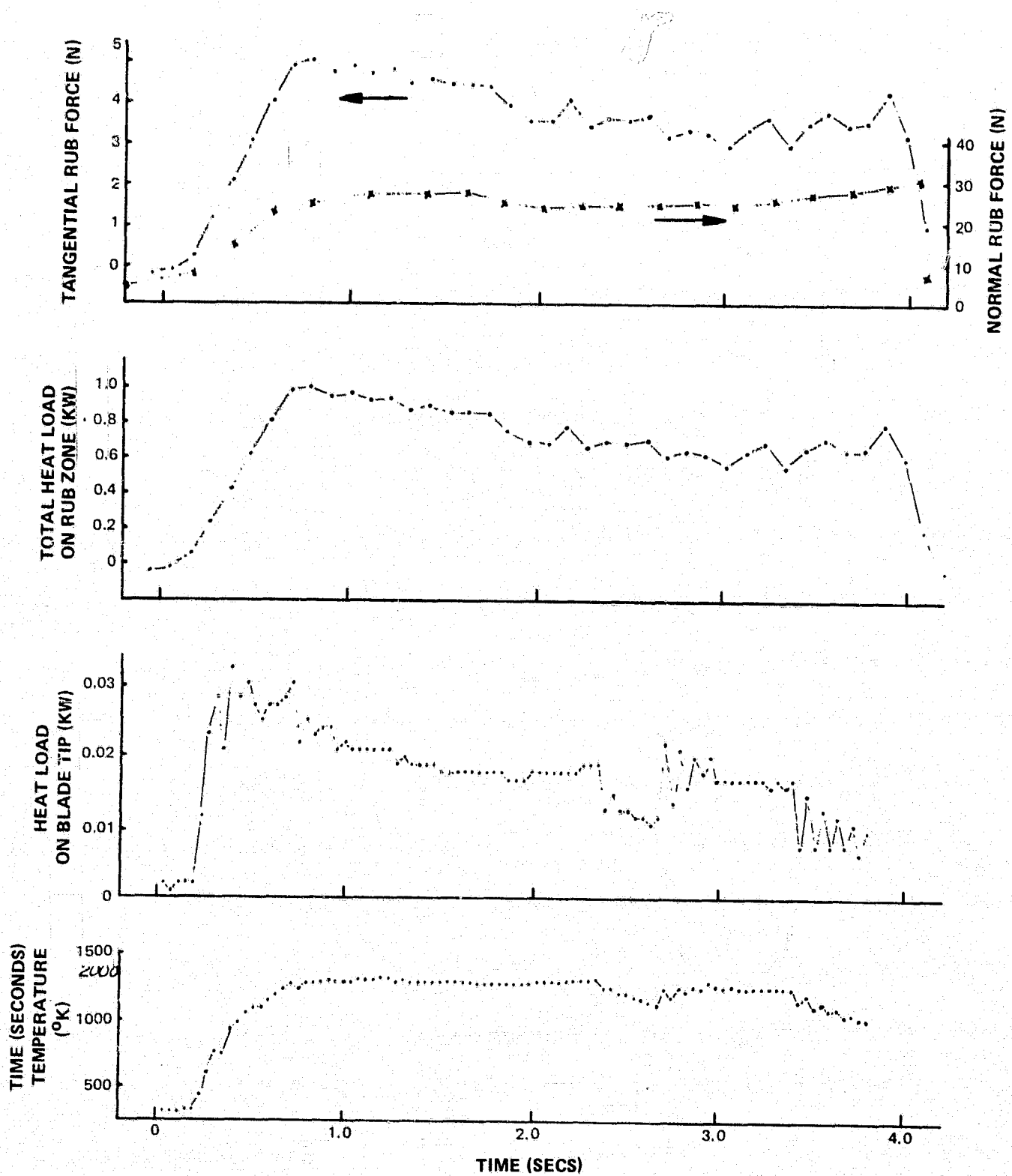
Figure 20. Task I Test 4 Data Reduction Results

ORIGINAL PAGE IS
OF POOR QUALITY



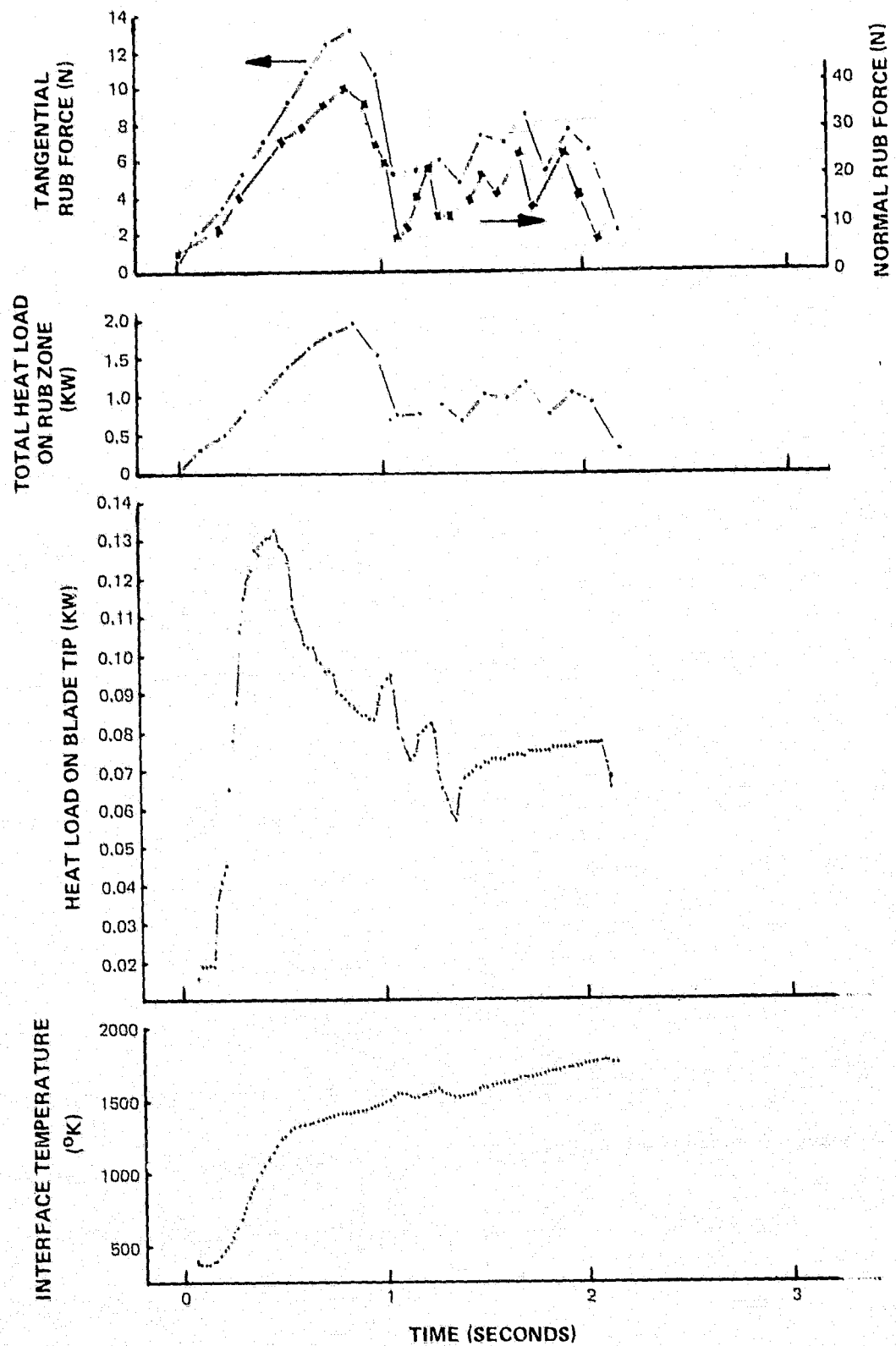
Test 5 ($i = .25$ mm/sec, $v = 213$ mps, $h = 1.74$ mm, $\delta = 1.0$ mm, $\rho = 19\%$)

Figure 21. Task I Test 5 Data Reduction Results



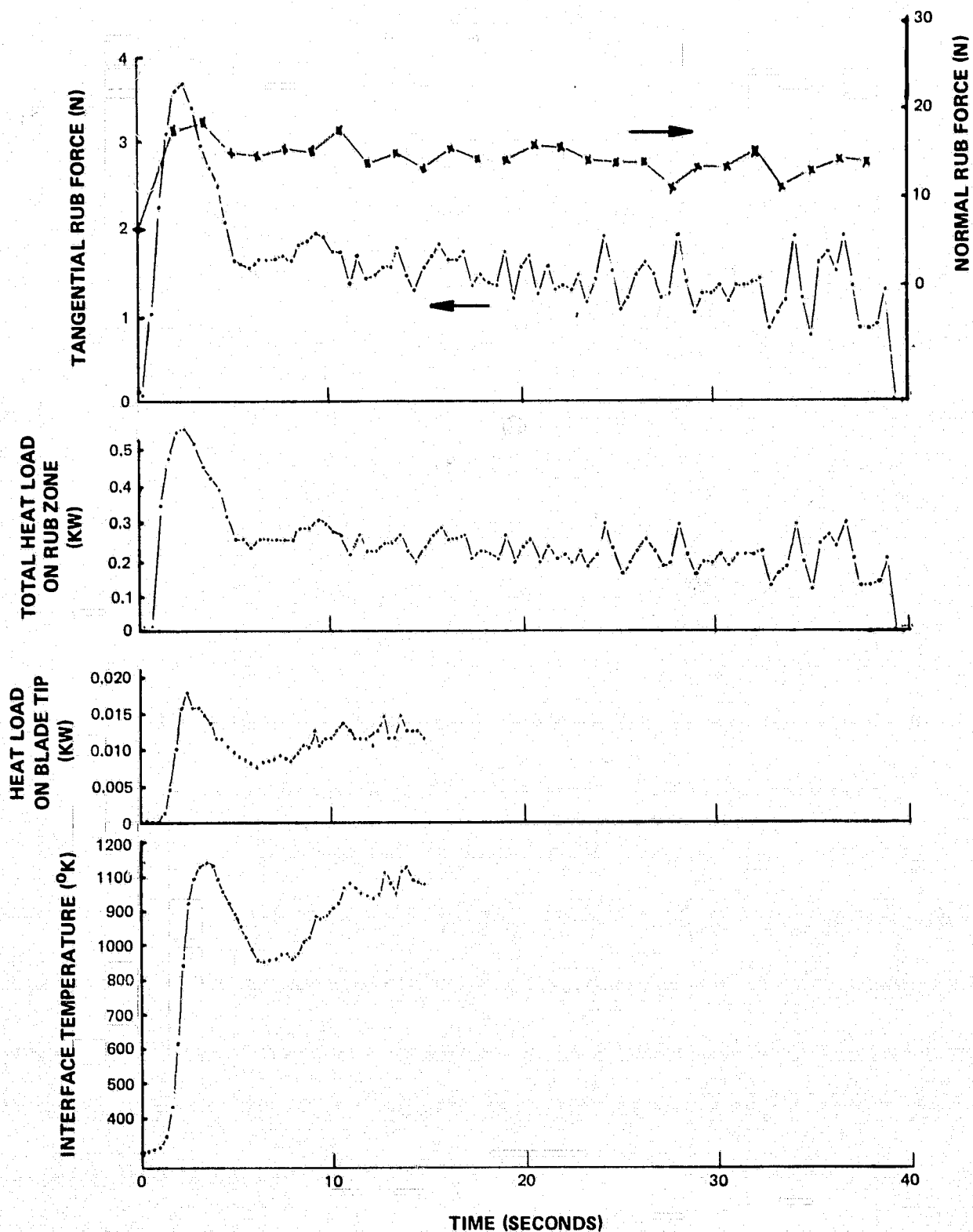
Test 8 ($i = .25$ mm/sec, $v = 213$ mps, $b = .56$ mm, $\delta = 1.0$, $\rho = 16\%$)

Figure 22. Task I Test 8 Data Reduction Results



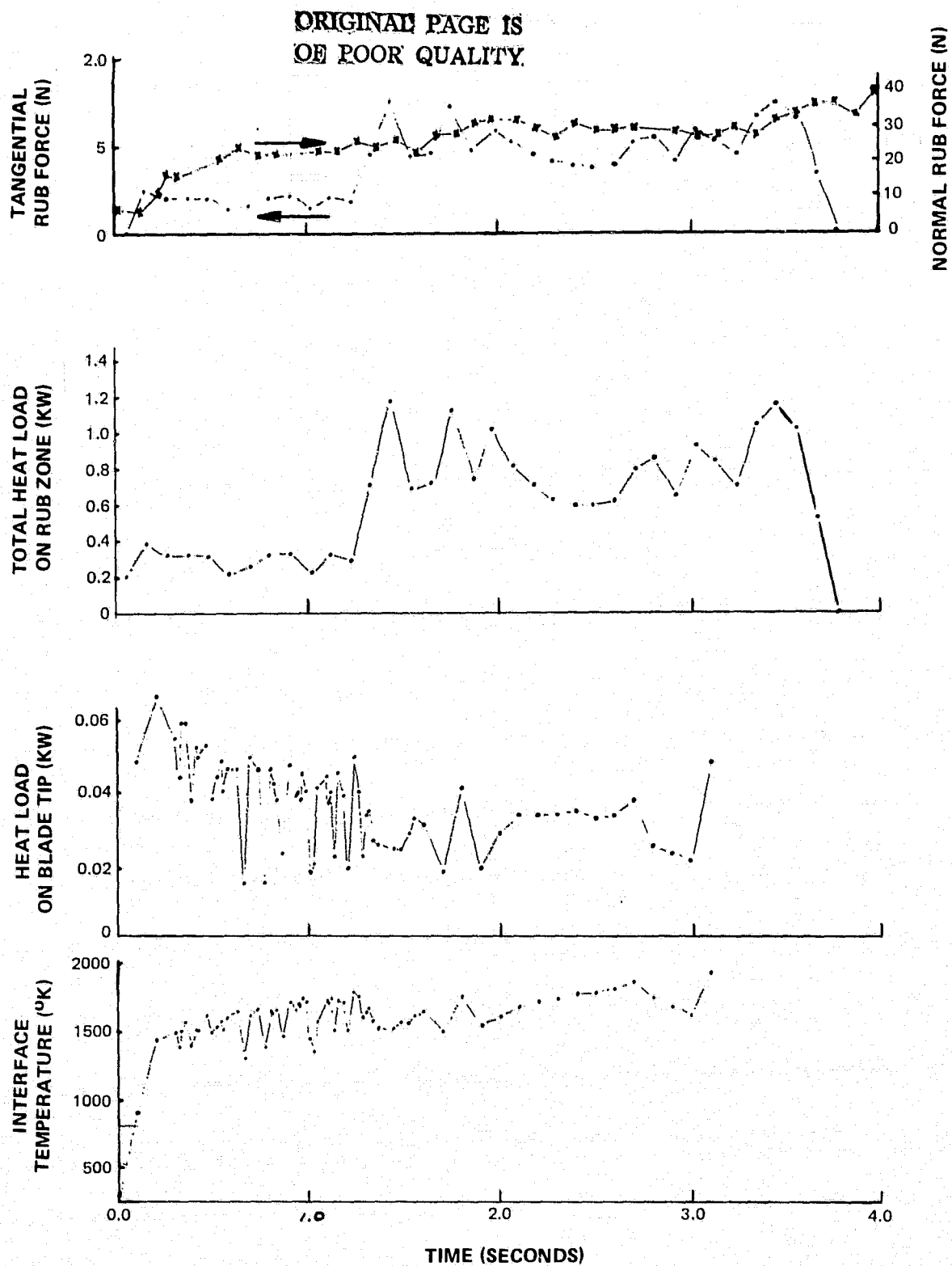
Test 9 ($i = .25$ mm/sec, $v = 152$ mps, $b = 1.75$ mm, $\delta = .5$ mm, $\rho = 19\%$)

Figure 23. Task I Test 9 Data Reduction Results



Test 11 ($i = .025$ mm/sec, $v = 152$ mps, $b = 0.56$ mm, $\delta = 1.0$ mm, $\rho = 19\%$)

Figure 24. Task I Test 11 Data Reduction Results



Test 12 ($i = .25$ mm/sec, $v = 152$ mps, $b = 0.61$ mm, $\delta = 1.0$ mm, $\rho = 19\%$)

Figure 25. Task I Test 12 Data Reduction Results

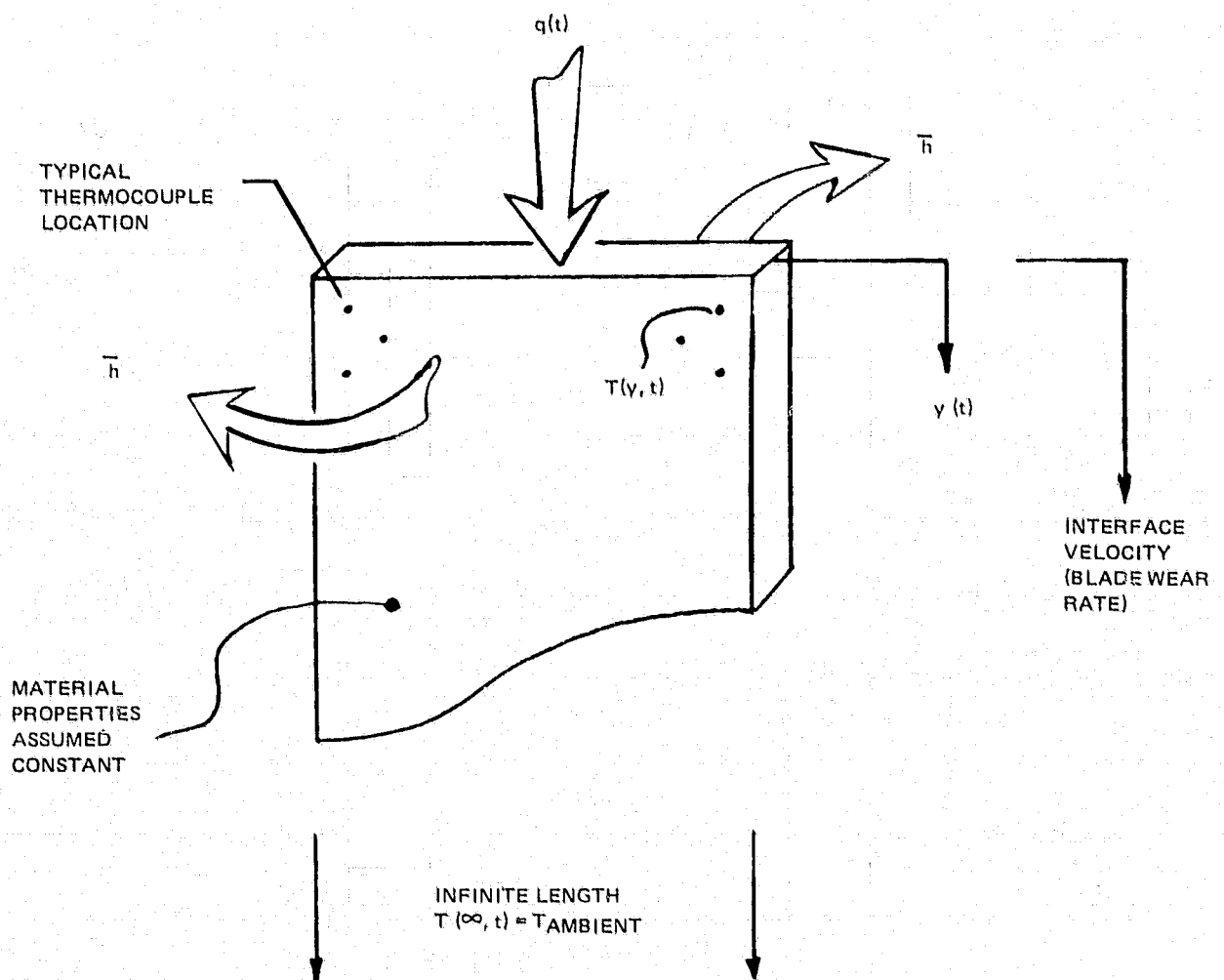


Figure 26. Model for Thermal Analysis of Blade

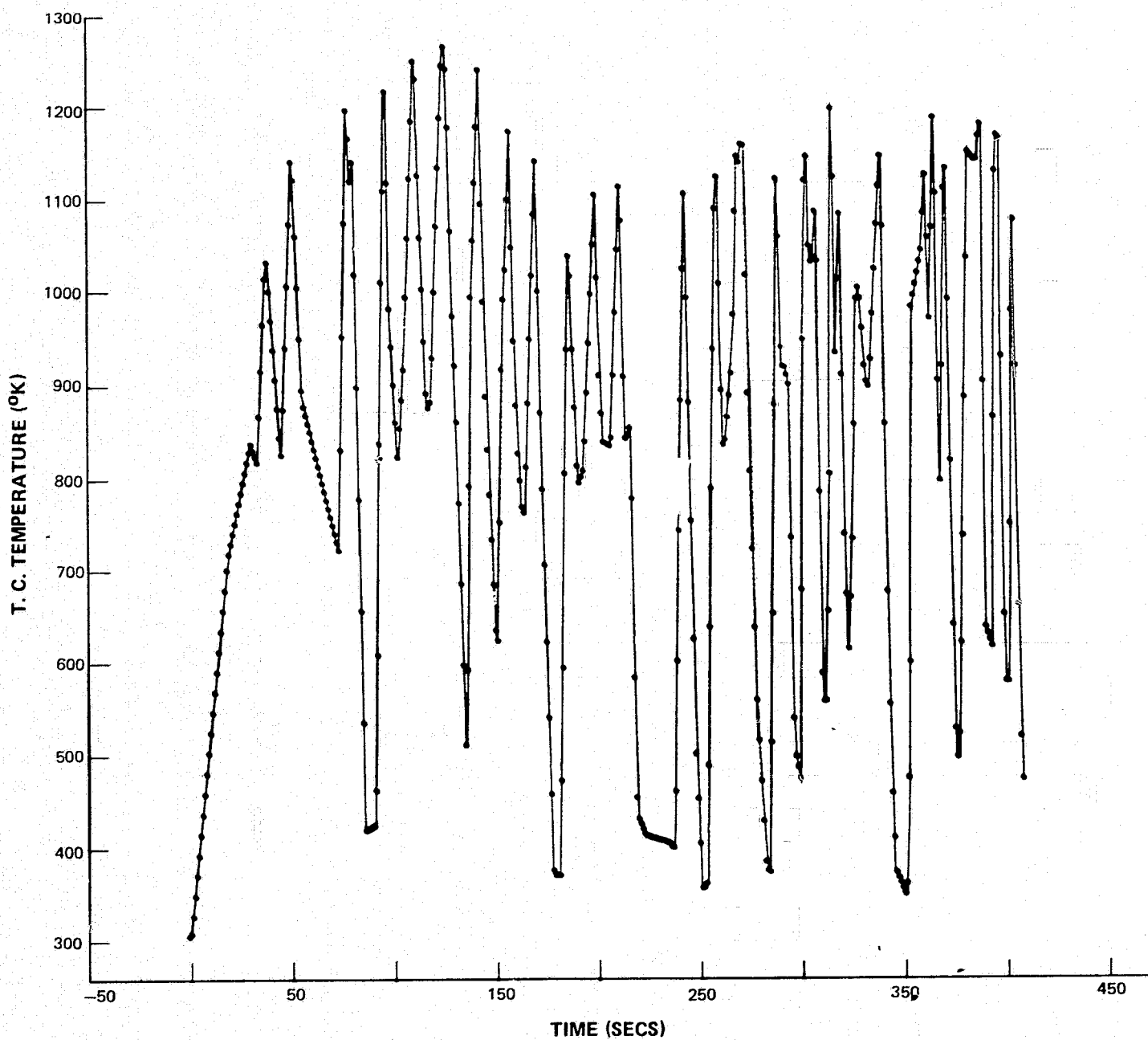


Figure 27. Test 7 – Thermocouple Trace During Test

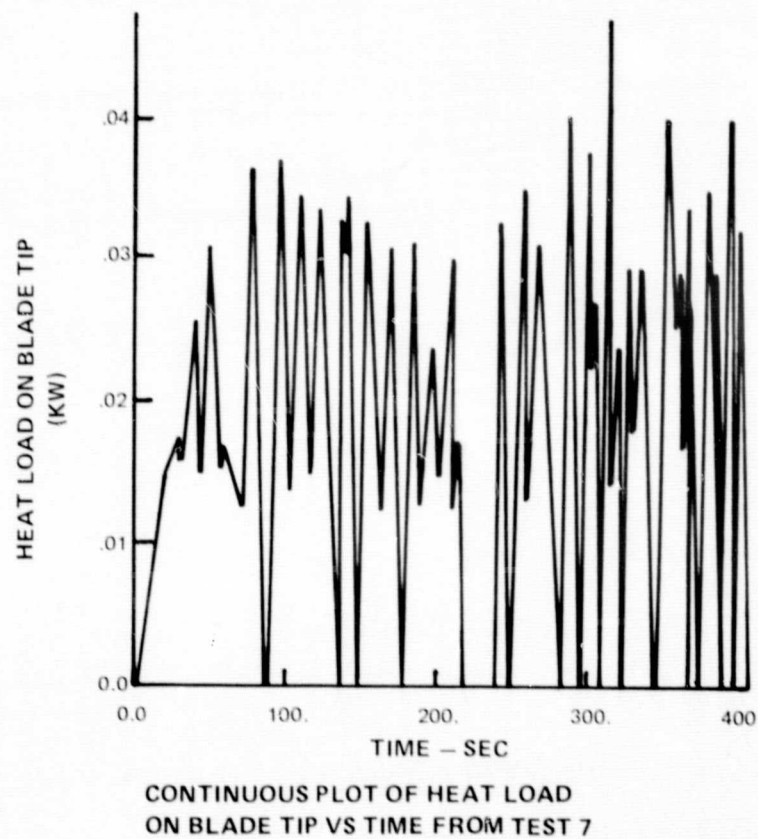
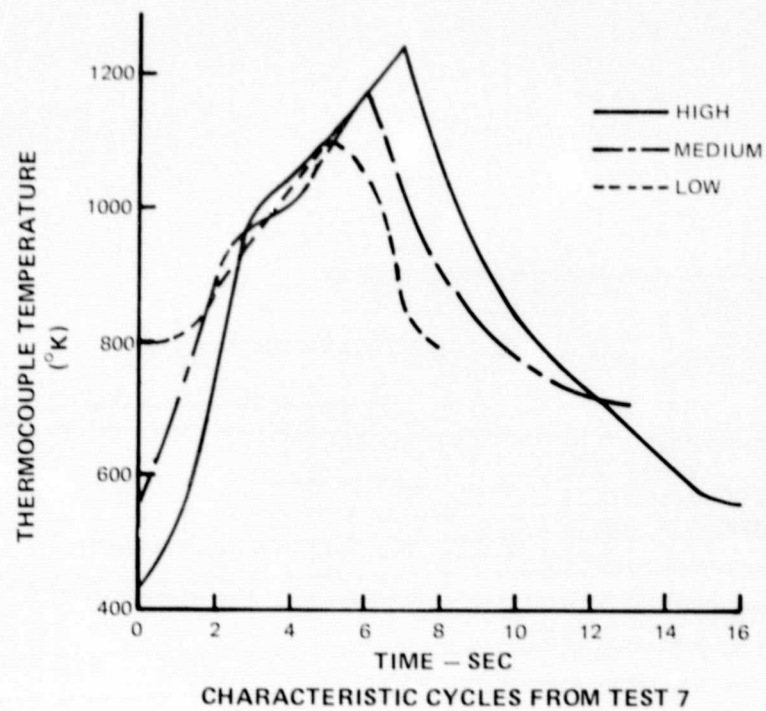
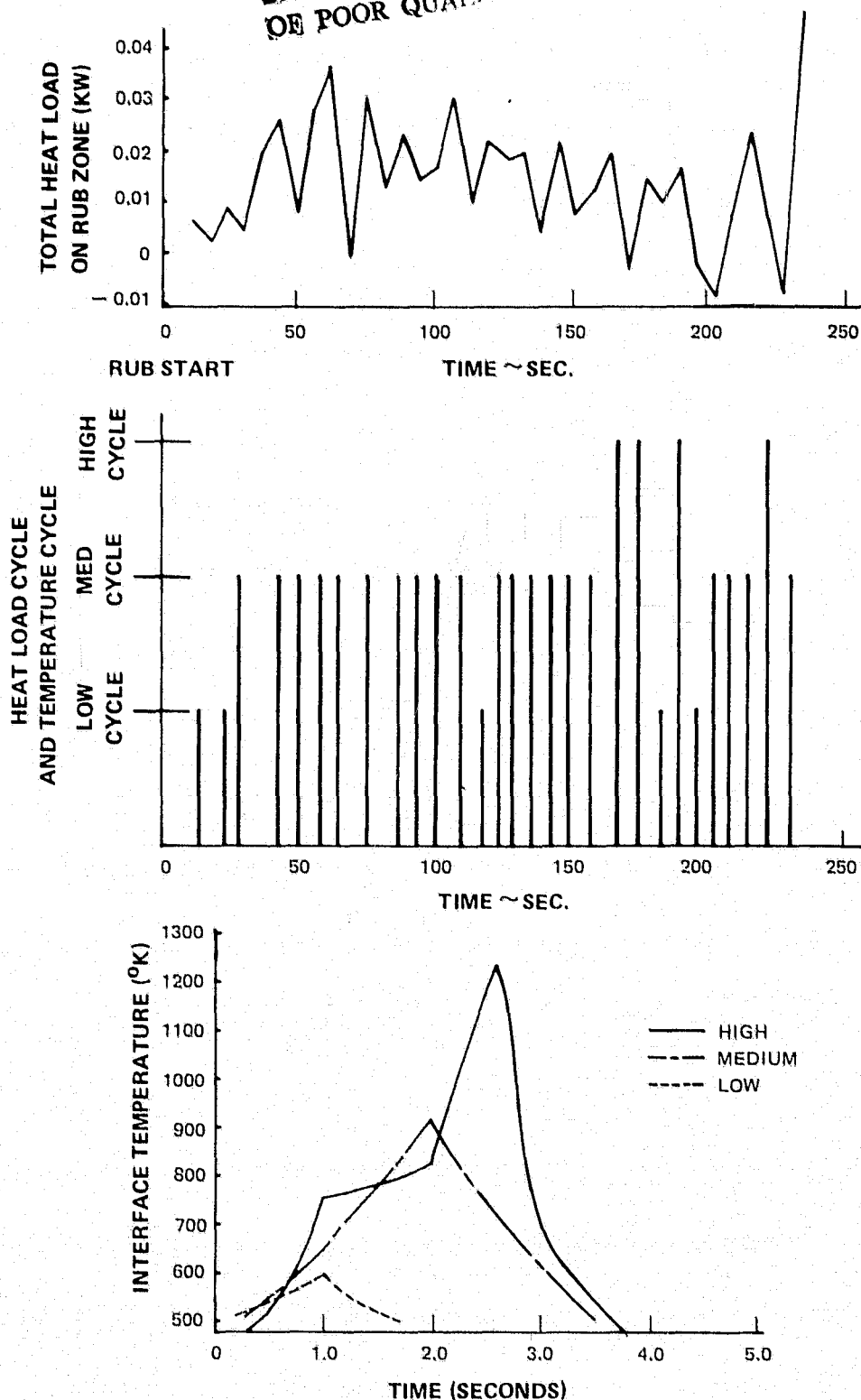


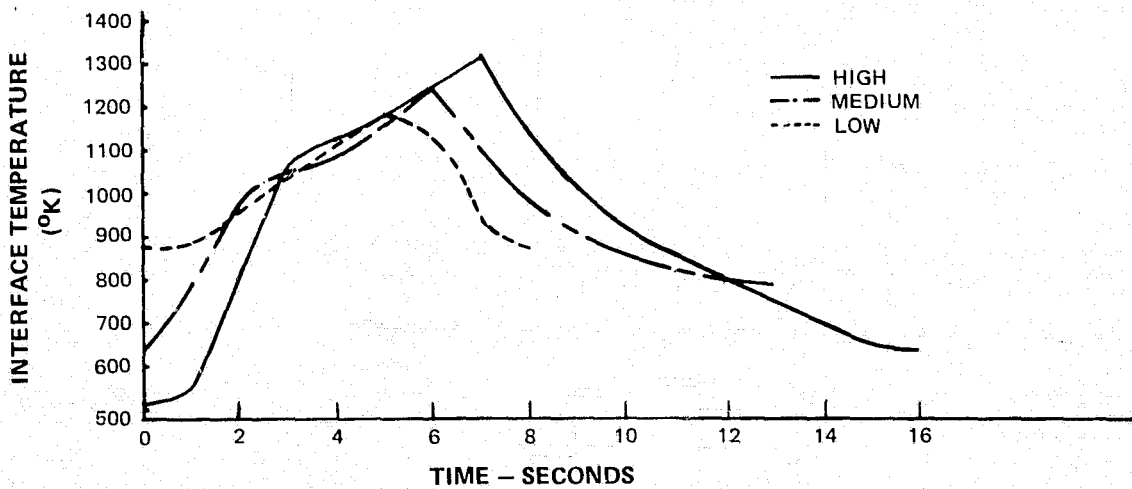
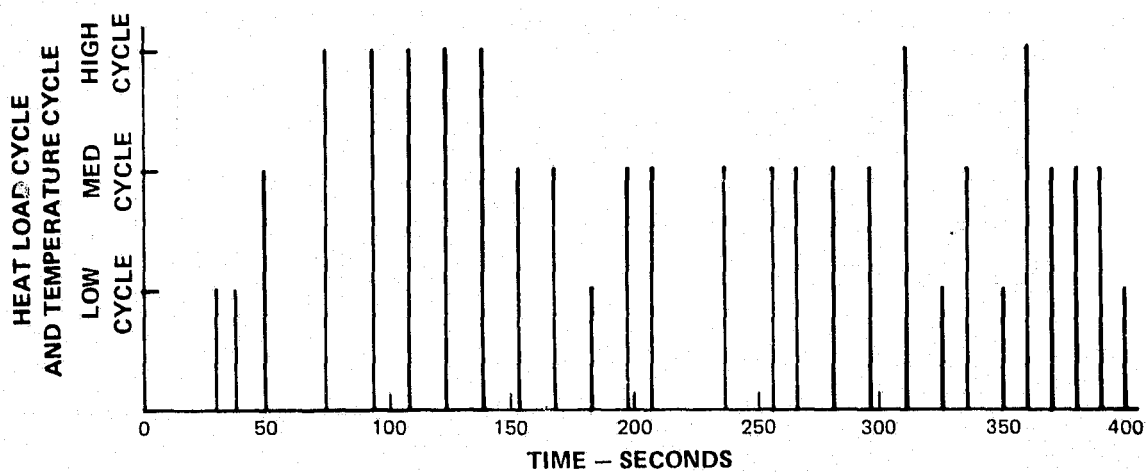
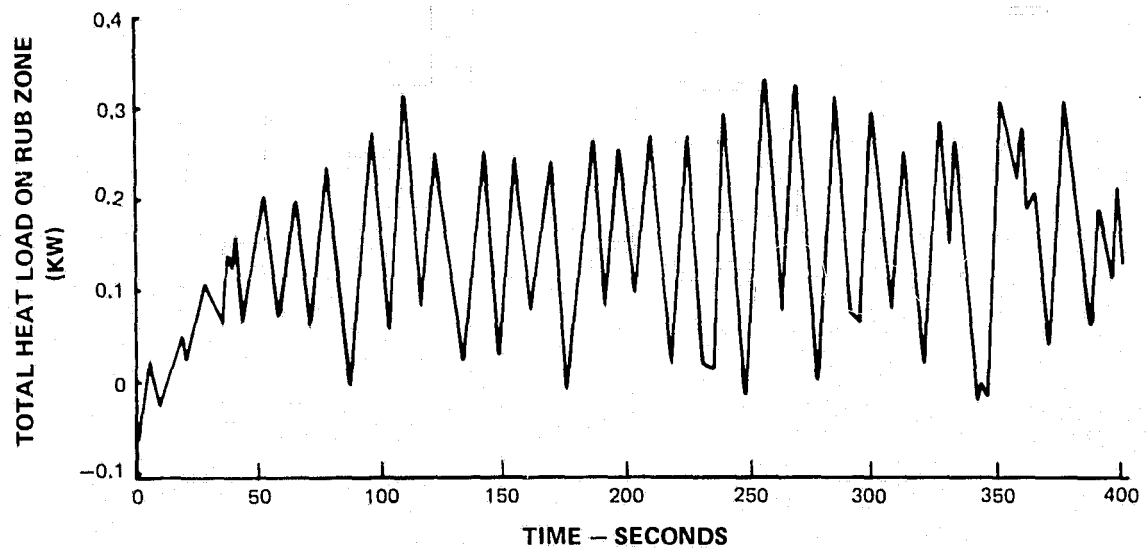
Figure 28. Test 7 - Blade Heating Data Reduction

ORIGINAL PAGE IS
OF POOR QUALITY



Test 2 ($i = .0025$ mm/sec, $v = 213$ mps, $b = .53$ mm, $\delta = 0.5$ mm, $\rho = 19\%$)

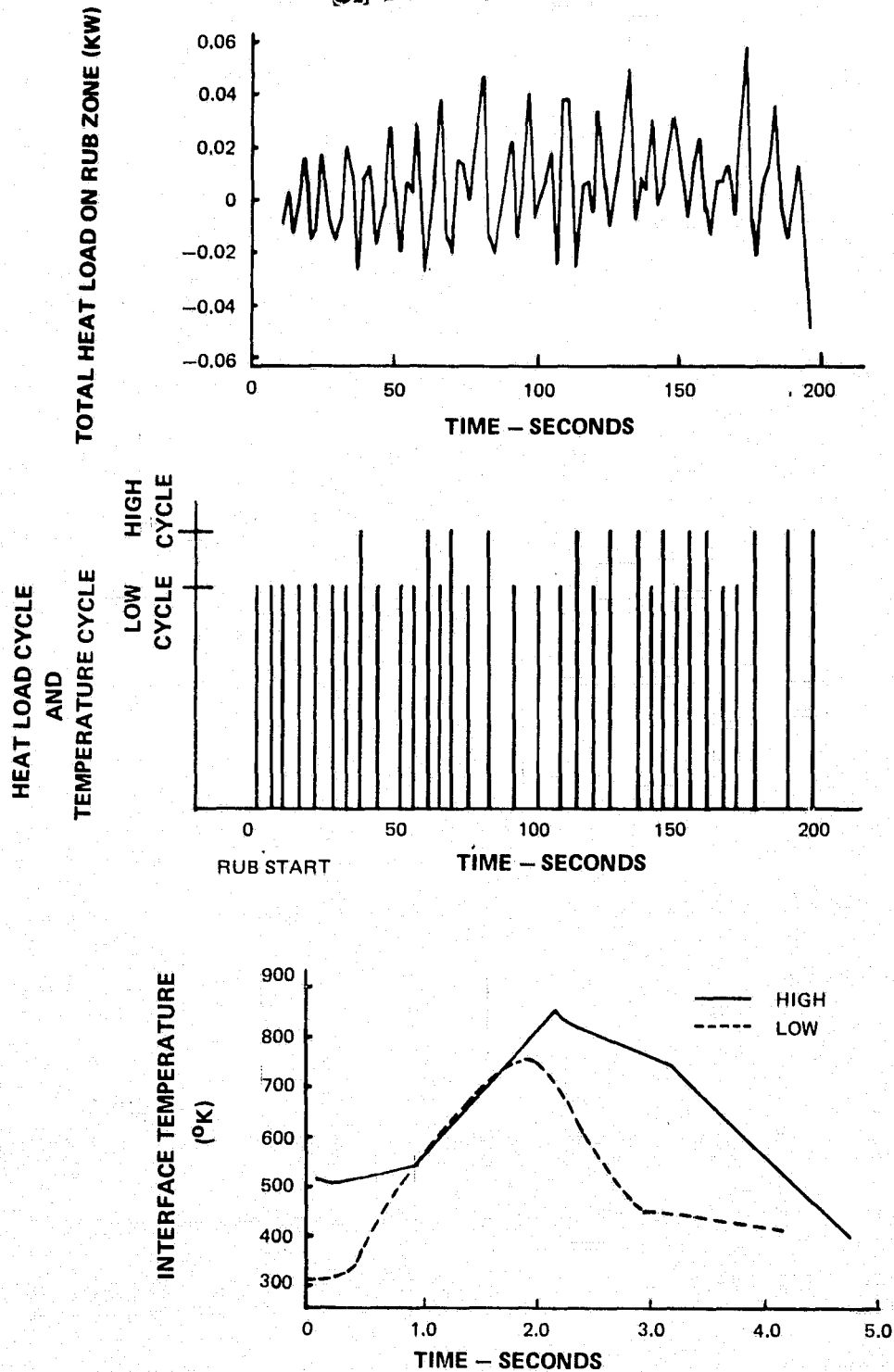
Figure 29. Task 1 Test 2 Data Reduction Results



Test 7 ($i = .0025$ mm/sec, $v = 152$ mps, $b = 1.75$ mm, $\delta = 1.0$ mm, $\rho = 16\%$)

Figure 30. Task I Test 7 Data Reduction Results

ORIGINAL PAGE IS
OF POOR QUALITY



Test 10 ($i = .0025$ mm/sec, $v = 213$ mps, $b = 0.52$ mm, $\delta = 0.5$ mm, $\rho = 19\%$)

Figure 31. Task I Test 10 Data Reduction Results

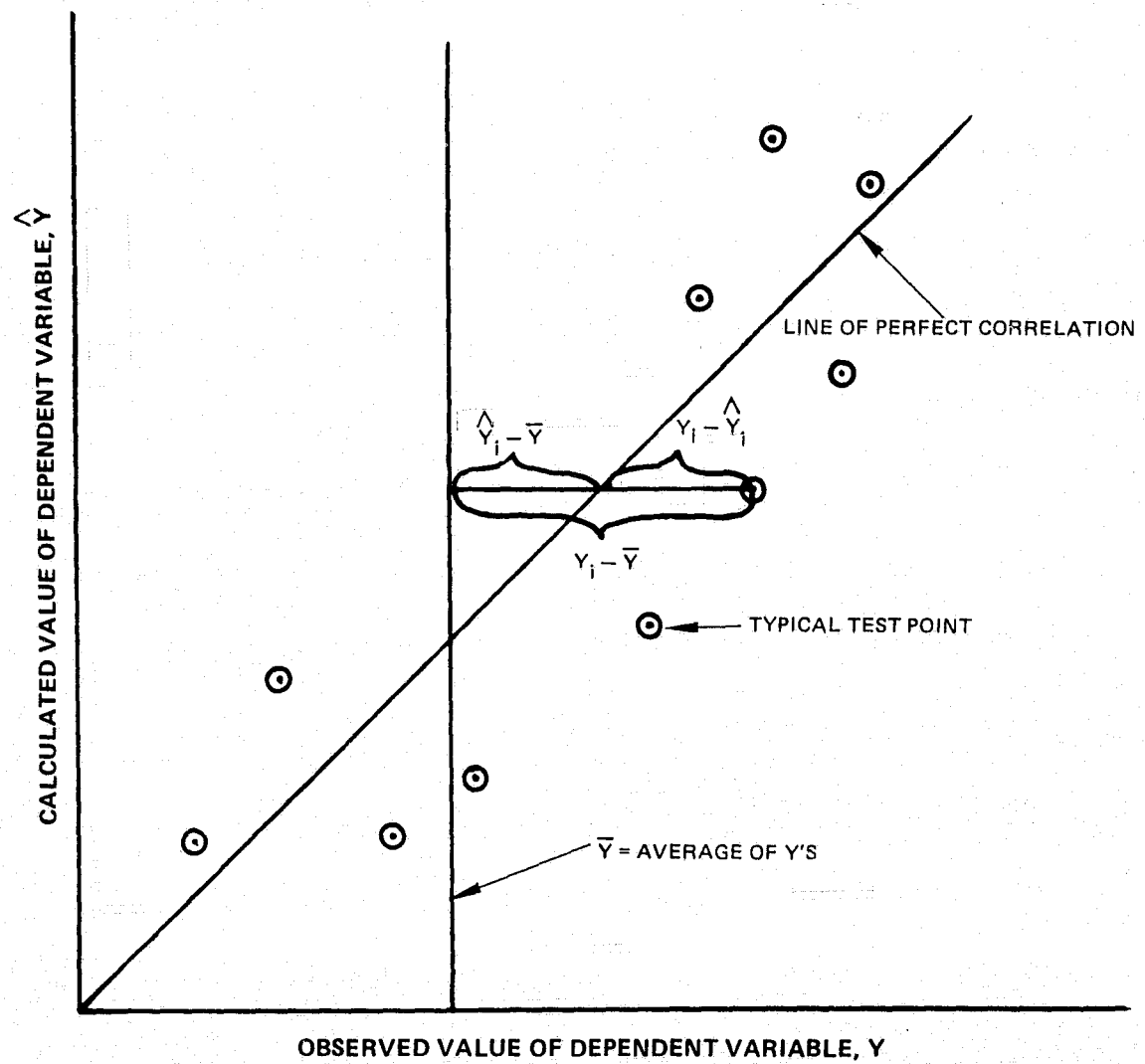


Figure 32. Data Fit to Model Using Least Squares Criterion

ORIGINAL PAGE IS
OF POOR QUALITY

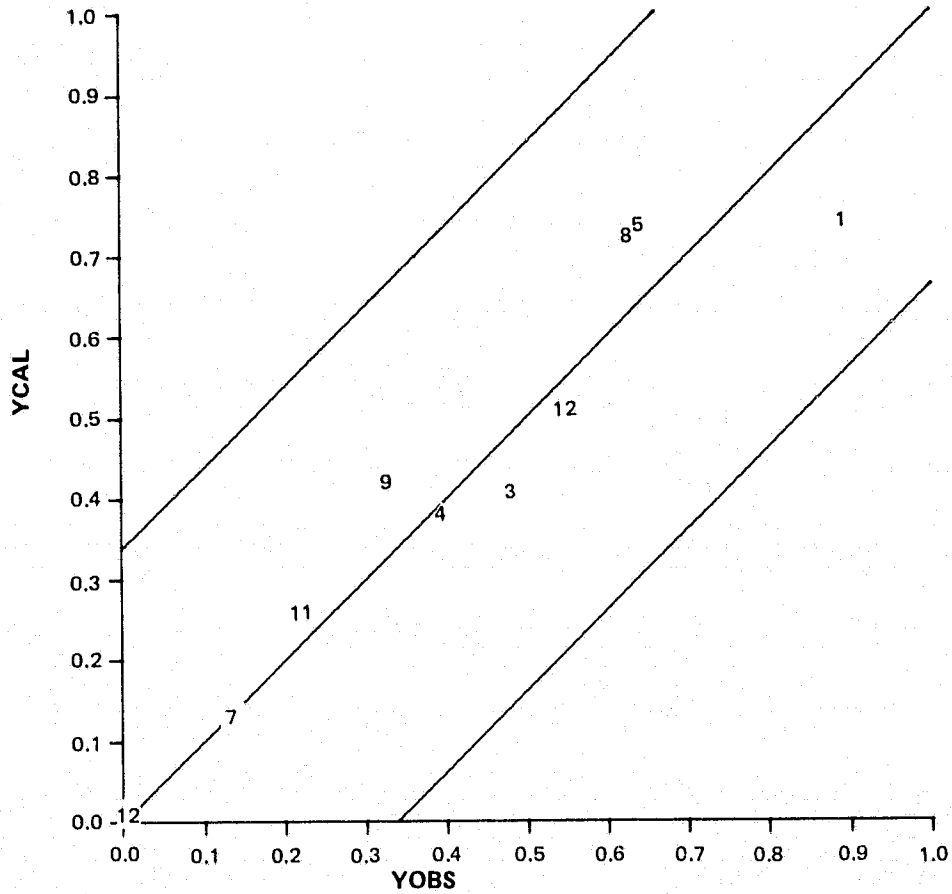


Figure 33. Regression Analysis for Task I Average Total Energy

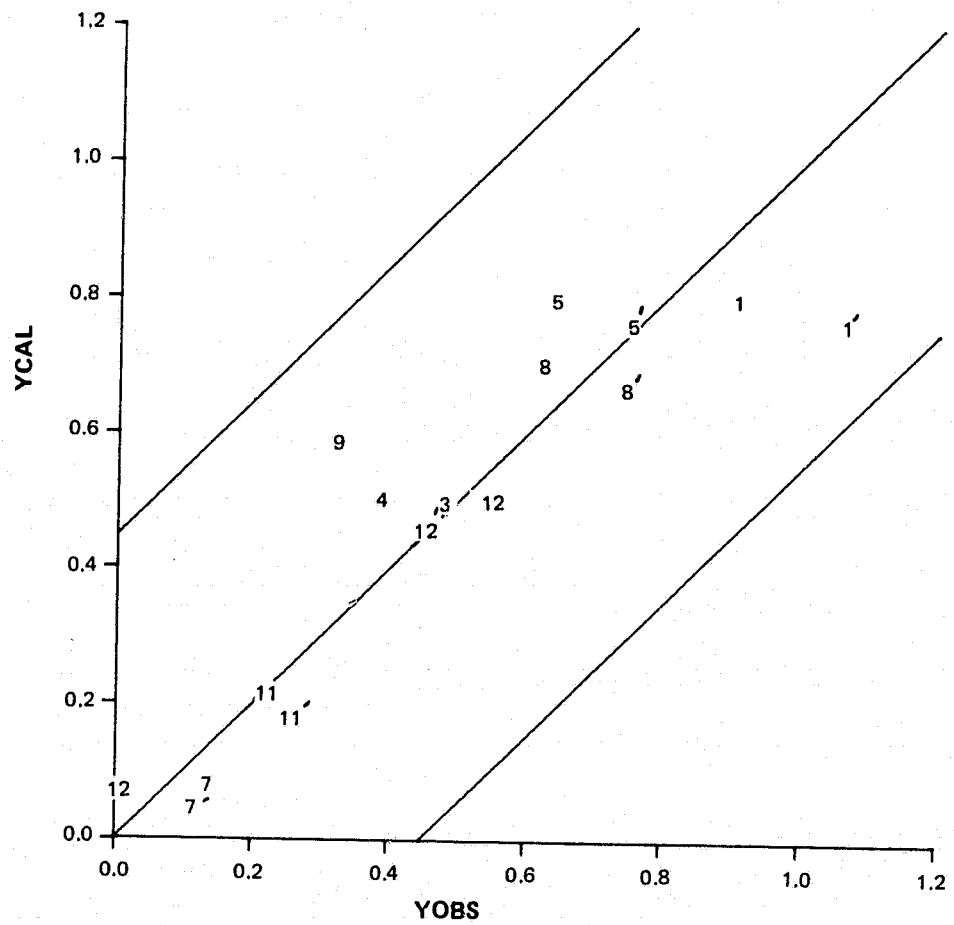


Figure 34. Regression Analysis for Task I Average Total Energy, Including Data from Expansion of 1.0 mm Tests

ORIGINAL PAGE
OF POOR QUALITY

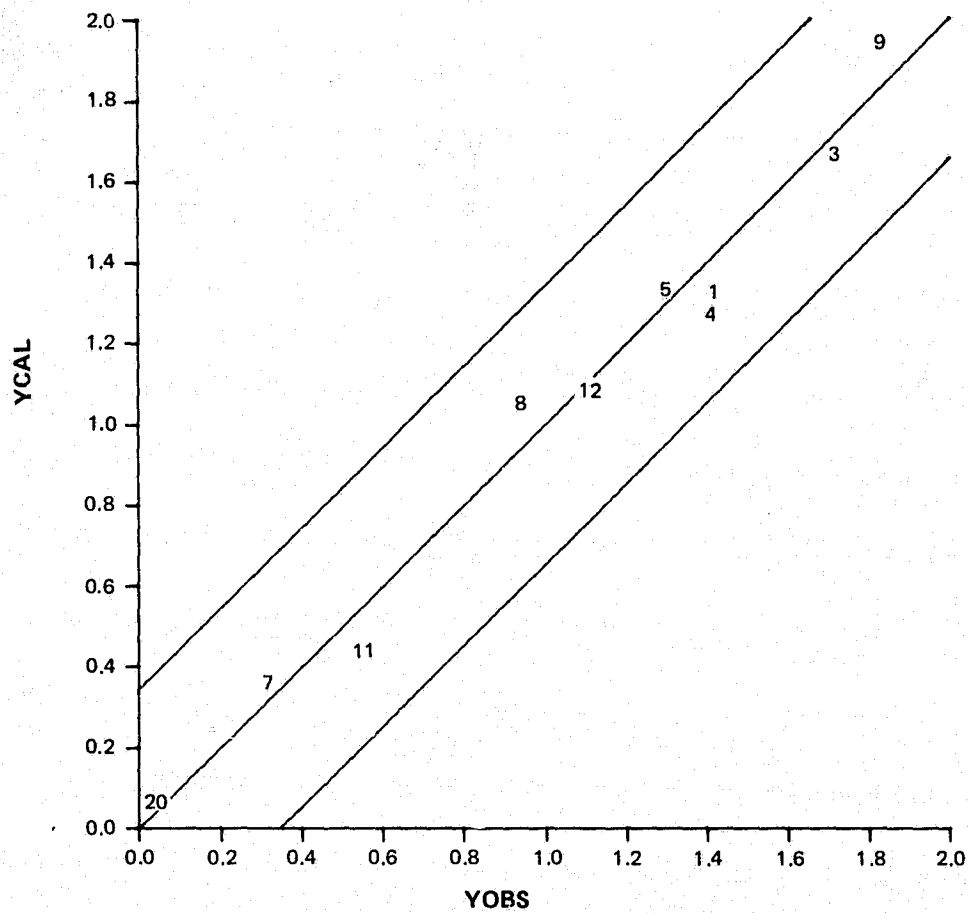


Figure 35. Regression Analysis for Task I Peak Total Energy

C-2

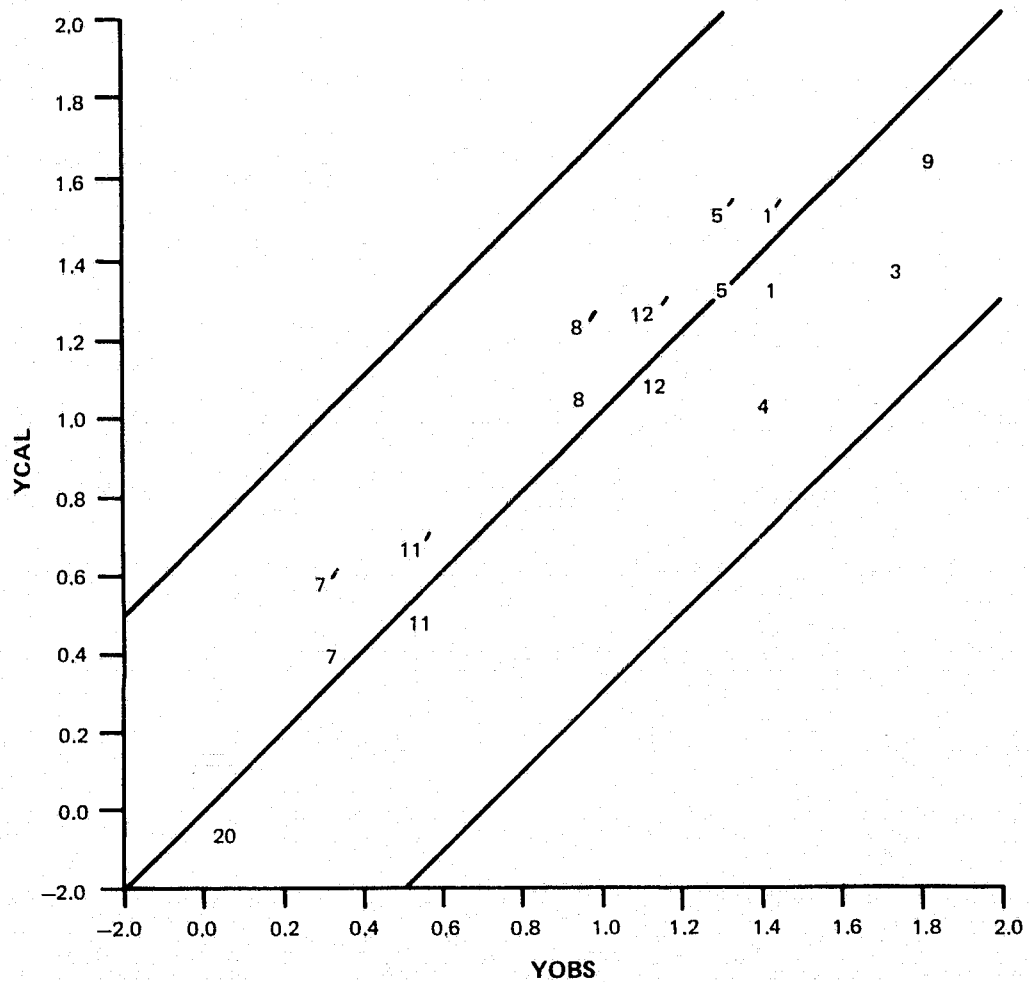


Figure 36. Regression Analysis for Task I Peak Total Energy, Including Data from Expansion of 1.0 mm Tests

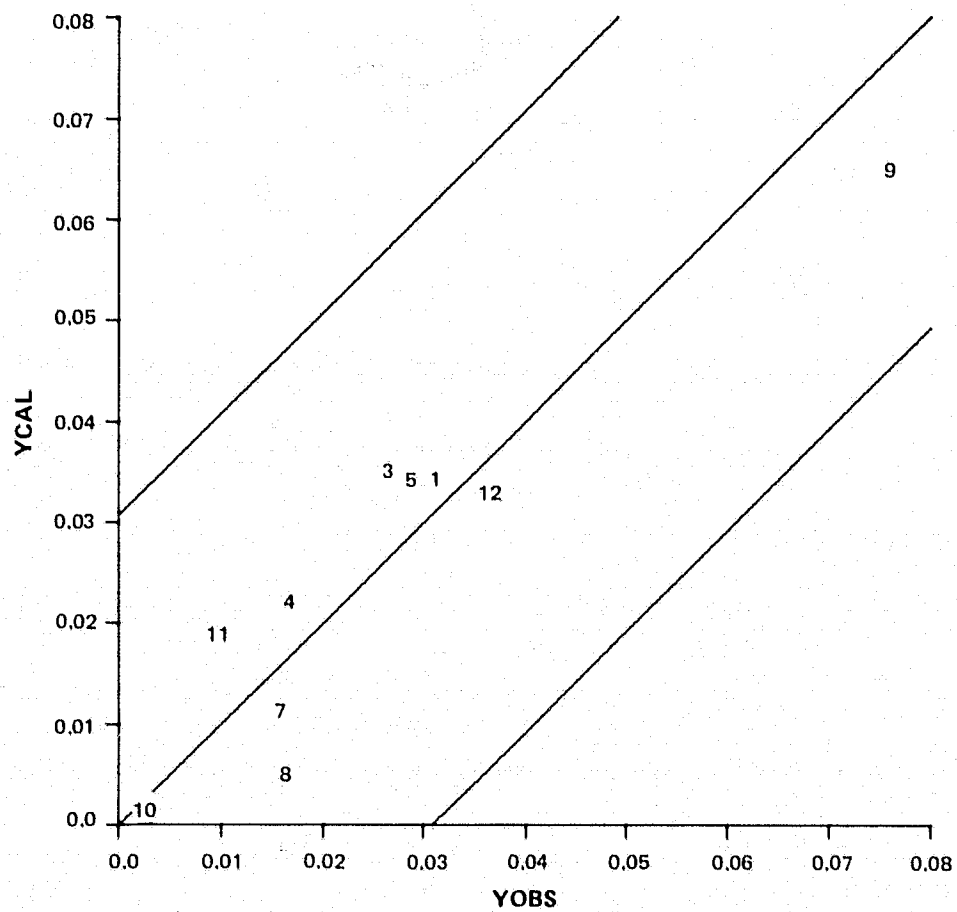


Figure 37. Regression Analysis for Task I Average Heat to Blade

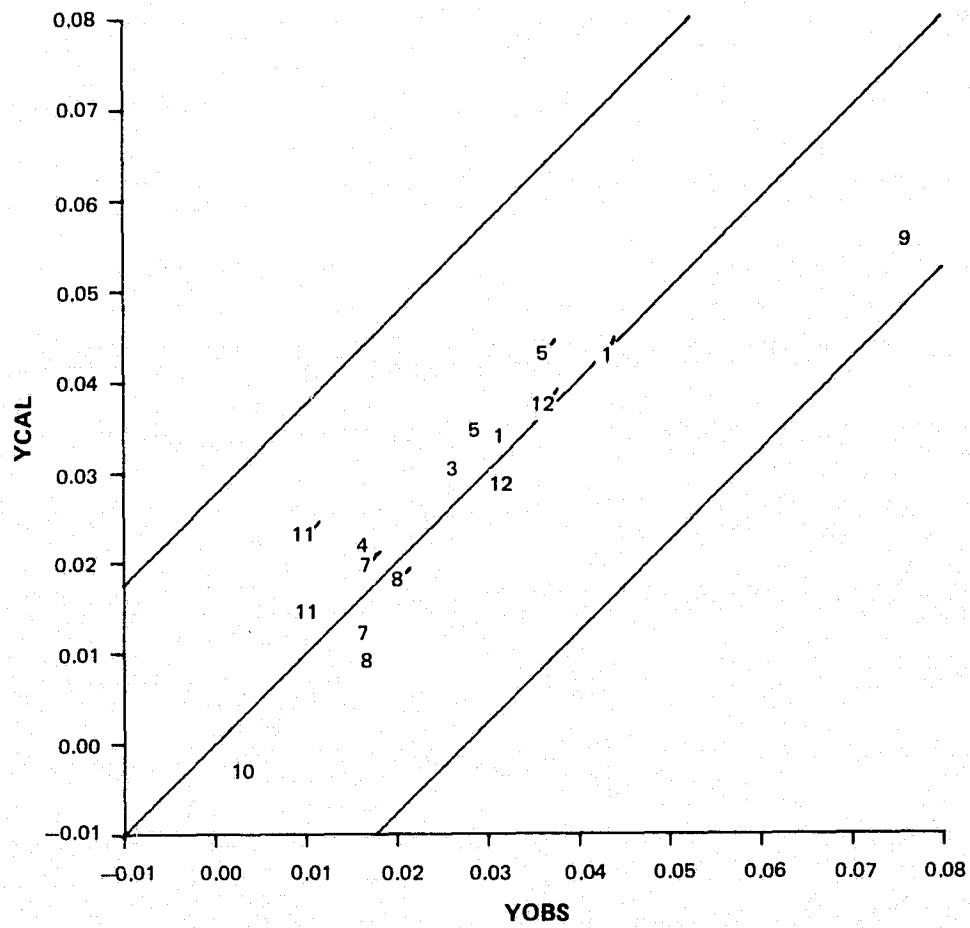


Figure 38. Regression Analysis for Task I Average Heat to Blade, Including Data from Expansion of 1.0 mm Tests

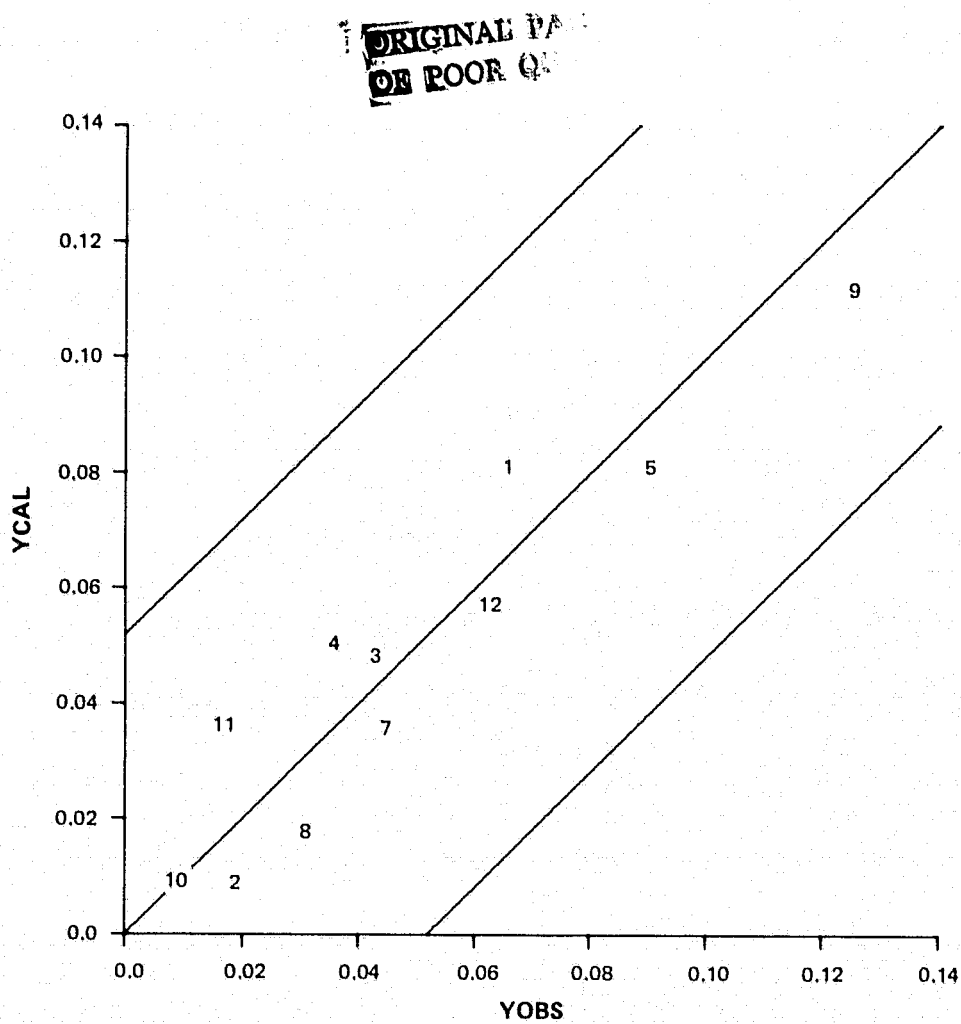


Figure 39. Regression Analysis for Task I Peak Heat to Blade

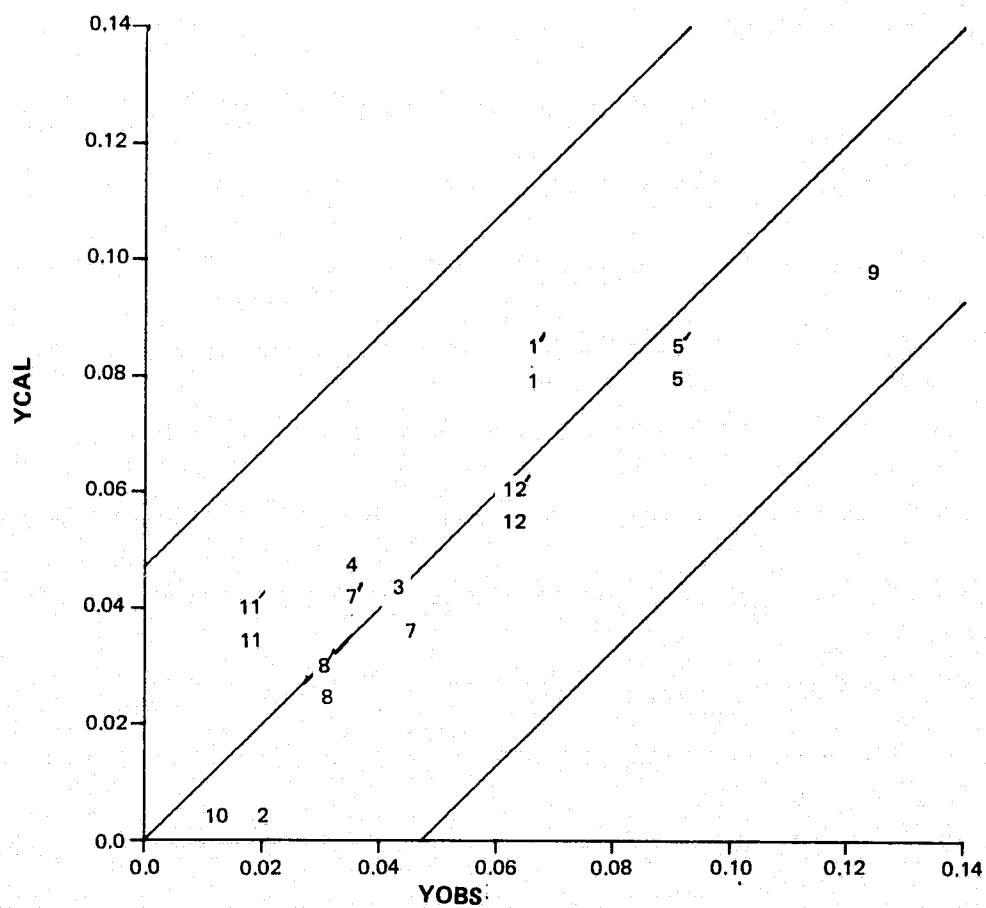


Figure 40. Regression Analysis for Task I Peak Heat to Blade, Including Data from Expansion of 1.0 mm Tests

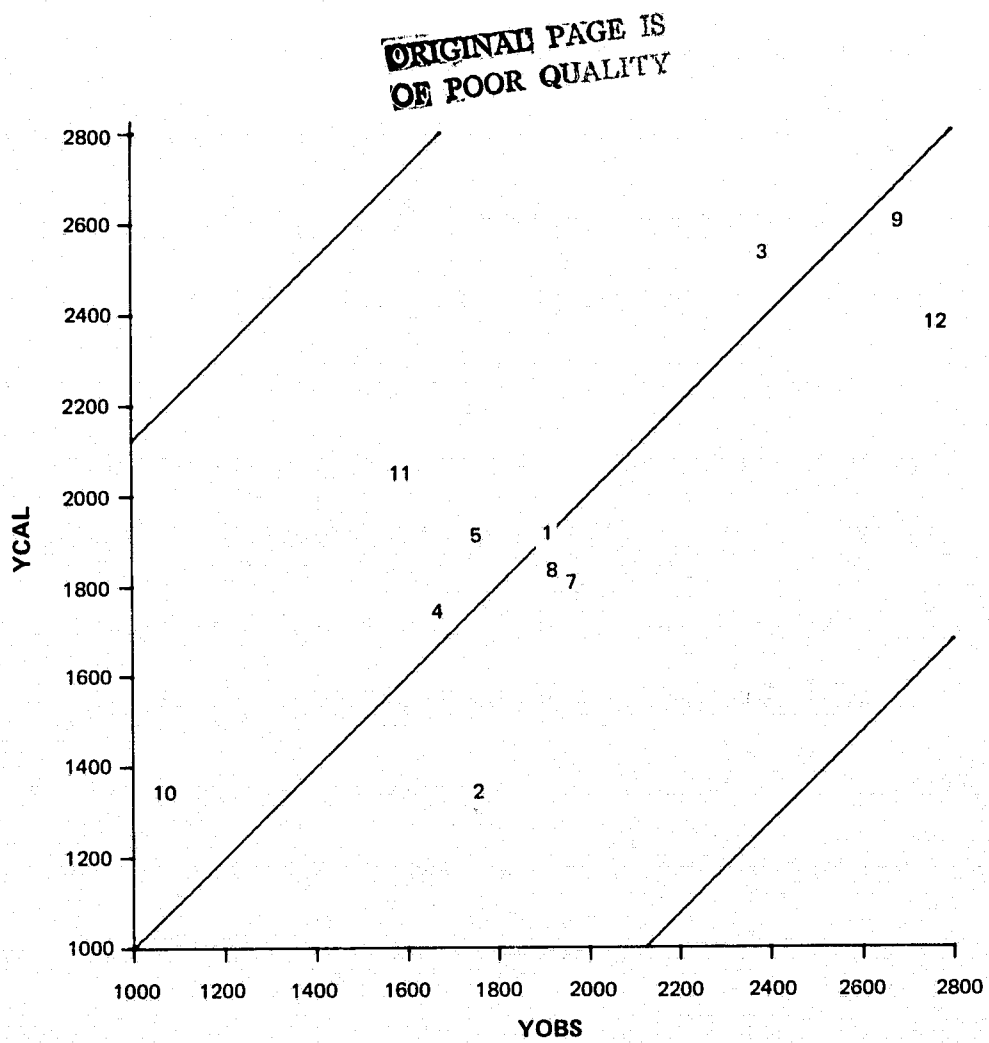


Figure 41. Regression Analysis for Task I Maximum Blade Temperature

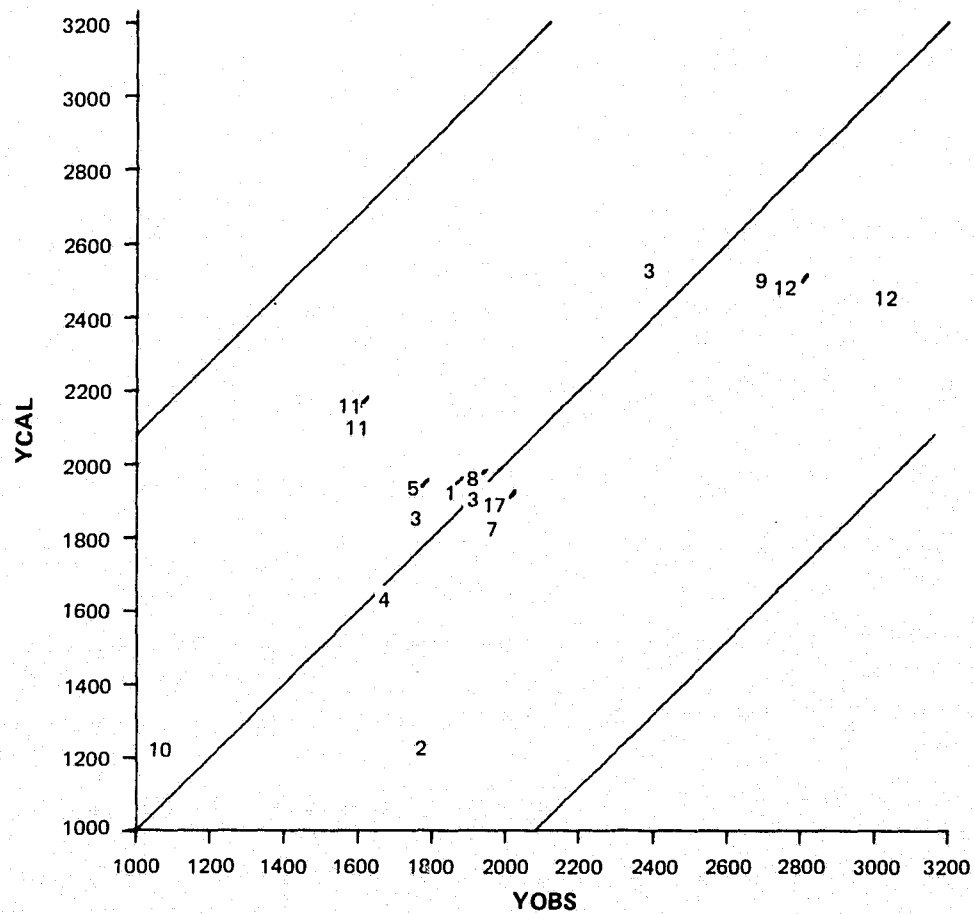


Figure 42. Regression Analysis for Task I Maximum Blade Temperature, Including Data from Expansion of 1.0 mm Tests

ORIGINAL PAGE IS
OF POOR QUALITY

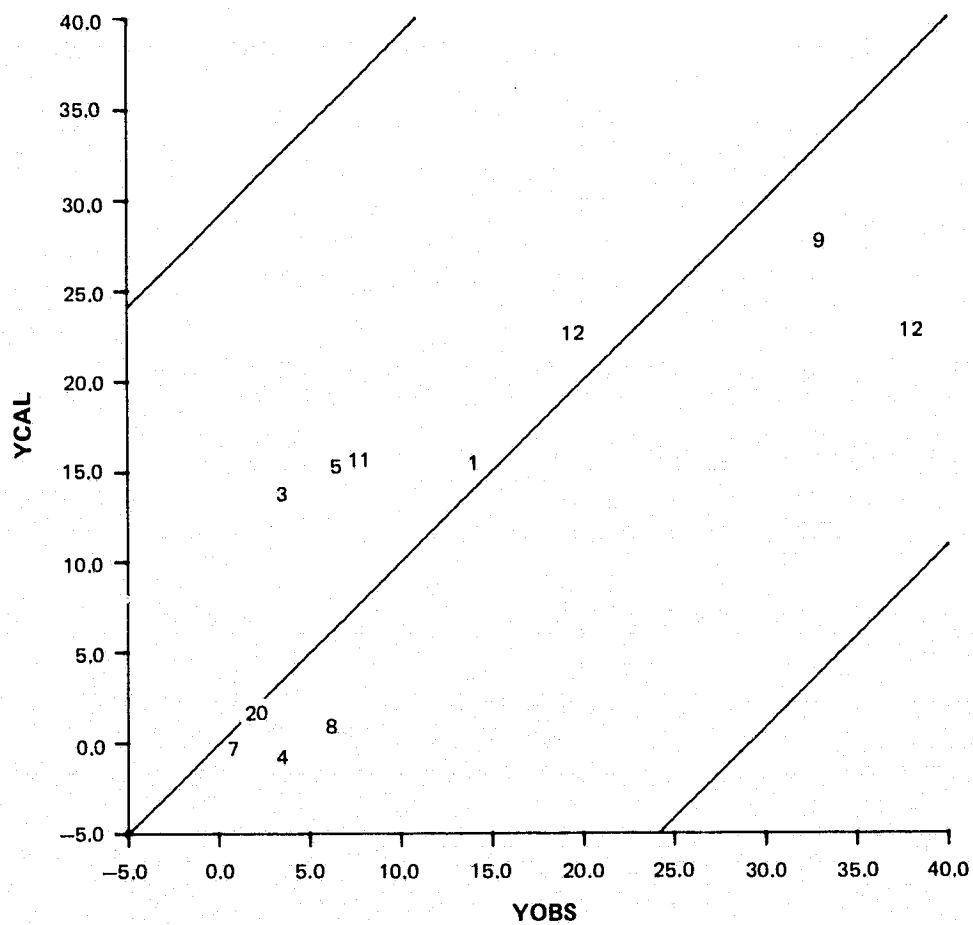
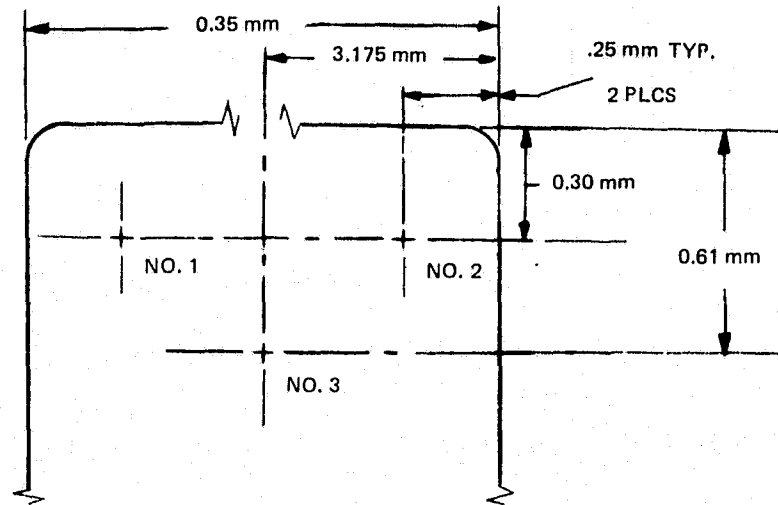
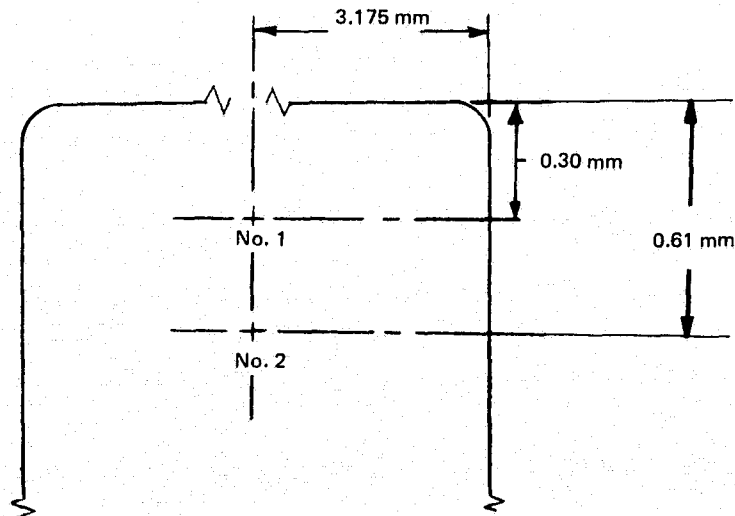


Figure 43. Regression Analysis for Task I Adjusted Blade Wear and Transfer

ORIGINAL PAGE IS
OF PHOTO



**TC CONFIGURATION FOR TEST 12 AND
SINGLE-BLADED TASK III TESTS**



**TC CONFIGURATION FOR EACH BLADE OF
MULTI-BLADED TASK III TESTS**

Figure 44. Task III Blade Thermocouple Installation

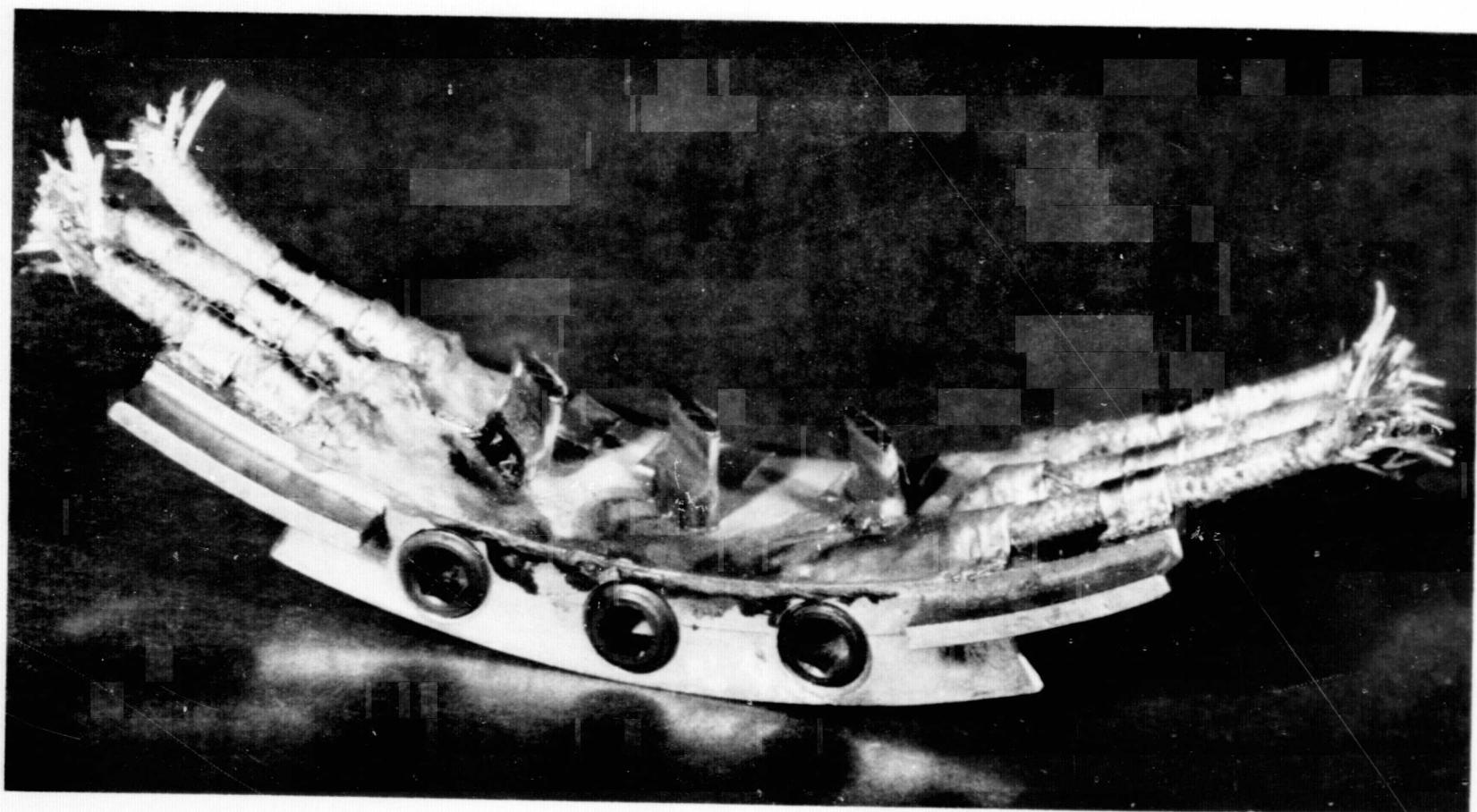
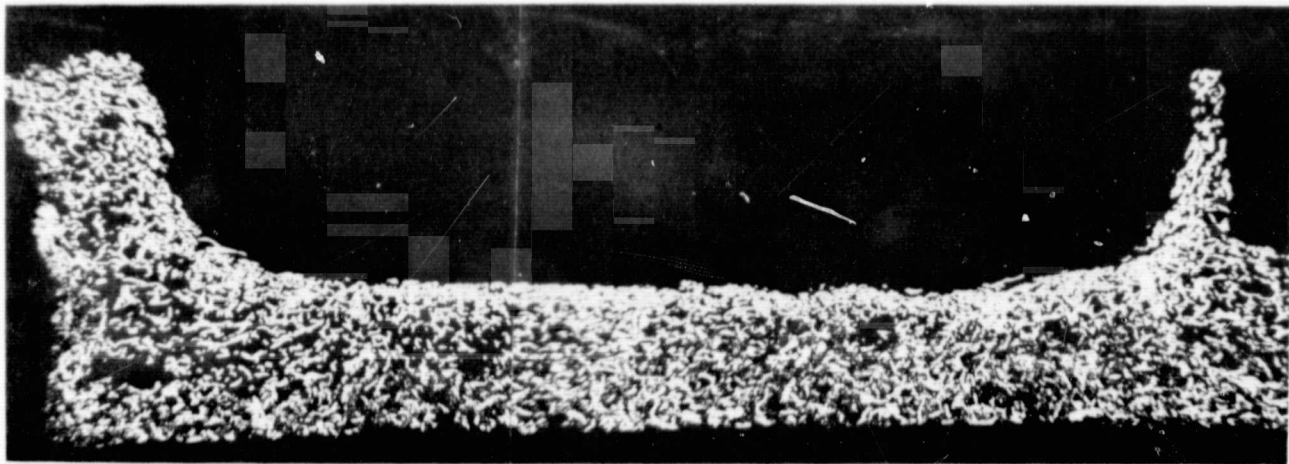
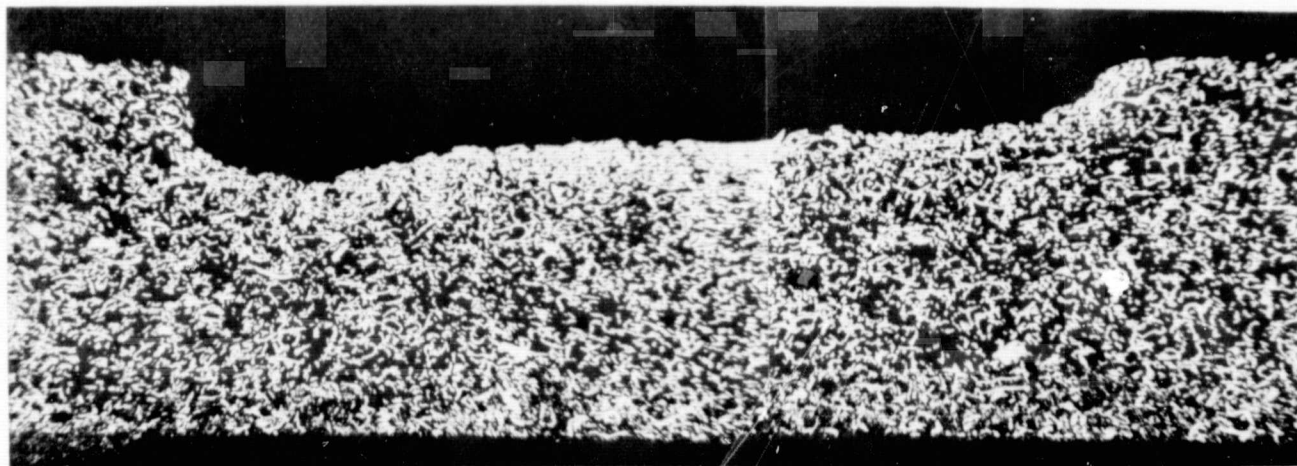


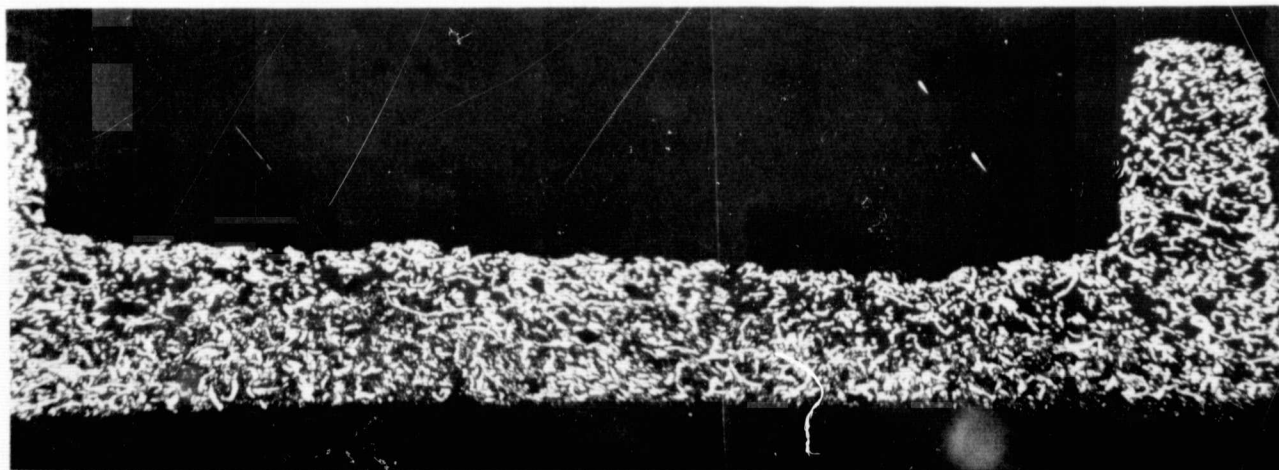
Figure 45. Test Setup for Task III, Multi-bladed Test



Test 13 (1, Ni, $i = 0.25$ mm/sec, $v = 213$ mps, $b = 0.48$ mm, $\delta = 1.0$ mm, $\rho = 16\%$)

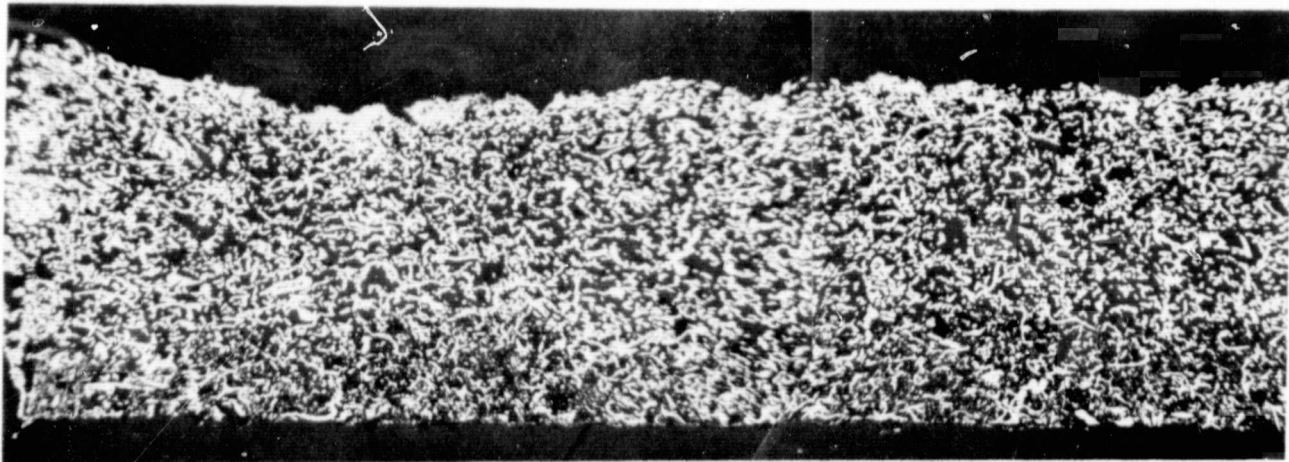


Test 14 (3, Ti, $i = 0.25$ mm/sec, $v = 152$ mps, $b = 0.55$ mm, $\delta = 1.0$ mm, $\rho = 19\%$)

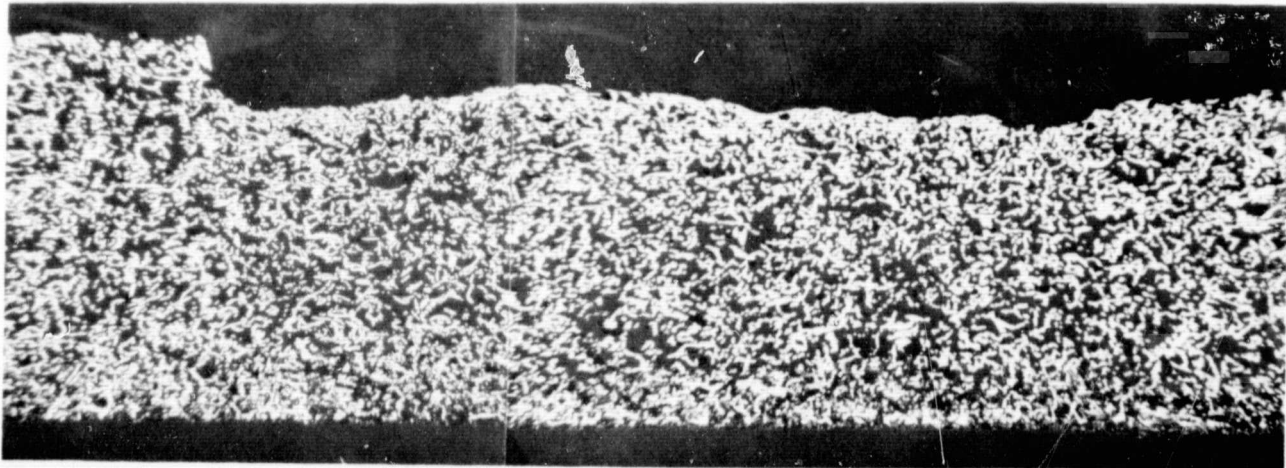


Test 15 (1, Ni, $i = 0.025$ mm/sec, $v = 213$ mps, $b = 1.70$ mm, $\delta = 1.0$ mm, $\rho = 16\%$)

Figure 46. Cross-sections of Seals from Task III Tests (Mag: 25x)



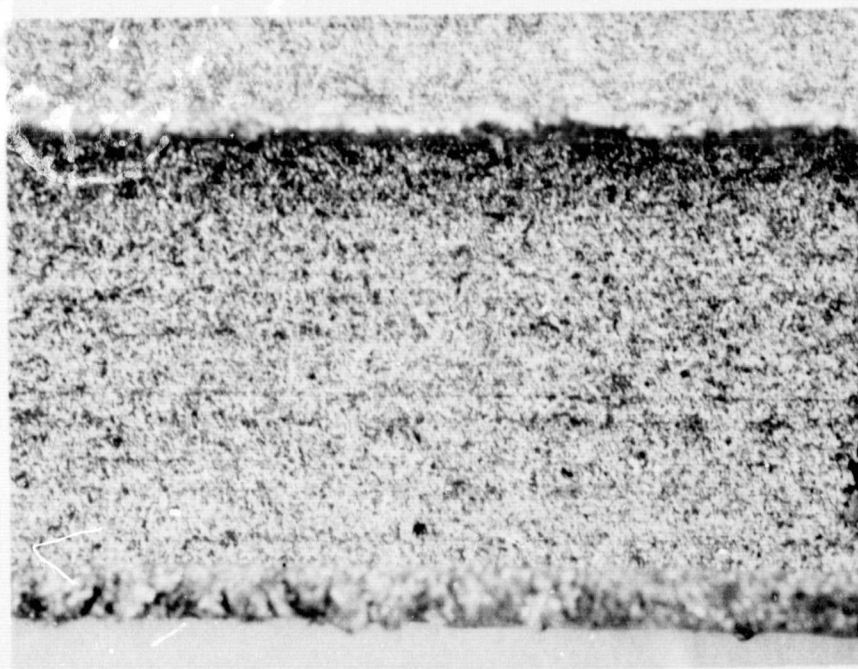
Test 16 (3, Ti, $i=0.25$ mm/sec, $v=152$ mps, $b=1.71$ mm, $\delta=1.0$ mm, $\rho=19\%$)



Test 17 (1, Ni, $i=0.25$ mm/sec, $v=152$ mps, $b=1.68$ mm, $\delta=1.0$ mm, $\rho=19\%$)

Figure 47. Cross-sections of Seals from Task III Tests (Mag: 25x)

ORIGINAL PAGE IS
OF POOR QUALITY

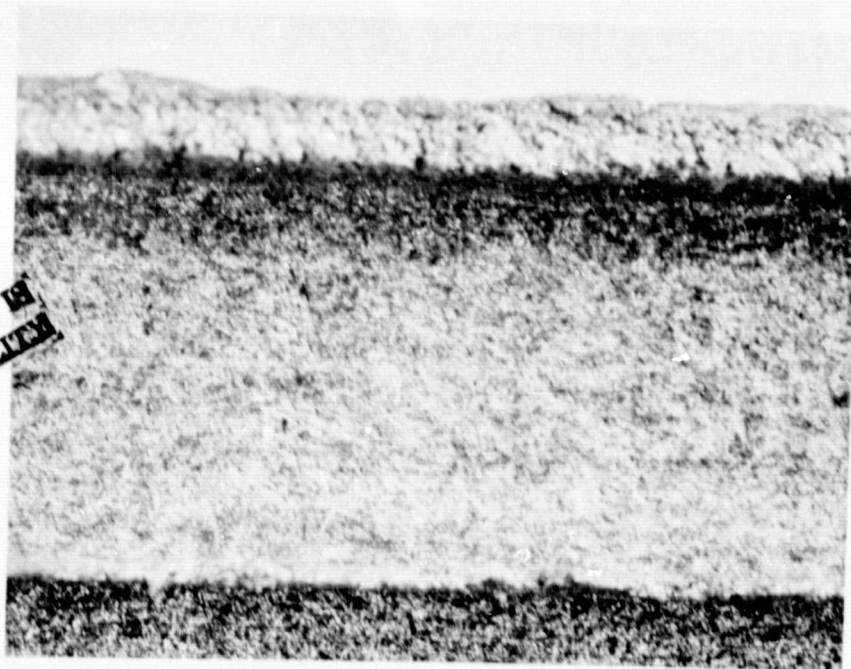


Test 15 (1, Ni, $i = 0.025$ mm/sec, $v = 213$ mps, $b = 1.70$ mm, $\delta = 1.0$ mm, $\rho = 16\%$)

Figure 48. Photograph Showing Absence of Smearing and Glazing on Seal Surface for Test 15 (Mag: 10x)

ORIGINAL PAGE IS
OF POOR QUALITY

ORIGINAL PAGE IS
OF POOR QUALITY



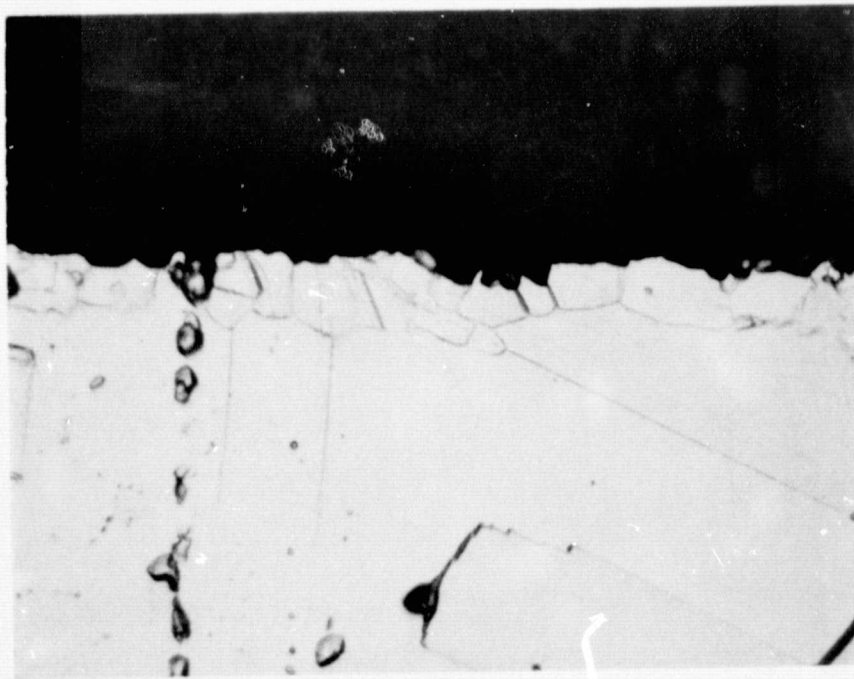
Test 13 (1, Ni, $i = 0.25$ mm/sec, $v = 213$ mps, $b = 0.48$ mm, $\delta = 1.0$ mm, $\rho = 16\%$)

Figure 49. Photograph Showing Absence of Smearing and Glazing on Seal Surface for Test 13 (Mag: 10x)



Test 15 (1, Ni, $i = 0.025$ mm/sec, $v = 213$ mps, $b = 1.70$ mm, $\delta = 1.0$ mm, $\rho = 16\%$)

Figure 50. Blade Rub Surface from Test 15 (Mag: 100 x)



ORIGINAL PAGE IS
OF POOR QUALITY

Test 13 (1, Ni, $i = 0.25$ mm/sec, $v = 213$ mps, $b = 0.48$ mm, $\delta = 1.0$ mm $\rho = 16\%$)

Figure 51. Sections of Recrystallization at the Blade Rub Interface for Test 13 (Mag: 500x)



Test 17 (1, Ni, $i = 0.25$ mm/sec, $v = 152$ mps, $b = 1.68$ mm, $\delta = 1.0$ mm, $\rho = 19\%$)

Figure 52. Cross-section of Blade from Test 17 Showing Decomposition of the Grain Structure (Mag: 100x)



Test 17 (1, Ni, $i = 0.25$ mm/sec, $v = 152$ mps, $b = 1.68$ mm, $\delta = 1.0$ mm, $\rho = 19\%$)

Figure 53. Seal Surface from Test 17 Showing Heavy Surface Glazing (Mag: 10x)



Test 13 (1, Ni, $i = 0.25$ mm/sec, $v = 213$ mps, $b = .48$ mm, $\delta = 1.0$ mm, $\rho = 16\%$)

Figure 54. Cross-section Through Blade from Test 13 Showing Region of Maximum Transfer (Mag: 100x)

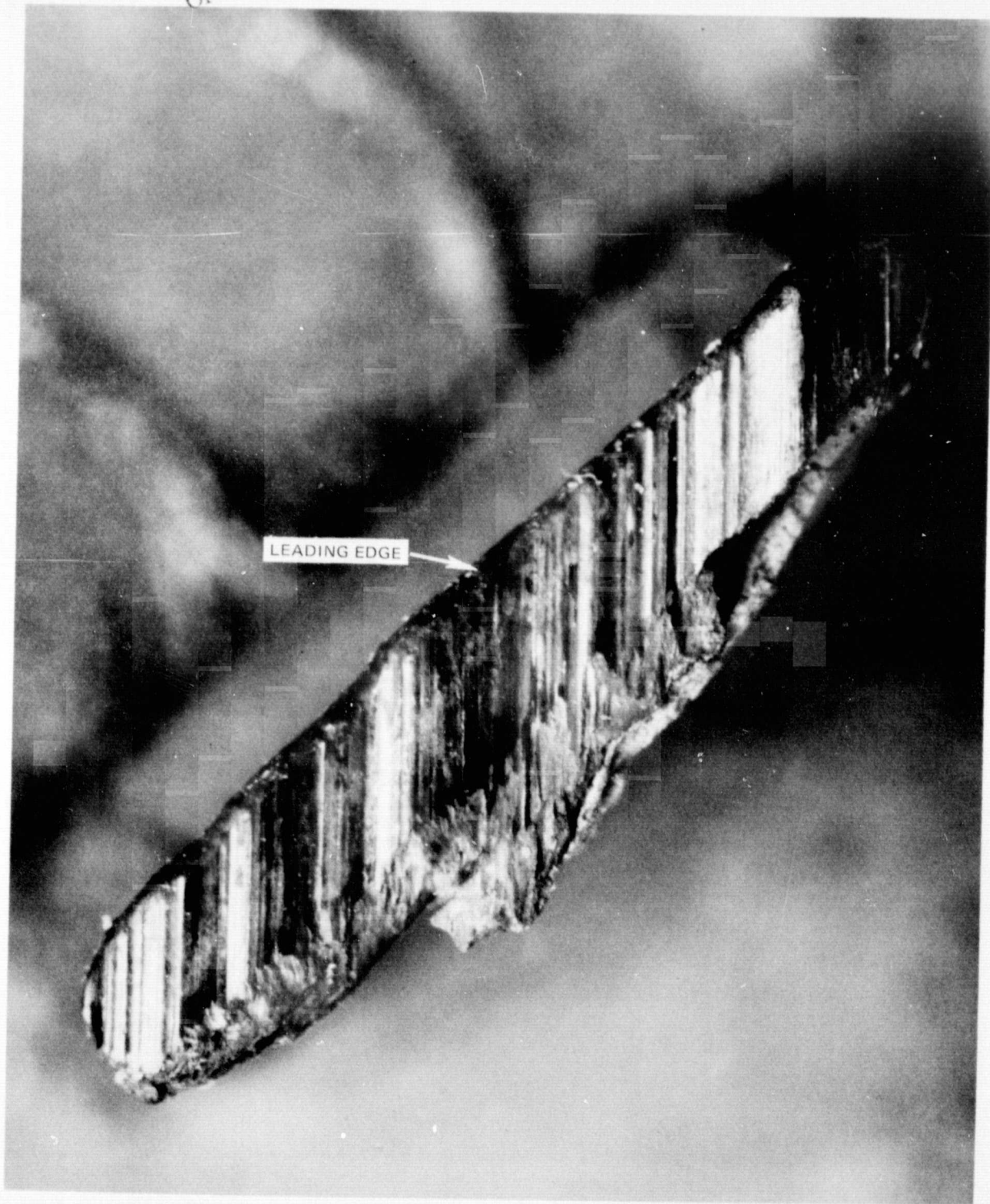
ORIGINAL PAGE IS
OF POOR QUALITY



Test 14 (3, Ti, $i = 0.25$ mm/sec, $v = 152$ mps, $b = 0.55$ mm, $\delta = 1.0$ mm, $\rho = 19\%$)

Figure 55. Blade Tip #1 from Test 14 (Mag: 50x)

ORIGINAL PAGE IS
OF POOR QUALITY



Test 14 (3, Ti, $v = 0.25$ mm/sec, $v = 152$ mps, $b = 0.55$ mm, $\delta = 1.0$ mm, $\rho = 19\%$)

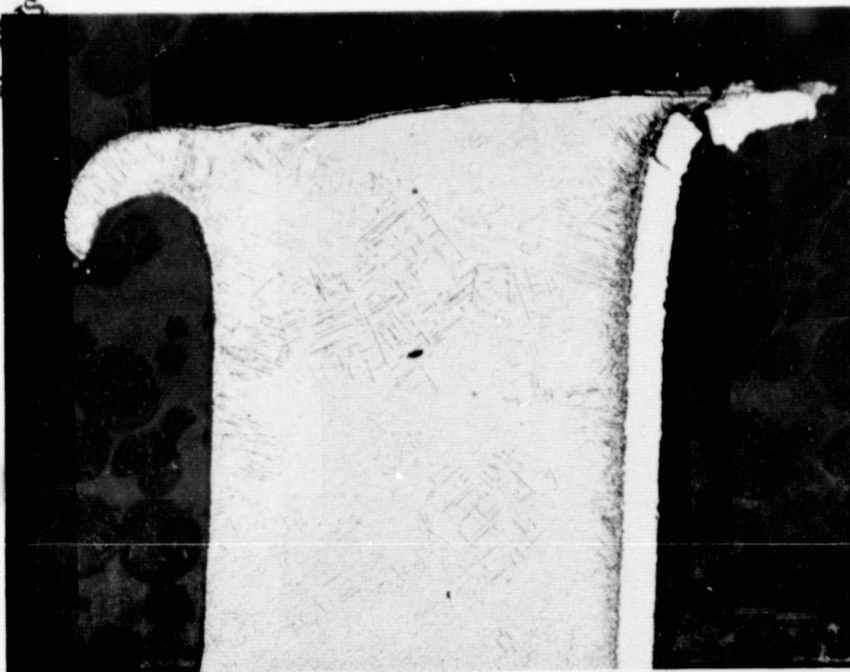
Figure 56. Blade Tip #2 from Test 14 (Mag: 50x)



Test 14 (3, Ti, $i = 0.25$ mm/sec, $v = 152$ mps, $b = 0.55$ mm, $\delta = 1.0$ mm, $\rho = 19\%$)

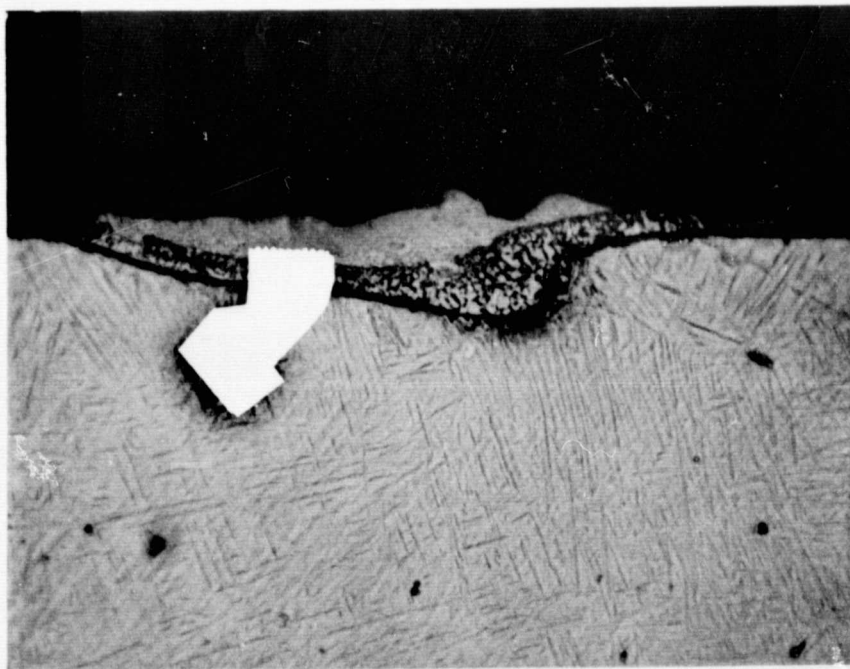
Figure 57. Blade Tip #3 from Test 14 (Mag: 50x)

ORIGINAL PAGE
OF POOR QUALITY



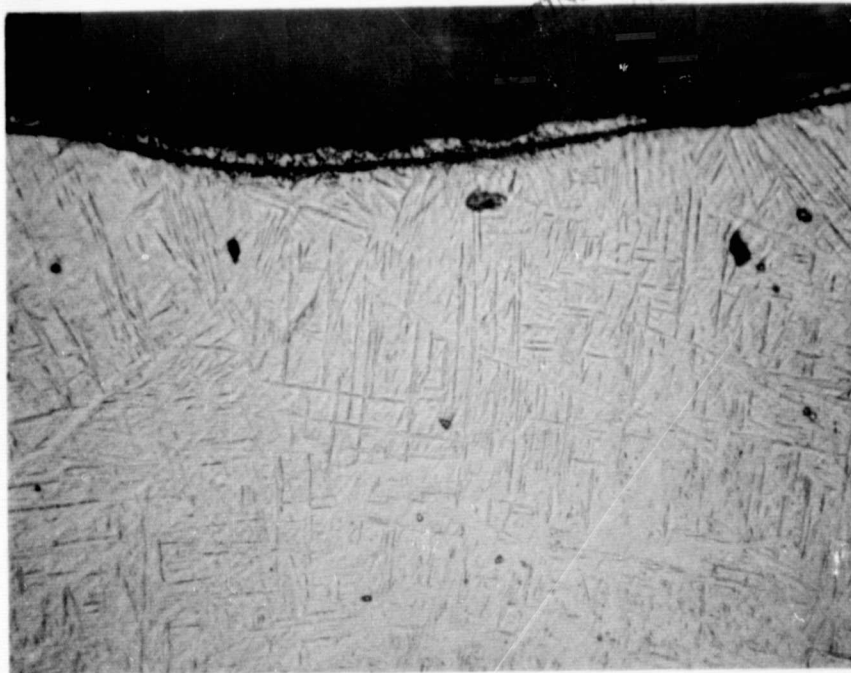
Test 14 (3, Ti, $i = 0.25$ mm/sec, $v = 152$ mps, $b = 0.55$ mm, $\delta = 1.0$ mm, $\rho = 19\%$)

Figure 58. Burrs at Leading (Left) and Trailing Edges (Right) of Blade Tip from Test 14 (Mag: 100x)



Test 14 (3, Ti, $i = 0.25$ mm/sec, $v = 152$ mps, $b = 0.55$ mm, $\delta = 1.0$ mm, $\rho = 19\%$)

Figure 59. A Section of the Rub Surface Where Mixing has Occurred (Mag: 500x)



Test 14 (3, Ti, $i = 0.25$ mm/sec, $v = 152$ mps, $b = 0.55$ mm, $\delta = 1.0$ mm, $\rho = 19\%$)

Figure 60. Photograph of Blade Tip Showing Surface Layer of Titanium with Traces of Hastelloy X for Test 14 (Mag: 500x)



Test 14 (3, Ti, $i = 0.25$ mm/sec, $v = 152$ mps, $b = 0.55$ mm, $\delta = 1.0$ mm, $\rho = 19\%$)

Figure 61. Photomicrograph of the Rubstrip for Test 14 Showing Densification at the Rub Surface (Mag: 10x)

ORIGINAL PAGE IS
OF POOR QUALITY.



Test 16 (3, Ti, $i = 0.25$ mm/sec, $v = 152$ mps, $b = 1.71$ mm, $\delta = 1.0$ mm, $\rho = 19\%$)

Figure 62. Blade Tip #1 from Test 16 (Mag: 30x)

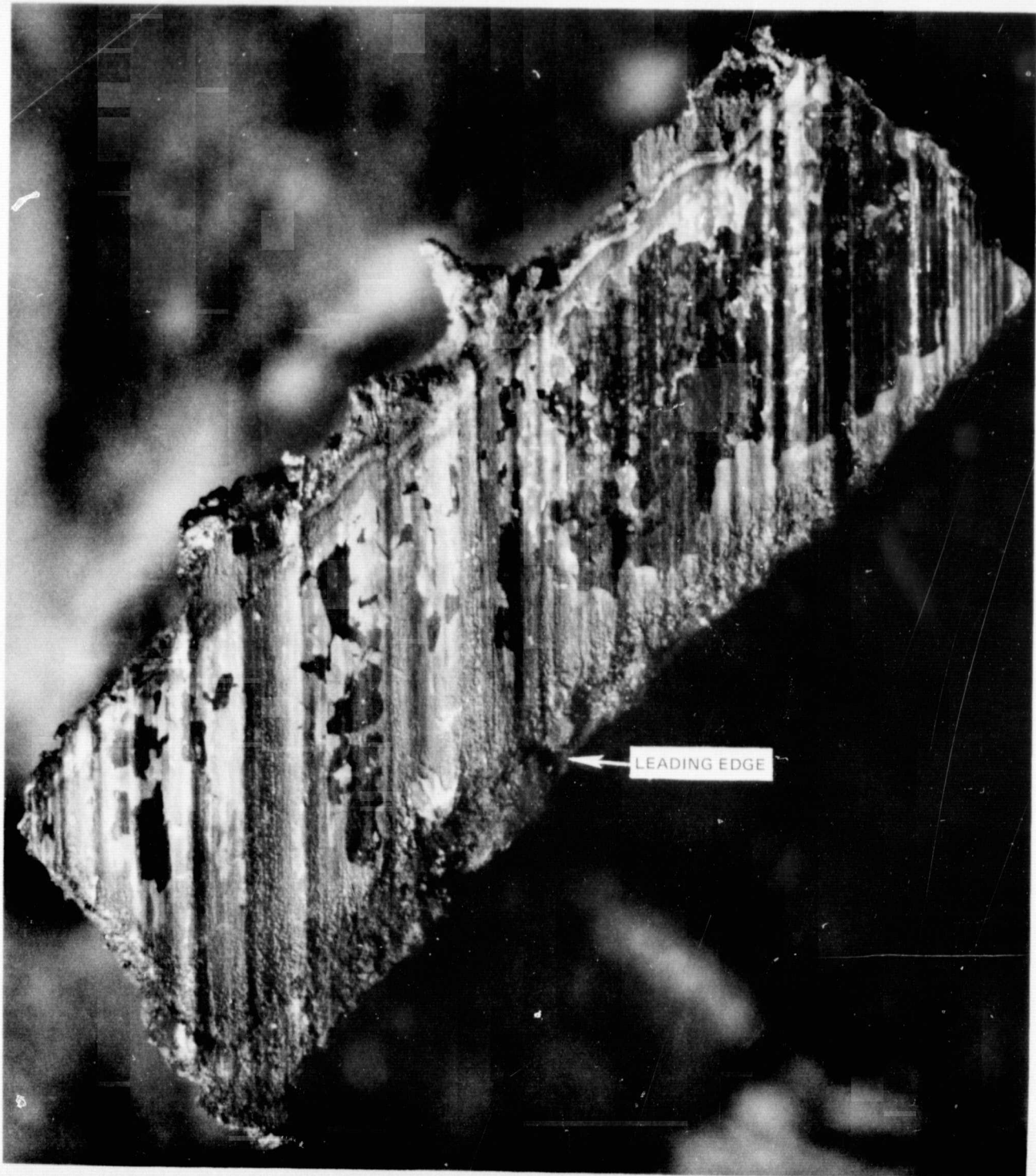
ORIGINAL PAGE IS
OF POOR QUALITY



Test 16 (3, Ti, $i = 0.25$ mm/sec, $v = 152$ mps, $b = 1.71$ mm, $\delta = 1.0$ mm, $\rho = 19\%$)

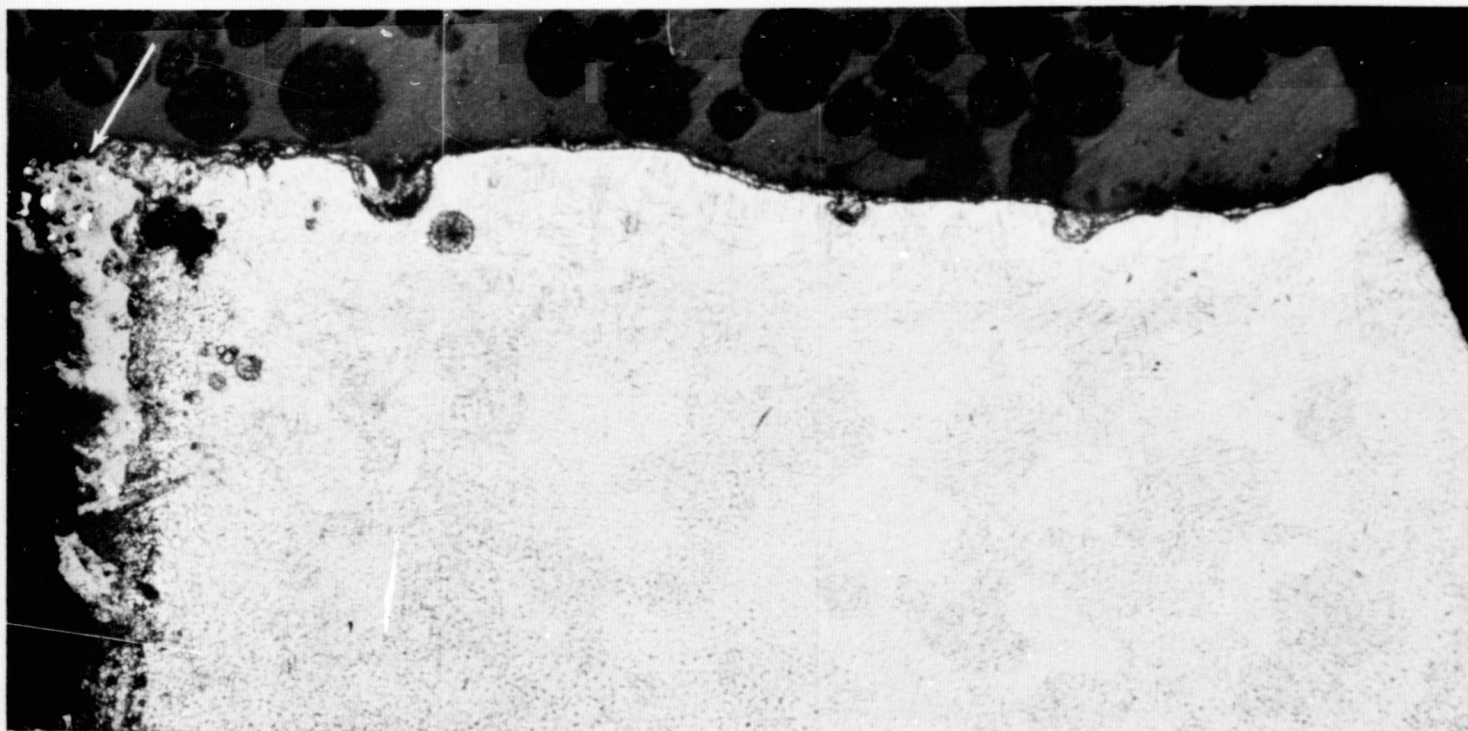
Figure 63. Blade Tip #2 from Test 16 (Mag: 30x)

ORIGINAL PAGE IS
OF POOR QUALITY



Test 16 (3, Ti, $i = 0.25$ mm/sec, $v = 152$ mps, $b = 1.71$ mm, $\delta = 1.0$ mm, $\rho = 19\%$)

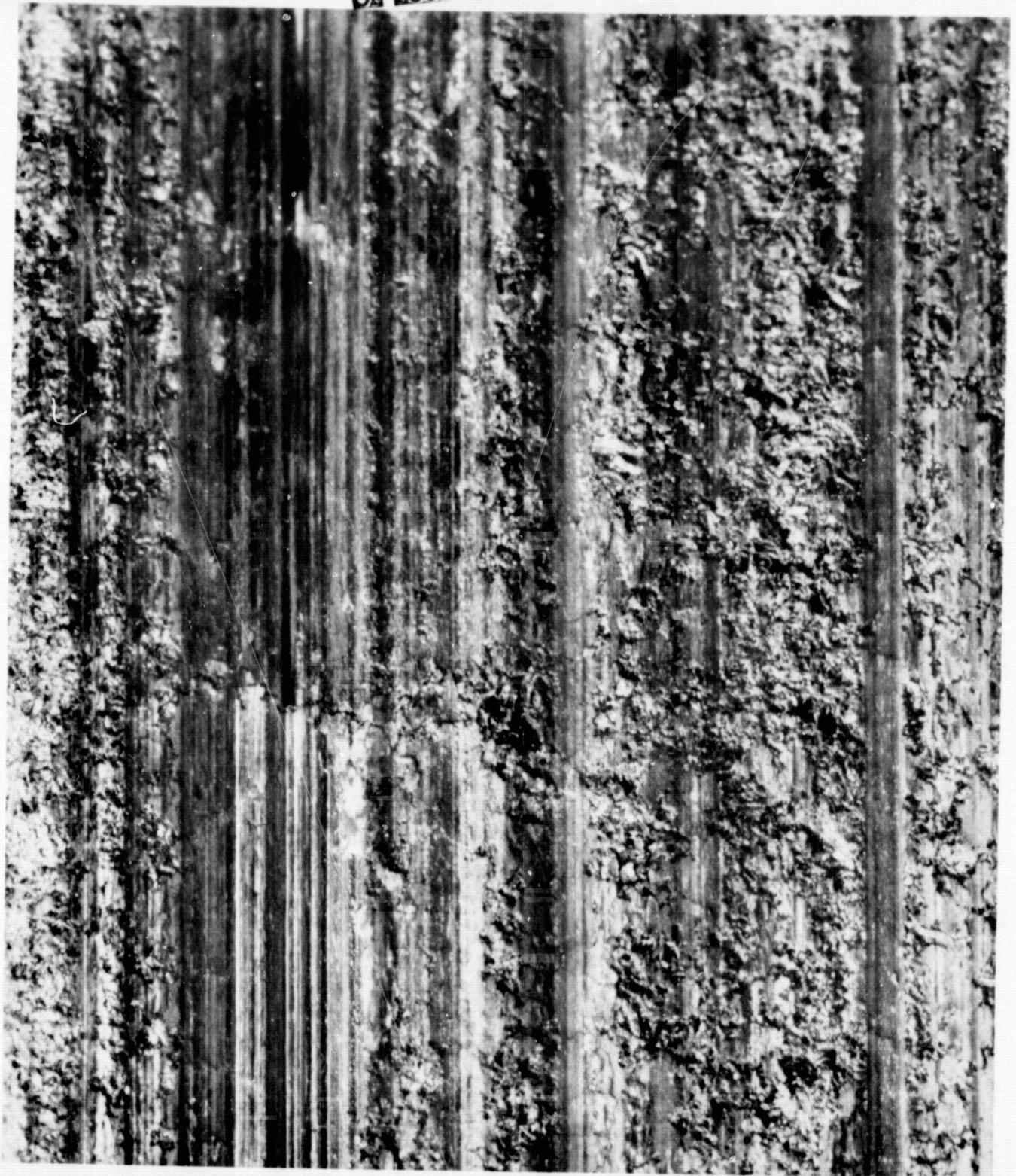
Figure 64. Blade Tip #3 from Test 16 (Mag: 30x)



ORIGINAL PAGE IS
OF POOR QUALITY

Test 16 (3, Ti, $i = 0.25$ mm/sec, $v = 152$ mps, $b = 1.71$ mm, $\delta = 1.0$ mm, $\rho = 19\%$)

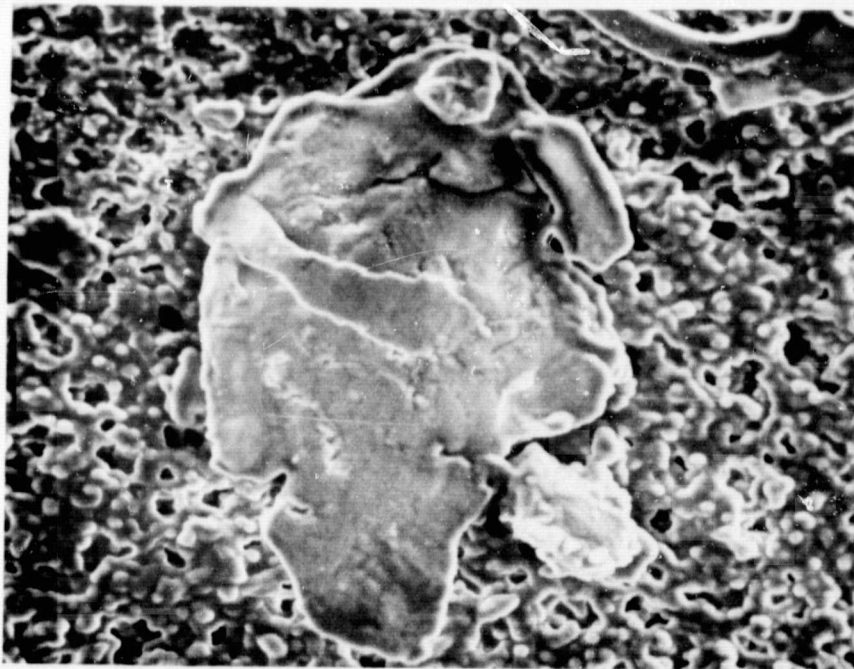
Figure 65. Cross Section of Blade from Test 16 Showing Burr at Leading Edge (Mag: 100x)



Test 16 (3, Ti, $i = 0.25$ mm/sec, $v = 152$ mps, $b = 1.71$ mm, $\delta = 1.0$ mm, $\rho = 19\%$)

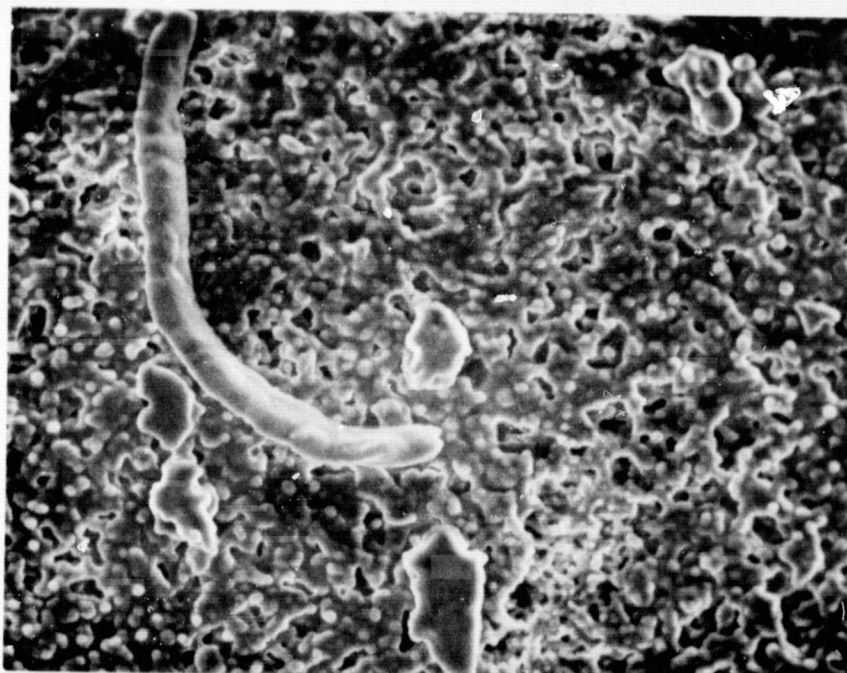
Figure 66. Plan View of Rubstrip from Test 16 Showing Heavily Glazed Striations

ORIGINAL PAGE IS
OF POOR QUALITY



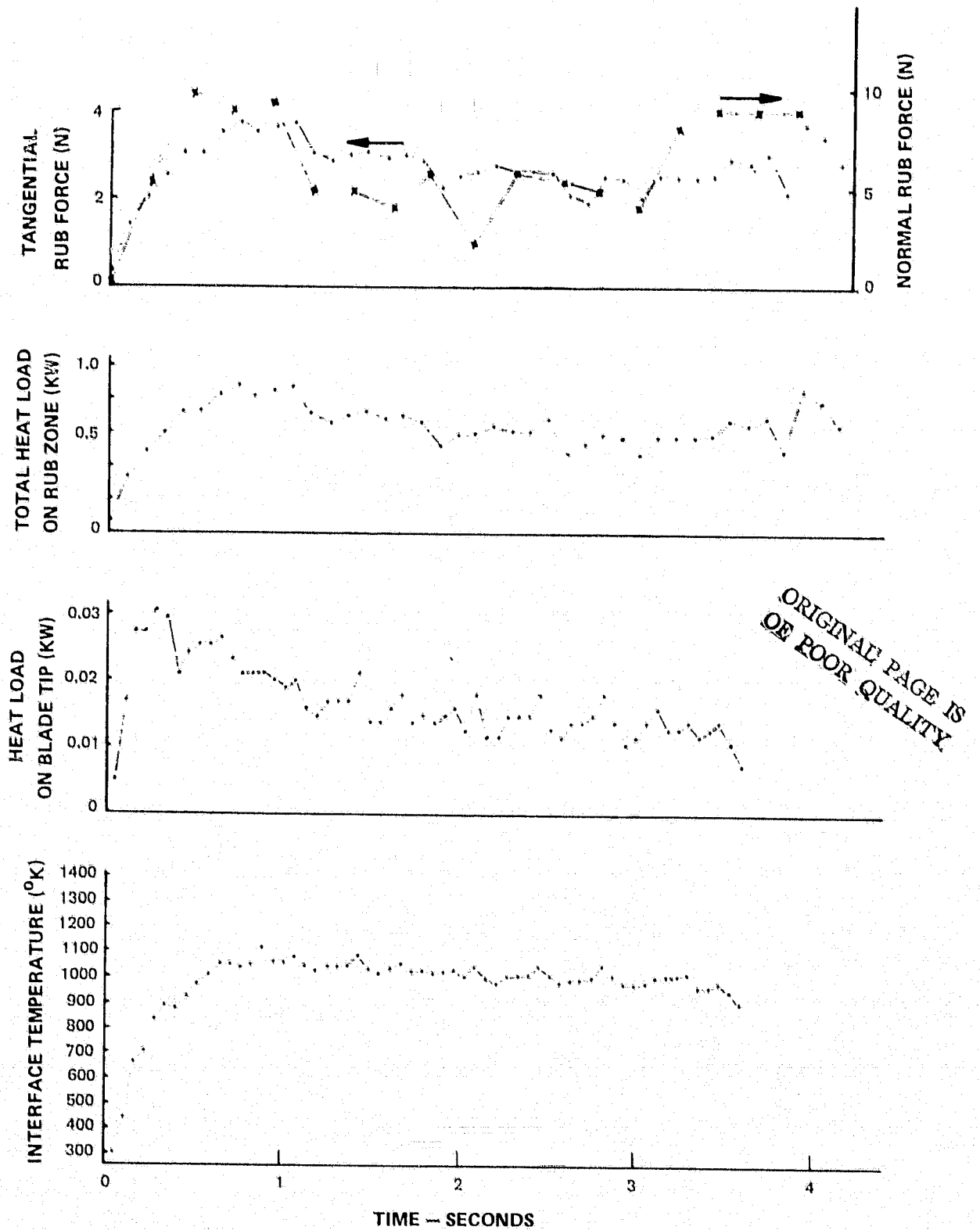
Test 14 (3, Ti, $i = 0.25$ mm/sec, $v = 152$ mps, $b = 0.55$ mm, $\delta = 1.0$ mm, $\rho = 19\%$)

Figure 67. Typical Particle of Rub Debris from Test 14 (Mag: 1000x)



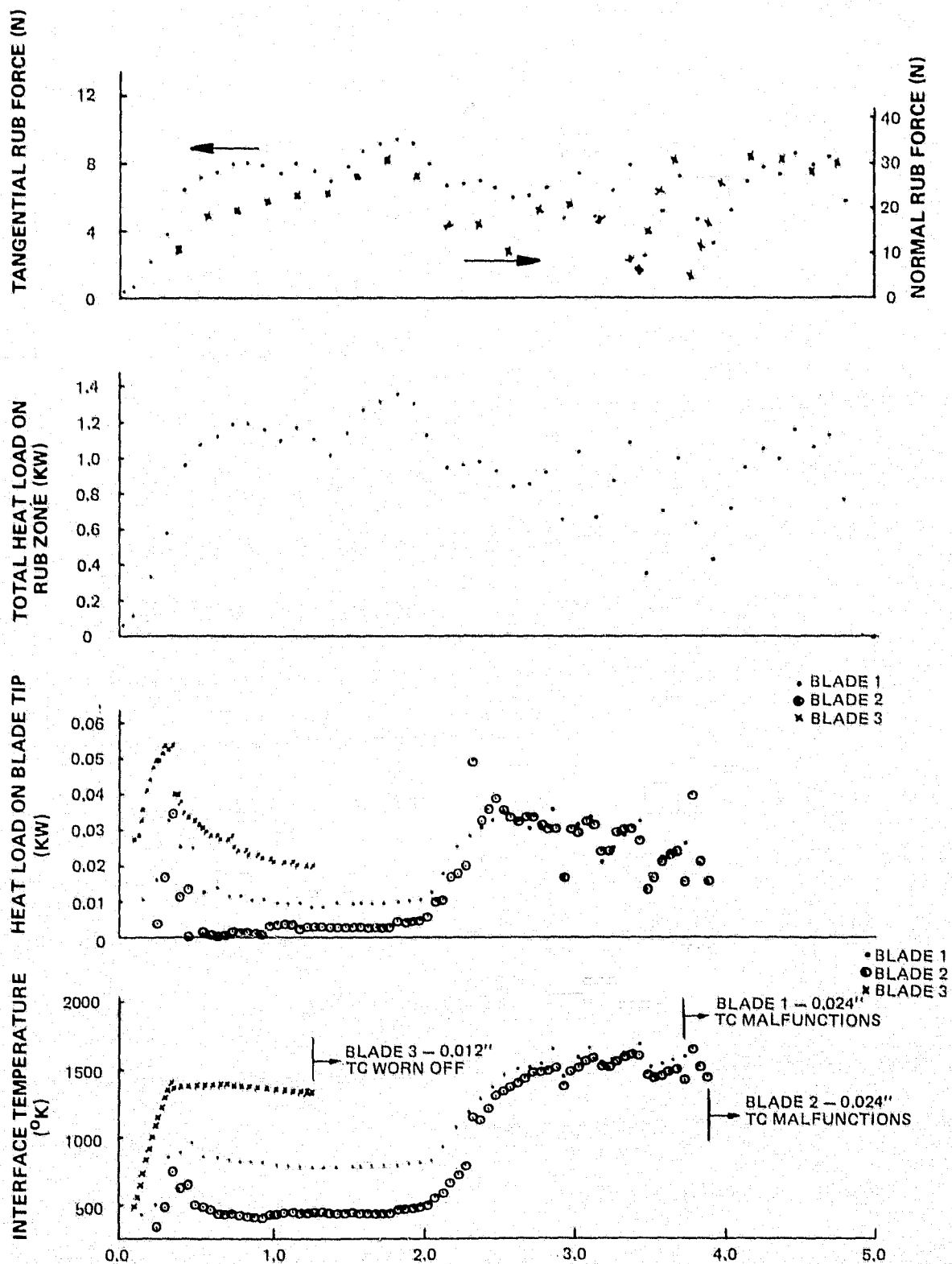
Test 14 (3, Ti, $i = 0.25$ mm/sec, $v = 152$ mps, $b = 0.55$ mm, $\delta = 1.0$ mm, $\rho = 19\%$)

Figure 68. Hastelloy X Abradable Seal Fiber Dislodged During Rub (Mag: 1000x)



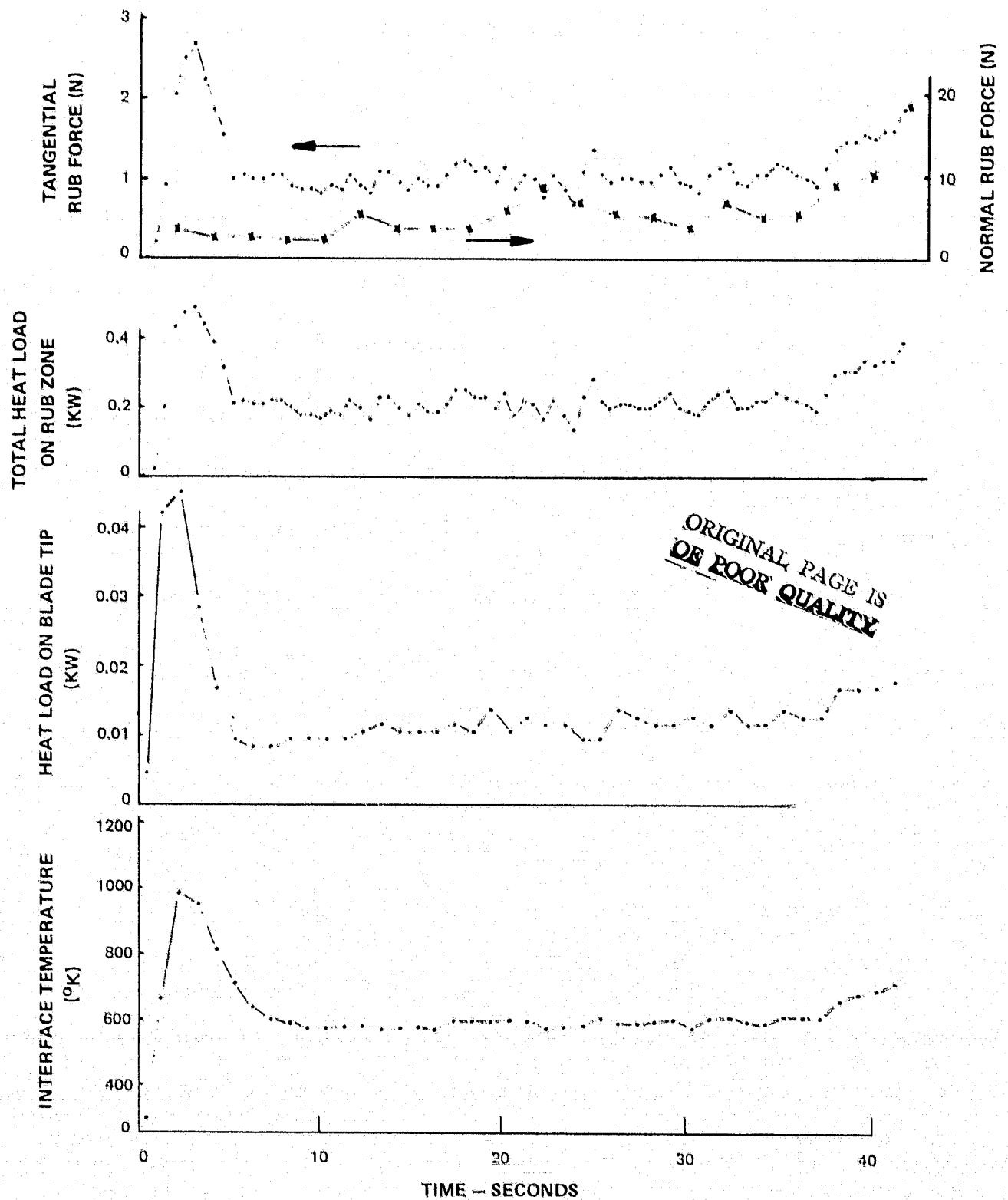
Test 13 (1, Ni, $i = .25$ mm/sec, $v = 213$ mps, $b = .48$ mm, $\delta = 1.0$ mm $\rho = 16\%$)

Figure 69. Task III Test 13 Data Reduction Results



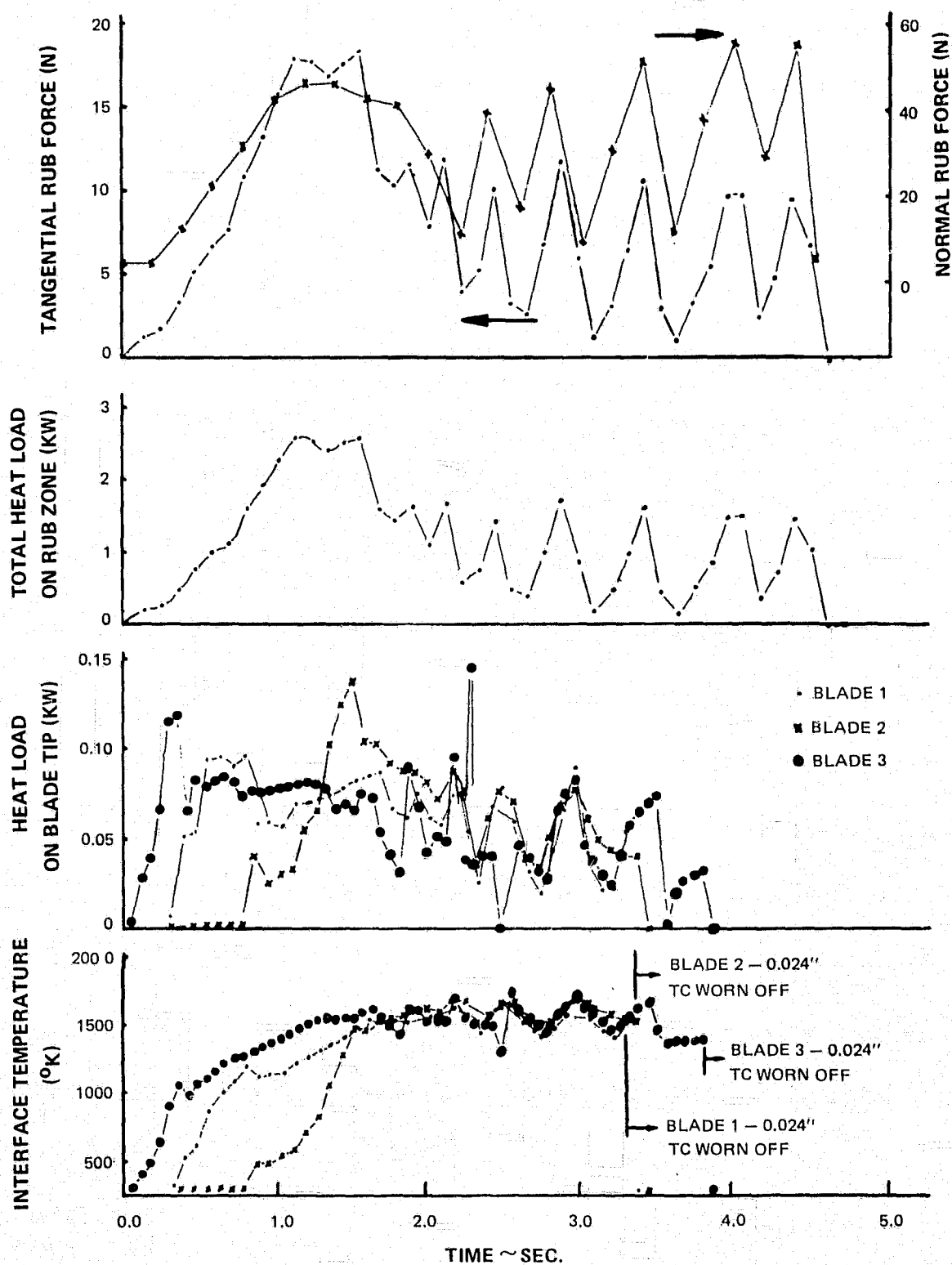
Test 14 (3, T_i , $i = .25$ mm/sec, $v = 152$ mps, $b = .55$ mm, $\delta = 1.0$ mm, $\rho = 19\%$)

Figure 70. Task III Test 14 Data Reduction Results



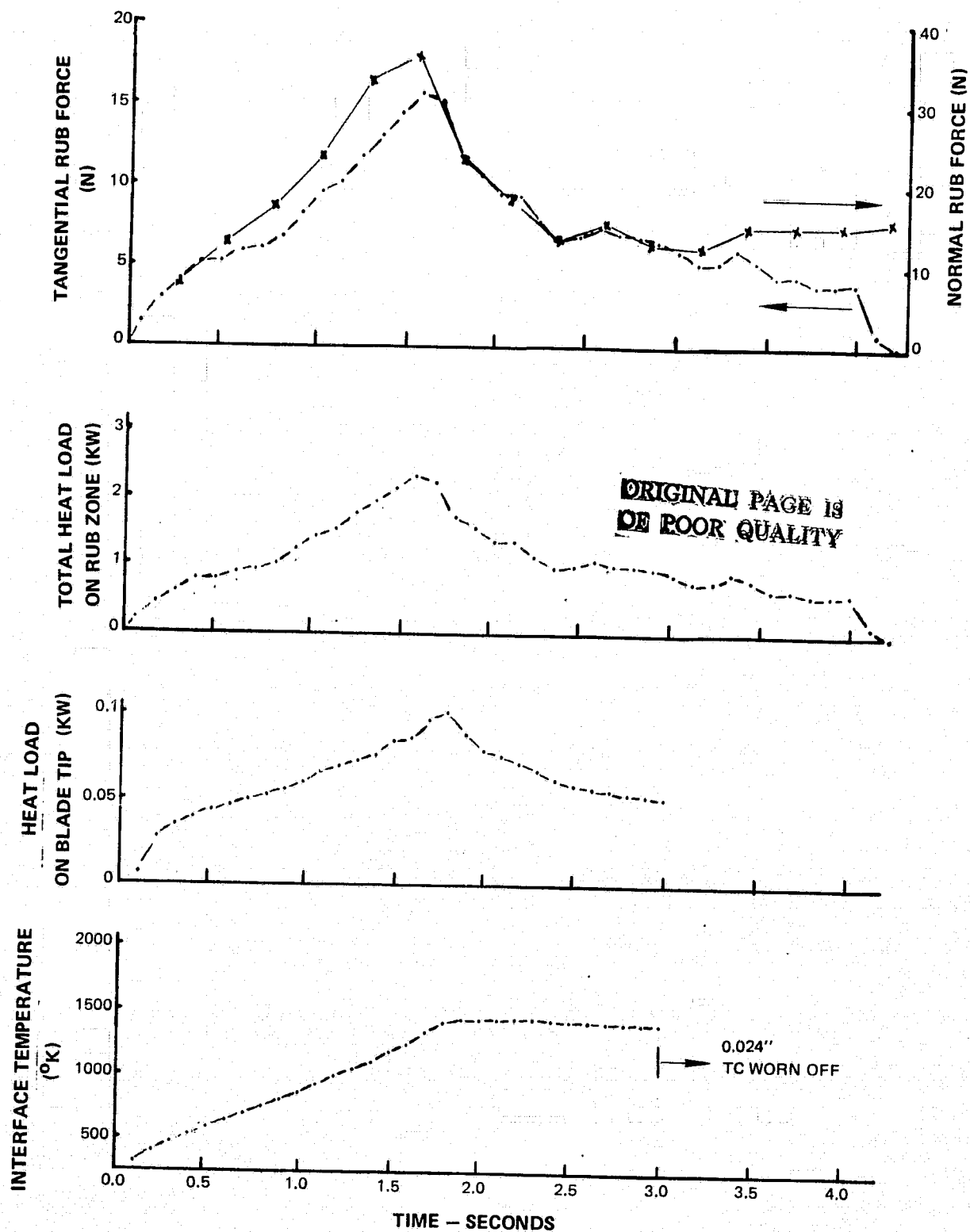
Test 15 (i, Ni, i = .025 mm/sec, v = 213 mps, b = 1.70 mm, δ 1.0 mm, ρ = 16%)

Figure 71. Task III Test 15 Data Reduction Results



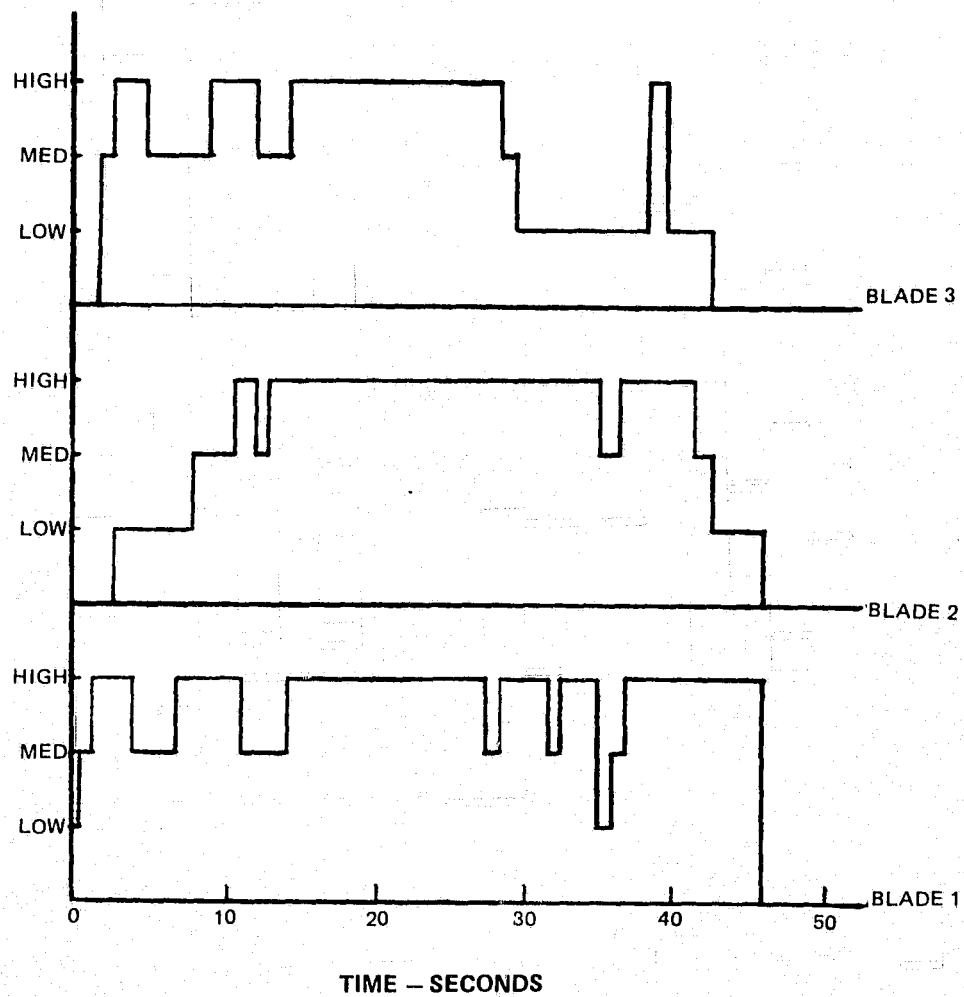
Test 16 (3, Ti, i = .25 mm/sec, v = 152 mps, b = 1.71 mm, δ = 1.0 mm, ρ = 19%)

Figure 72. Task III Test 16 Data Reduction Results



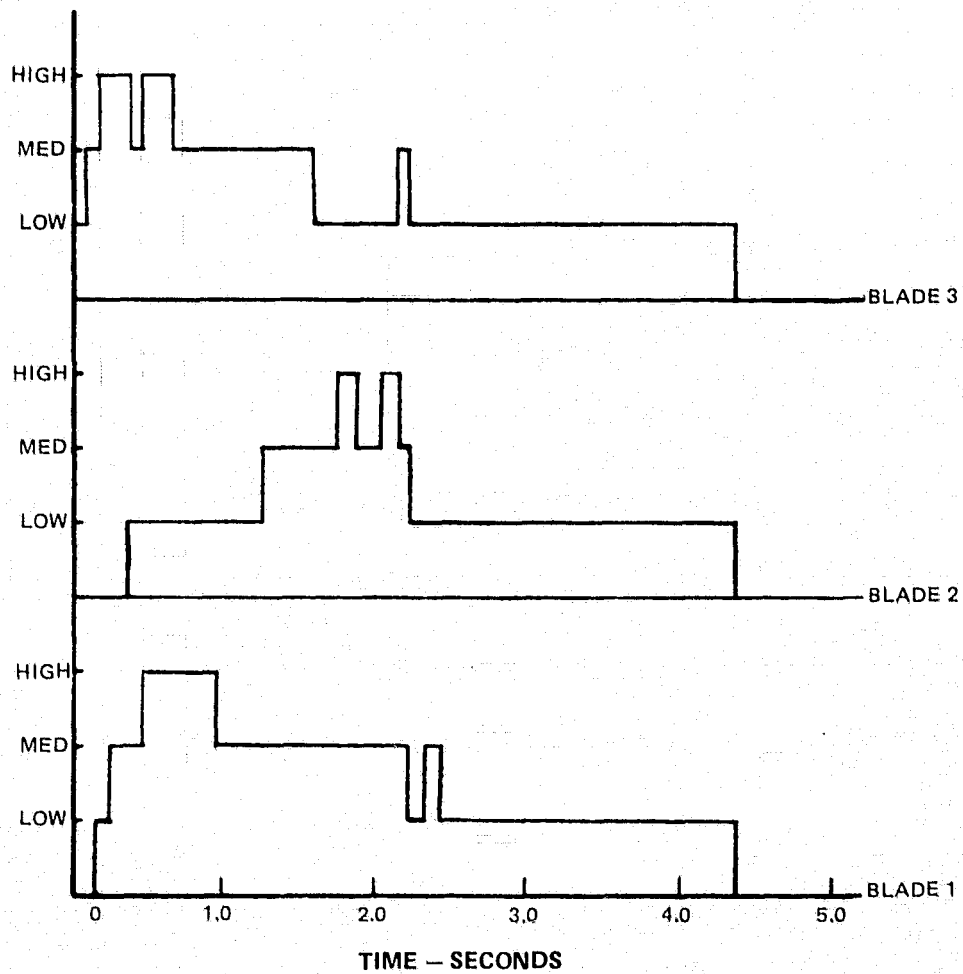
Test 17 (1, Ni, $i = .25$ mm/sec, $v = 152$ mps, $b = 1.68$ mm, $\delta = 1.0$ mm, $\rho = 19\%$)

Figure 73. Task III Test 17 Data Reduction Results



Test 14 (3, Ti, i = .25 mm/sec, v = 152 mps, b = .55 mm, δ = 1.0 mm, ρ = 19%)

Figure 74. Task III Test 14 Strain Gauge Results



Test 16 (3, Ti, i = .25 mm/sec, v = 152 mps, b = 1.71 mm, δ = 1.0 mm, ρ = 19%)

Figure 75. Task III Test 16 Strain Gauge Results

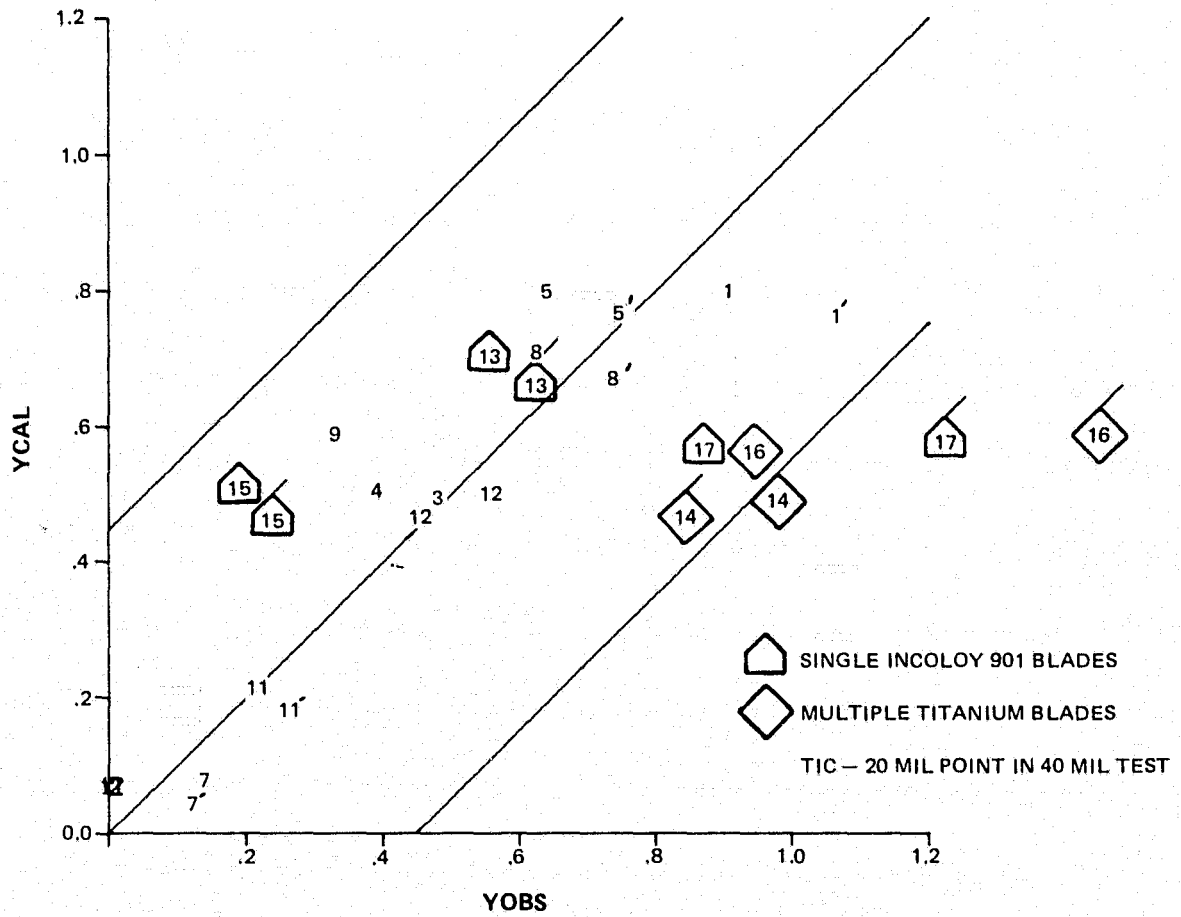


Figure 76. Comparison of Task III Data with Task I Model - Average Total Energy

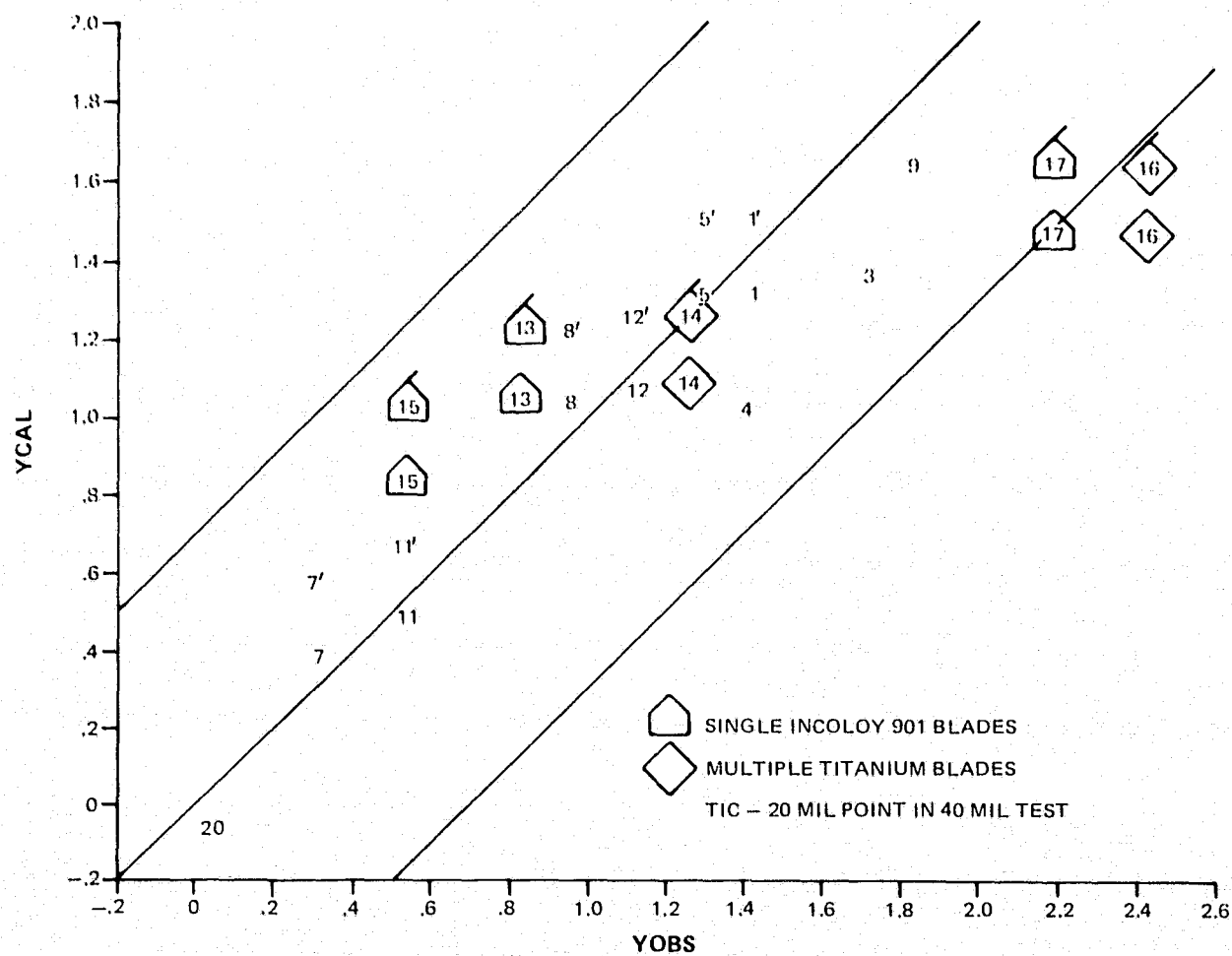


Figure 77. Comparison of Task III Data with Task I Model -- Peak Total Energy

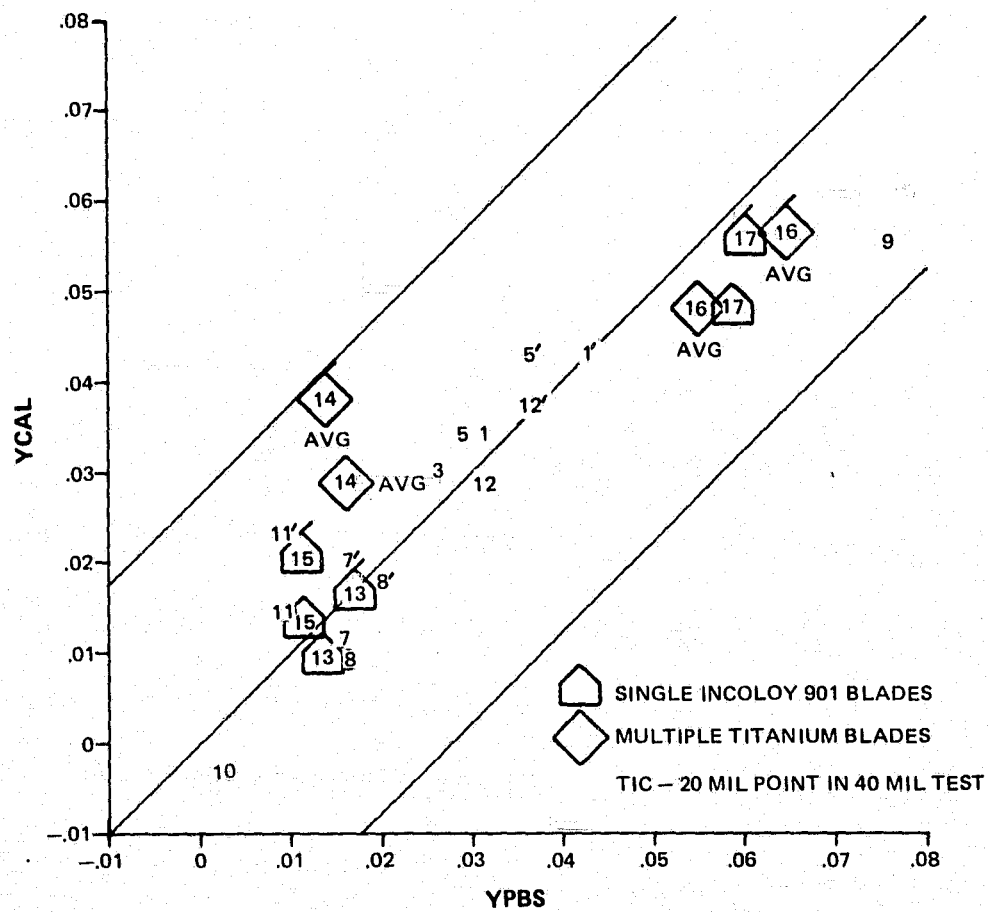
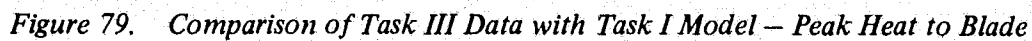


Figure 78. Comparison of Task III Data with Task I Model - Average Heat to Blade



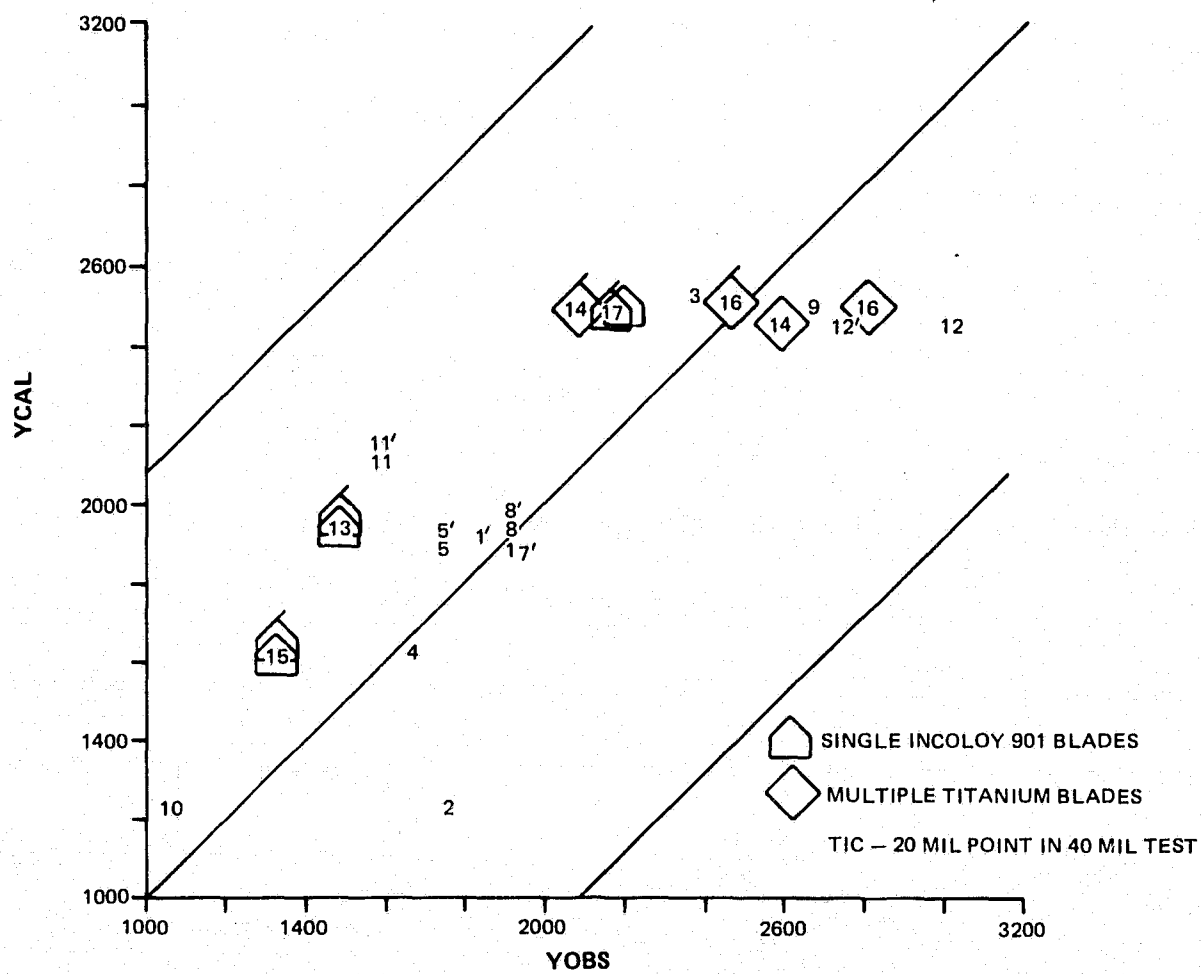


Figure 80. Comparison of Task III Data with Task I Model – Maximum Blade Temperature

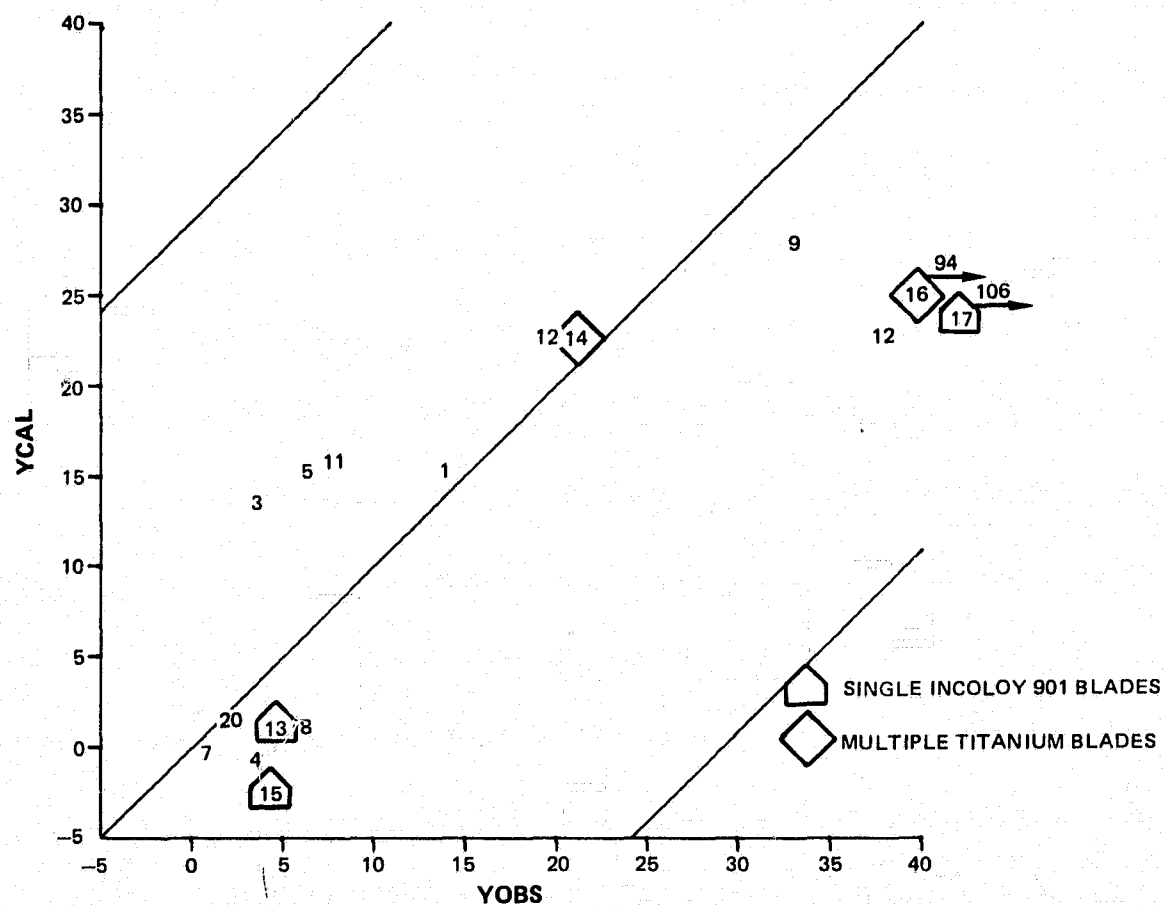


Figure 81. Comparison of Task III Data with Task I Model – Adjusted Blade Wear and Transfer